A piezoelectric translator for feedback in an optical probe.

Author:
Bendeli, Alexander

Publication Date:
1975

DOI:
https://doi.org/10.26190/unsworks/4903

A PIEZOELECTRIC TRANSLATOR FOR FEEDBACK IN AN OPTICAL PROBE

A. BENDELI

A thesis presented for part fulfilment towards
the degree of MASTER OF ENGINEERING SCIENCE
at the UNIVERSITY OF NEW SOUTH WALES

JUNE 1975

ACKNOWLEDGEMENTS

The author wishes to thank the director of CSIRO National Measurement Laboratory and in particular the group leader of the Length section for the time allocated to the implementation of this project. The author also very gratefully acknowledges the time and effort of Mr E.G. Thwaite and Associate Professor G. Johnston for counselling and supervising the work carried out at the laboratory.

TABLE OF CONTENTS

SYNOPSIS

1 INTRODUCTION

5 THE OPTICAL STYLUS

21 THE TRANSLATOR

30 THE FEEDBACK TRANSDUCER

44 EXPERIMENTAL RESULTS AND APPARATUS

54 CONCLUSION

APPENDIX I

APPENDIX II

REFERENCES

SYNOPSIS.

Surface roughness parameters are conventionally derived from mechanical stylus measurements. Non-contacting measurements offer certain advantages and a feasability study for an optical probe is undertaken. Several components which might be used in the apparatus are examined and evaluated. The probe is based on a research originally carried out by O. Dupuy in 1964. The design involves the use of an electromechanical translator displacing a lens such that a light spot is always focused on the surface to be measured. For our purposes, the spot is derived from focusing a laser beam and the translator is fabricated from a piezoelectric ceramic. Evaluation of the translator revealed hysteresis and non-linearities which must be reduced since a linear device is required. Several schemes for linearizing are discussed and an interferometric displacement measuring method using an "optical wedge" is evaluated. An improved defocusing detector using fibre optics has been implemented in a prototype and displacements of 100 nm were readily measured. Sensitivities up to 12 nm/V were achieved. Limitations due to laser intensity fluctuations prevented any higher sensitivities from being attained.

INTRODUCTION

The project's ultimate goal is to design an instrument which will indicate the profile of a surface without actually making contact with that surface. It is to be stressed that the following is a feasibility study of a non-contacting optical profilometer based on a research originally carried out by Dupuy (1964) at the "Institut d'Optique, France".

The topology of a surface can be understood as a superposition of two processes; a periodic component resulting typically from the characteristics of the machining process and a stochastic component which is a random element superimposed on the periodic structure to result in the overall surface texture. Various statistical models of surfaces have been developed (Davies 1954, 1961, Porteus 1961, 1963). Topology is a three dimensional phenomenon so that the measurement of a line profile (as carried out by a stylus instrument) results in a partial loss of information. Several surface topology measurement methods are summarized in the following paragraphs (Mollenhauer, 1973).

Contact method. Using a stylus instrument results in a profile section measurement. It has sometimes been found that inconsistent results are obtained from the measurement of the same surface by a variety of stylus instruments. This may be due to insufficient precise calibration methods or the fact that the surface measured was not isotropic or again that the variations are statistical. There is no evidence, however, of an overall basic inadequacy in the stylus method and indeed it is the most satisfactory

method currently available for obtaining detailed quantitative information about the statistical nature of surfaces. It is worth mentioning that certain commercial instruments such as "Talystep", can achieve a vertical resolution of better than 2.5 nanometres and a horizontal resolution limited by the apex radius of the stylus (typical stylus tip radius = 1.27 μm).

Non contact. Most of the recent development is due to Dupuy in the profile measurement field. Non-contacting three dimensional evaluations using interference microscopes have also been developed (Tolensky, 1970). Due to the high magnifications of these microscopes, only small areas are observable. Three dimensional measurements using capacitance probes and scanning microscopes have also been tried (Phelan, 1971). Demmel (1954), Westberg (1973), Edwin (1973) investigated relationships between normal stylus parameters and photometrical parameters.

Comparison methods using the human finger have been found to have a surprisingly high sensitivity to roughness and frequency. However, the method is of no real value as precise quantitive measurements cannot be achieved.

The calibration of surface roughness measuring instruments is normally carried out using physical standards such as etched, ruled or evaporated surfaces. Recently, several calibration methods have been developed in order to eliminate wavelength and range limitations which are an important limitation with these standards, see for example Sharman (1968), Bendeli & Al (1974). Practically all surface roughness measuring equipment utilizes a mechanical pickup stylus in contact with and traversing the surface to be

investigated. Here, the pickup element functions rather similarly to the stylus in a commercial record player. In metrology, however, the stylus output is filtered to remove surface components below a set of specified cut-off wavelengths. Situations arise when the surface of the specimen to be measured is very delicate and must not be scored by the measuring apparatus (eg optical coatings). It is obvious that a non-contact measurement has to be performed in such cases. Various advantages are often attributed to non-contacting measurement in any field. The main advantage as the name itself implies, is a non-disturbance of the parameter being measured. In some cases, the physical state of the surfaces makes contacting measurement impossible and non contacting mandatory, eg. flow velocity measurement of hot steel. A variety of examples can be drawn from working industrial applications of this non contacting concept, eg. photoelectric batch counters, optical correlator for non contacting velocity measurement, laser interferometry for short or long range distance measurement, capacitive pick-up elements for submicron length measurement, air jet pressure gauges for deviations from nominal dimensions in automotive parts etc.

The aim of this project is twofold. Firstly, to establish a means of generating precise linear displacements over a wide range. Secondly, by using this linear translator, to design a non contacting "probe". This term will be defined as a device which explores surface irregularities without actual physical contact with the latter. The behaviour and performances of the probe would be similar to a mechanical stylus and

must follow the peaks and troughs present in the surface. Capacitive measurements will not be considered here as they tend to integrate the topology of the entire surface under the capacitor's plate, which often covers an area of greater magnitude than that to be dealt with. A spot of light projected through an optical system onto the surface under test will function as an "optical stylus" analogous to a diamond stylus used in conventional surface measurement equipment.

The preliminary design parameters laid out for such a probe are the ability to respond to signals from DC to 1 kHz, to operate with a range of ± 20 micrometres and to have a sensitivity in the nanometre region (say 3 - 5 nm). Several existing probing instruments have been developed, eg. the topografiner; Young (1966), scanning electron microscope. A review of surface microtopography is given in Young (1971). The optical method seems to be the most promising for general laboratory work as it does not necessitate special high vacuum vessels and sophisticated electron microscopes. Although the construction of a non-contacting probe is the ultimate aim of this project, the performance of several components of this apparatus need examination before the construction of the probe could be undertaken. The ensuing discussion expounds these investigations.

Throughout this context, the term "translator" will define an electro-mechanical device whose input is electrical and output is of a mechanical nature. A "transducer" will define a component, not necessarily electro-mechanical, whose output is an electrical signal in response to some stimuli such as displacement, velocity, acceleration or other.

THE OPTICAL STYLUS

The optical stylus

Several non contacting methods for examining a surface and obtaining a profile or a topographical picture of a section of the surface have already been developed. Notably, a scanning electron microscope reaching a vertical resolution of 150 nm and a horizontal resolution of 10 nm was quoted by Young (1971). This instrument projects a focused electron beam on the specimen surface. The beam is rastered across the surface in synchronism with the X and Y deflection of a cathode ray oscilloscope (or TV monitor). Scattered electrons from the surface are collected, amplified and made to modulate the intensity of the CRO trace. Information from each point on the surface is obtained and displayed to reveal the three dimensional topography of the specimen.

A "topografiner" developed at the National Bureau of Standards is another high resolution non-contacting apparatus (Young, 1966). A sharply pointed emitter is scanned above the specimen surface by two piezoelectric drivers. A constant current is passed through the field emission point thus establishing a fixed field at the emitter surface. Once the emitter to specimen distance is fixed, the voltage between the two can be calculated according to Laplace's equation. As the emitter is scanned across the surface, changes in voltage are measured and fed to a servo system which applies the appropriate correcting voltage to a third piezoelectric translator thus keeping the emitter to specimen voltage constant. The correcting voltage corresponds directly to the emitter position and can be used to record the profile. The quoted vertical and horizontal resolutions are 3 nm and 400 nm respectively

(with a tip radius of 0.1 - 1μm). The limitation of both the scanning electron microscope and the topografiner is that their operation must be carried out in vacuum. Other quantitive methods of measuring surface roughness parameters are under development, but as yet these are unable to directly yield the detailed topography of a surface. These instruments usually give a measure of the light intensity reflected from the surface. A correlation is then established between these results and the surface roughness parameters as measured by conventional stylus apparatus in order to determine how closely the results approach each other. Due to different reflective coefficients of various metallic or dielectric surfaces, identical surface topographies on various materials would result in greater reflections from one surface than the other. Several schemes have been devised to reduce the effect of varying surface reflectivity.

The main part of the present project is based on a research carried out by O. Dupuy (1964, 1967), who obtained encouraging results for the design of an optical probe. One handicap encountered with Dupuy's design is the relatively long time in obtaining a surface profile. The scanning time quoted by Dupuy ranged from 10 to 120 minutes for a 5 mm sample length. Over such extended periods, thermal gradients are likely to alter the "average surface plane" relative to that at the start of the measurement. This is especially a problem if precision down in the nanometre region is sought.

Principle of the Dupuy experiment.

The apparatus consists of a means of projecting the image of a pinhole onto the surface under examination. The diffraction - limited image is reflected back through the imaging objective. It is then focused in the plane of a knife edge and just above its edge. Vertical movement of the surface (which is analogous to a peak or a valley) defocuses the spot. This defocusing displaces the focal point of the spot to a new plane parallel to the original plane position but further ahead or behind the knife edge. The knife edge intercepts part of the light beam depending on the vertical displacement of the surface. Displacement of the lens to refocus the image in the knife edge plane will give a measure of the vertical motion of the surface. The unit is insensitive to some degree to the reflective property of the surface under examination. The greatest advantage lies in the fact that no vacuum chambers are necessary. When the measurements are performed fast enough, thermal problems can be reduced and the instrument can become a more viable commercial proposition. It is in this area that the author will suggest improvements to the measurement technique.

Review of the Foucault method

Consider a point source S in figure 1 lying on the optic axis of a lens L at some distance p from the lens centre. The image will be located at a distance p^1 according to the lens law $\frac{1}{f} = \frac{1}{p} + \frac{1}{p^1}$ where f is the focal length of the lens L. A knife edge B is located in the image plane. Situated behind the blade is an observer looking at the lens and seeing it uniformly illuminated when the blade does not interrupt the beam.

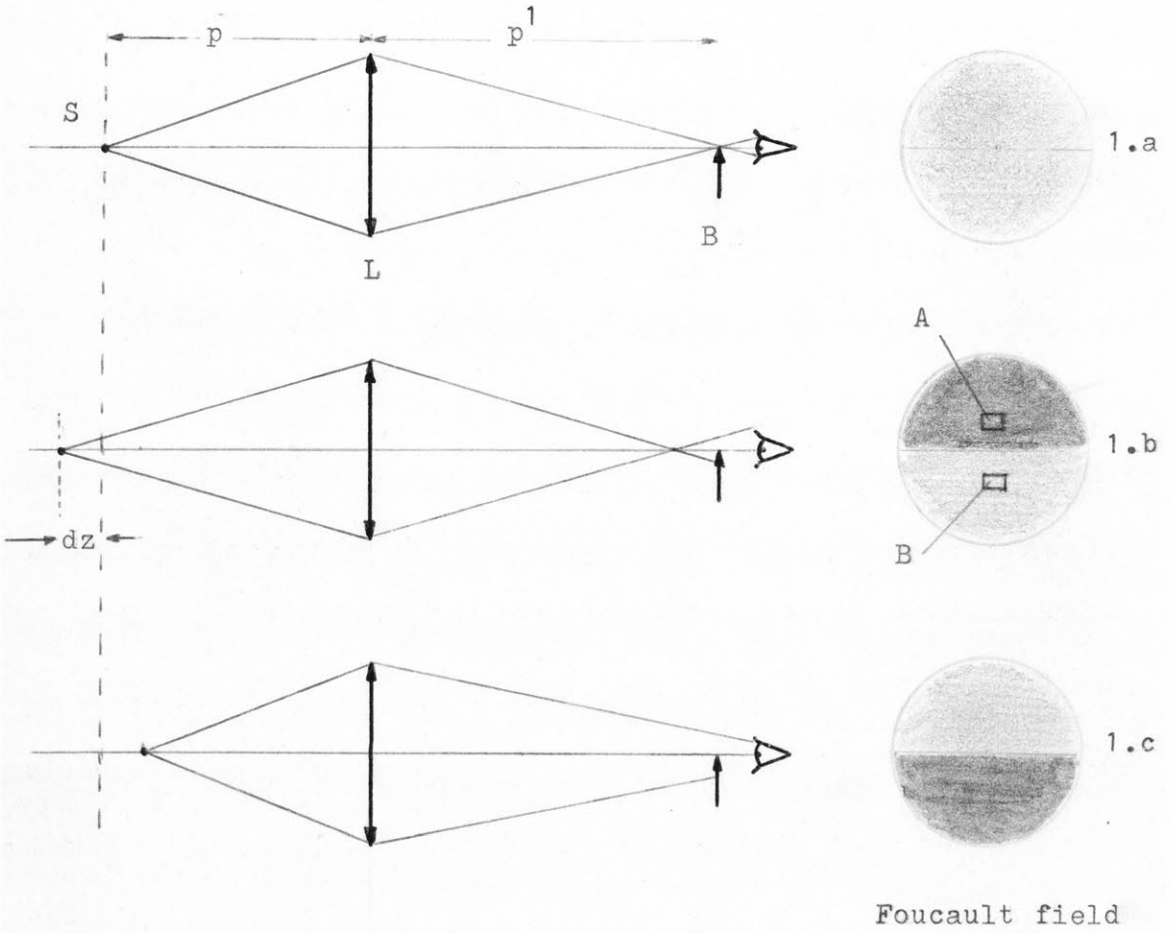

Figure. 1

If the blade is moved in its plane but perpendicular to the optic axis, the observer sees an area of the lens extinguish uniformly as the blade is progressively moved across the field until total extinction occurs. The blade is then returned to a position where the lens is uniformly illuminated (figure 1a). If the point source is moved by a small amount dz away from the lens, the image will be situated between the lens and the blade. Some of the rays will be intercepted by the blade and one half of the lens field will extinguish (figure 1b). Similarly, if the source is moved in the opposite direction, the other half of the lens field will extinguish (figure 1c). Therefore, we have a means of determining precisely the exact location of a point source by photometric equalization of the two half fields. The actual instrument uses a slight variation of this principle to determine the position of a spot on a surface. Assume S is displaced away from the lens by an amount dz giving a field as shown in figure 1b. The lens will now be moved by the observer towards the point source such that the image is formed again in the plane of the blade and the lens field is uniformly illuminated. A measure of the lens displacement will be directly related to the displacement of the point source. The observer has become the feedback path and uses his visual threshold to ensure that the lens field is uniformly lit. The error in the position of the source when the longitudinal sightings are made is given by a formula proposed by Arnulf (1929) and revised by Dupuy (1969). The relation is an extension to Rayleigh's criterion for the resolution of two sources. The general form of the equation is:

$$dz = \tfrac{1}{2} \cdot \frac{W}{m.n.\sin^2(\frac{a}{2})} \qquad (1)$$

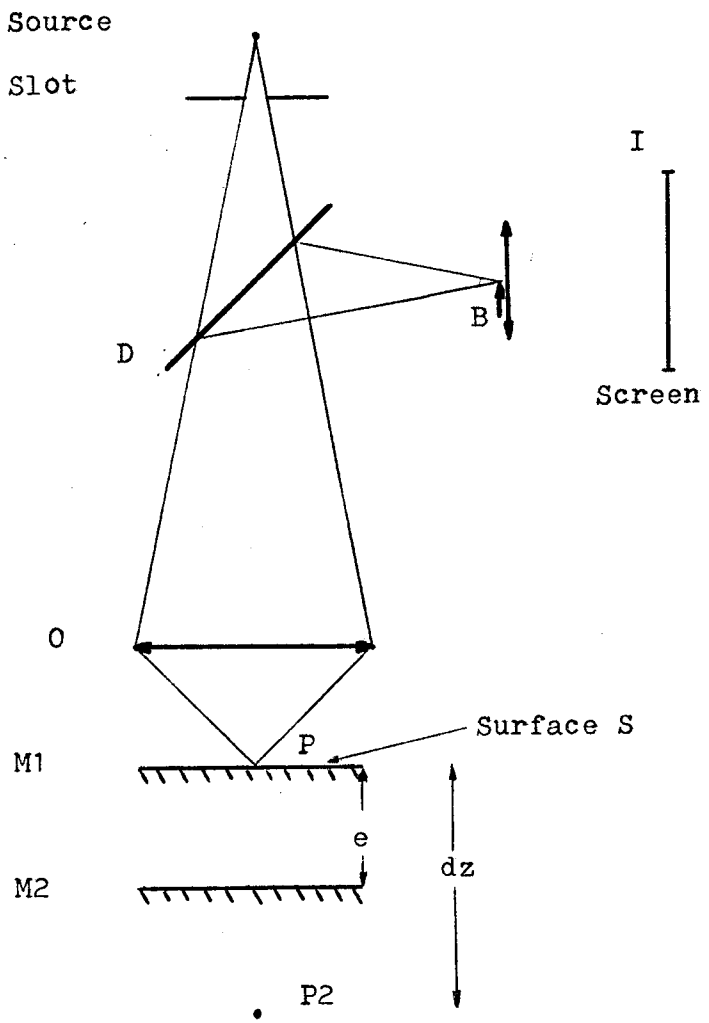

Figure. 2

dz = minimum detectable displacement of the source

W = illumination wavelength

n sin a = numerical aperture of the sighting objective

m = empirical numerical coefficient which depends on various factors such as contrast, illumination intensity, diameter of the eye pupil, minimum detectable change in intensity. m equals 20 for visual sightings.

The optical set-up

A simplified schematic of the system is shown in figure 2. Light of wavelength W illuminates a circular aperture and the resulting diffraction is obtained at P. Point P is situated on the surface plane M. D is a semi reflective beam splitter and O the sighting objective. The minimum size image that can appear at P is limited by the resolving power of O. For a diffraction limited optical system, the image of a circular aperture consists of a central bright disc known as Airy's disc. The radius of the disc at P is $r = \frac{1.22\ W}{2 \cdot n \cdot \sin(a)}$ (2)

Light is reflected back from the surface through O, then deflected by D and an image is formed in the plane of the knife edge B. A lens placed against the blade projects an image similar to those shown in figures 1a, b, c on screen I. When the surface is moved from M_1 to M_2 by an amount e, the relative position of the spot P_2 is at a distance dz from p so that dz = 2e. In actual measurement situations, the surface is displaced laterally at a uniform rate and it is the texture of the surface

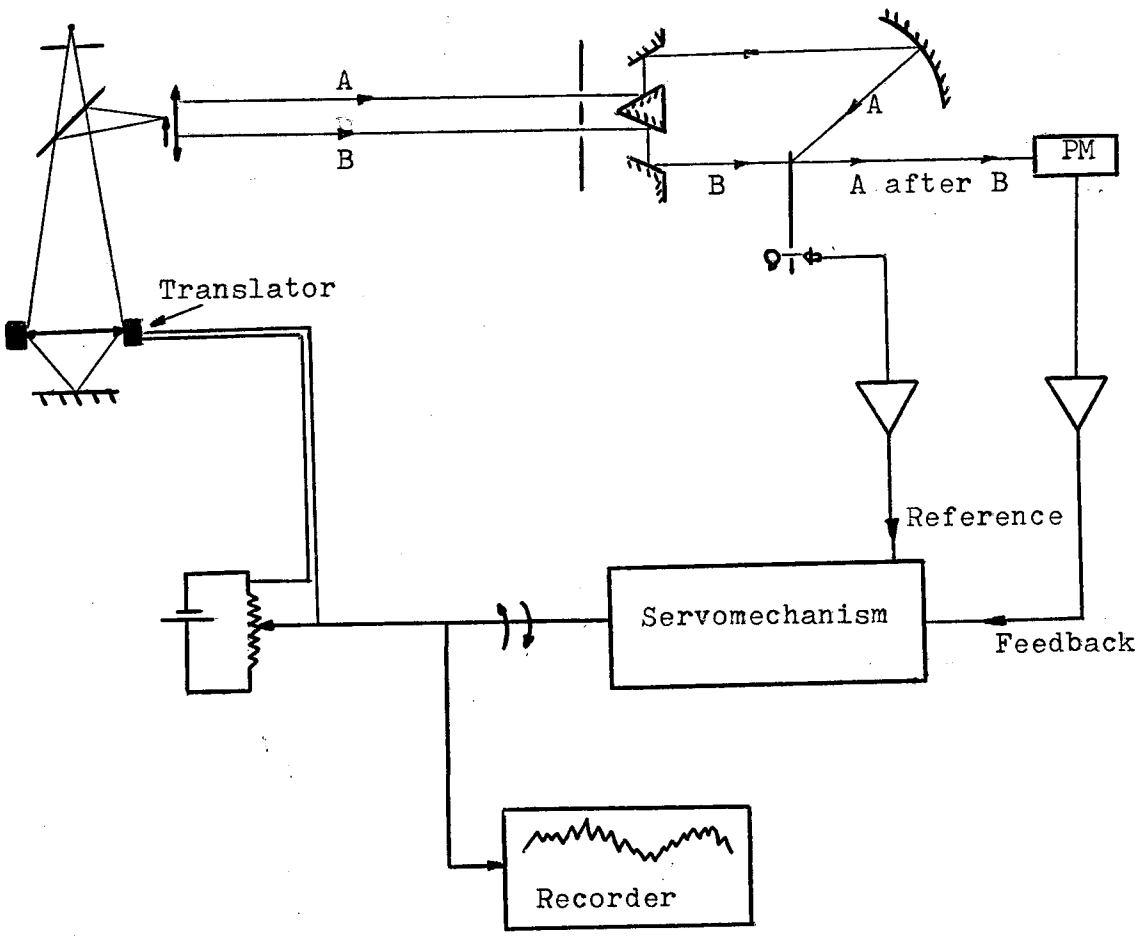
A
B
A
B
A after B
PM
Translator
Reference
Servomechanism
Feedback
Recorder

Figure. 3

which gives the impressions of vertical displacements. An improvement by a factor of two in locating the surface S has been achieved over the original Foucault method as now $e = \frac{1}{4} \cdot \frac{W}{m.n.\sin^2(\frac{a}{2})}$ (3)

Dupuy (1967) quotes a theoretical precision of .001 micrometres with a lens of numerical aperture of 0.95 and a loss in precision with decreasing numerical factor m. A schematic of the instrument developed by Dupuy is shown in figure 3. A brief description follows. The main objective is supported by an electromagnetic translator. The two sampling areas A and B are sequentially projected onto a photomultiplier PM by means of a rotating toothed disc which is coated with a highly reflective layer. The photomultiplier amplitude output signal represents the intensity difference between the two areas A and B. A reference signal is also generated by the toothed disc as it modulates the light path between a lamp/photocell arrangement. The reference and photomultiplier output are phase compared to determine the direction of travel of the translator. The amount of translation is determined by the amplitude of the peak AC signal from the PM. The comparison is made in a servomotor which drives the shaft of a voltage divider. The voltage divider output is then applied to the translator. The translator is displaced until the illumination of areas A and B is equalized and the PM output is zero. The translator's voltage then represents the surface profile as the surface is lateraly displaced under the objective.

Proposed set up

It is to be stressed at this point that the following is a feasability study of the scheme before embarking on a final design. No

Figure. 4

servomechanisms or complex optical/mechanical arrangements were necessary at this stage. The theoretical precision of .001 μm as stated by Dupuy for the sighting, using a lens of NA 0.95, implies an illuminating wavelength of 0.405 μm. The early experimental values quoted by Dupuy were .01 μm obtained with an NA 0.95 but further improvements on this figure were envisaged. In our case, to obtain a greater light output and to improve the contrast and threshold detection (ie an increase in the value of m) it was decided to use a He-Ne laser as the primary source of illumination. The objective available at National Measurement Laboratory has a NA of 0.65 and a magnification of X40. The numerical aperture of 0.65 results in a $\sin^2(\frac{a}{2})$ term of 0.12.

With photoelectric detection, m ranges from 400 to 2000 depending on the location of the photodiode in the Foucault field. Selecting m = 400, the theoretical precision expected for a wavelength of 0.6328 μm using relation 3 is .003 μm. This figure of .003 μ is aimed at but because of inadequacies and limitations of the mechanical system, performance of this particular set up is not expected to attain the calculated precision. A rigid structure to support most of the optical components and a means of deflecting a surface in a vertical direction was required. This was met by an instrument stand as shown on figure 4. This robust stand provided excellent stability but did not have an adequately smooth vertical adjustment. As a result, the deflection could be effected only in jumps determined by the knurled nut engaging the screw. Surprisingly enough, minimum movements in the order of one micrometre were effected.

Figure. 5

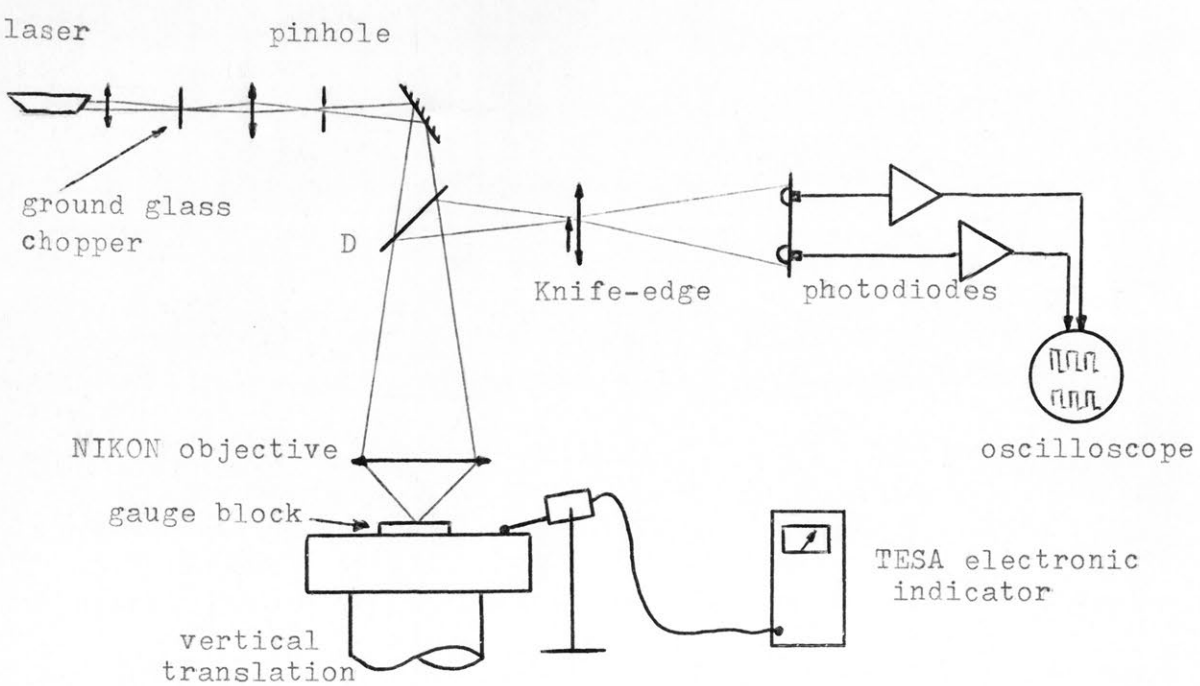

Figure. 6

Photographs in figures 4 and 5 depict the preliminary experimental set up constructed to determine the feasability of the project. A schematic appears on figure 6.

A parallel beam, illuminating a pinhole, was originally used as a point source whose image was projected on the surface. The beam traverses a half-silvered mirror D before reaching the surface (in this case, a gauge block).

The gauge block rests on a table which can be raised or lowered by the knurled nut previously mentioned. A "TESA" displacement indicator monitors the vertical displacement of the table. Upon reflection from the gauge block surface, the beam retraces its path through the objective and is reflected by D on to the knife-edge B. A lens then projects the Foucault image on a screen. Such an image was achieved by the above preliminary experimental arrangement. Raising and lowering the gauge block produced the expected alternating pattern on either side of the centre line of the Foucault image.

The actual image obtained was marred by a large number of stray interference patterns resulting from unwanted reflections, misalignments and imperfections in the lenses. At this stage, the minimum detectable displacement was 10 μm. The interference patterns were eliminated by introducing a rotating ground glass screen situated in the path of the beam emerging from the laser. The diffuser destroys the spatial coherence of the beam. By having a clearer image for visual observation, the precision increased to 3 micrometres with the possibility of estimating smaller displacements by interpolation.

A partial loss in intensity of the beam is incurred due to the ground glass diffuser, thus the ability of equalizing the illumination of the two areas by visual means was substantially decreased. To improve the threshold sensitivity, two PIN photodiodes were placed in the plane of the screen such that each diode samples one of the two halves of the image area. The response of the diodes is faster than the integration time of the eye. Their output when observed on an oscilloscope was a measure of the light intensity modulated by the granularity of the ground glass as it rotated. Estimation of equality between the two signals can be easily achieved after the diodes and amplifiers have been calibrated for equal output for similar input radiant power. When the two areas are equally illuminated a large initial DC offset is present at the amplifier's output. Any slight deflection of the surface will result in unbalanced intensitities and it becomes necessary to detect small signals on a large background signal. The problem is therefore one of signal to noise. This large standing DC offset cannot be eliminated by shifting the cathode ray oscilloscope controls and still afford detection of small outputs. Adding an equal and opposite voltage should eliminate the DC offset and so improve the detection of the small signals. This was not undertaken at this stage as another possibility worth investigating became apparent.

This new possibility relied on the idea of modifying the diffuser so that it could act as a light "chopper". Several strips of opaque paper were glued to the ground glass (as can be seen on figures 4, 5) to obtain an 'on/off' modulation of the light. Although this process reduces the

sensitivity of visual interpolation and interpretation of the intensity, it should not affect the sensitivity of the diodes during the 'ON' cycle, as the intensity during that period is identical to that prior to the modification. The resultant peak to peak AC signal received from the photodiodes has the same amplitude as the DC offset signal previously mentioned. It was therefore possible to AC couple the CRO and observe the modulated output received with the use of a higher sensitivity range on the vertical attenuator of the CRO. Equalization of illumination was achieved by observing and comparing the two signals from the photodiodes during the 'ON' cycle. This extended the minimum detectable movement down to 1 micrometre. The precision was still 300 times lower than the expected theoretical maximum precision for the lens and wavelength used. This was due to several factors which included inaccurate alignment of the optical system, lack of an efficient diffuser, collimating lens and pinhole arrangement. As the mechanical limitations of the displacement table were reached the experiment could not be carried any further.

A tentative electronic improvement is now proposed and a brief description of a system using two photodiodes and two amplifiers follows. The set up would be basically similar to the one shown on fig. 7 except that the source is modulated either by switching its power on or off or by a shutter mechanism. Furthermore, a second photodiode is situated about the axis such that it lies symetrically with the photodiode shown. As the source is switched, the light falling on the photodiodes will give rise to

two modulated photocurrents. Each current will alternatively represent the dark level output and the level of intensity for the null condition. Since under null conditions the resultant signal must be zero, the two photocurrents must be subtracted in a differential amplifier. A problem arises here because the diode sensitivities and thermal drifts are not matched. Furthermore, two large signals need to be subtracted to detect a smaller component thereby placing a demanding specification on the common mode rejection of the differential amplifier. Conceptually, it would be possible to AC couple the photocurrents, adjust the buffer amplifiers gain so that equal currents result, limit the swing during the off peaks such that most of the useless DC offset is eliminated and subtract two smaller signals to obtain the desired result. This possibility was not investigated at this stage although it was not discarded. Figure 9 is a summary of the process described above.

Improvements to the detecting system

It was next proposed to use only a single photodiode and amplifier to eliminate the problems of equalizing the sensitivities and other matters as mentioned previously. An investigation was carried out on several methods by which two areas could be separated for comparison on a single photodetector without having recourse to elaborate mechanical/ optical set ups. Two possibilities emerged ie, modulating the knife edge or modulating the light beam. It is expected that these methods will simplify the optical scheme and rotating silvered disc system used by Dupuy. Systems working on these alternatives will be described next.

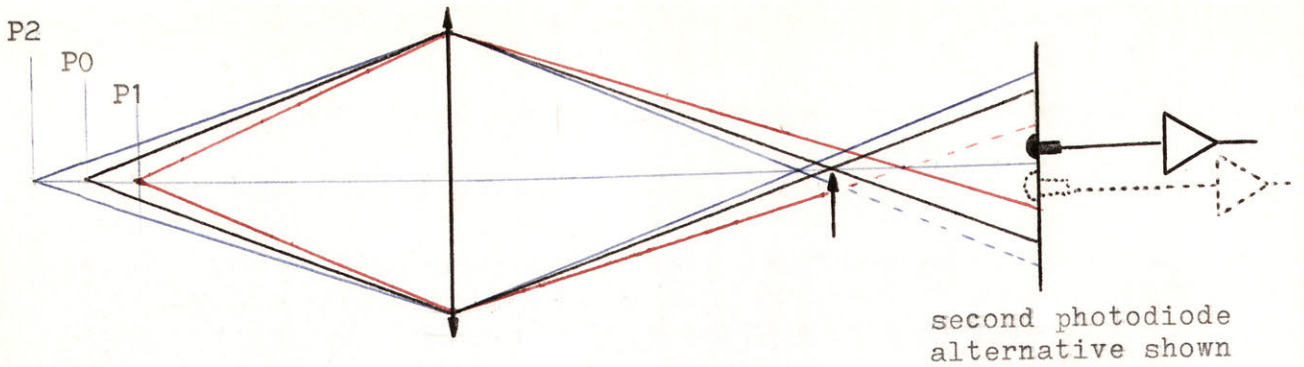

Figure. 7

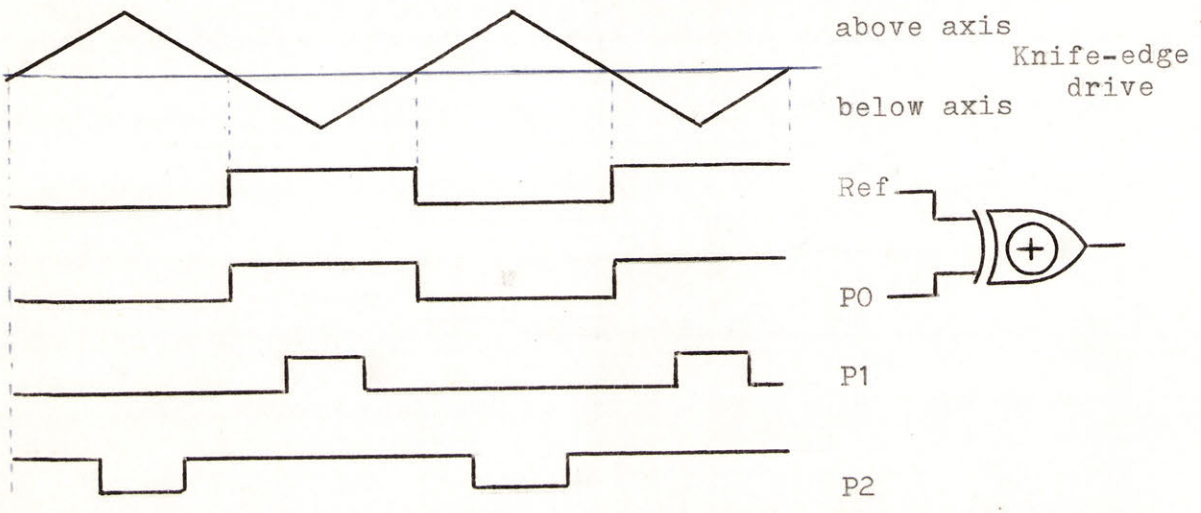

Figure. 8

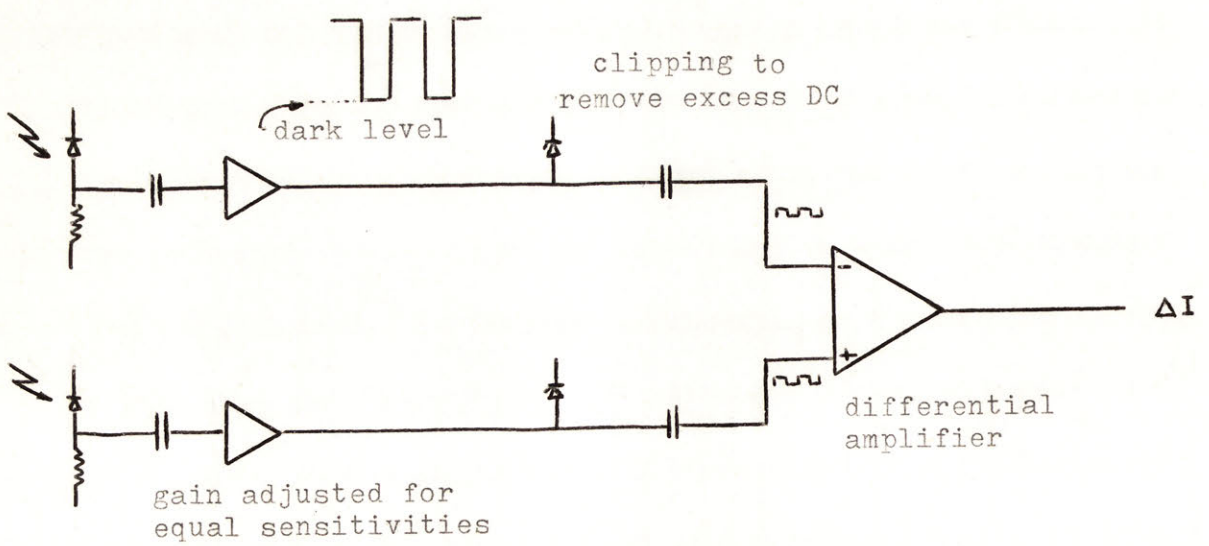

Figure. 9

(a) Knife edge modulation

Figure 7 represents the possible situations for the object to image relationship. Under balanced conditions, the image is located at the knife edge plane. The ray tracing for this condition is marked 1. A single photodiode is located at the screen and samples one of the two halves of the image. When the knife edge is driven above the optic axis, it intercepts the beam and no light reaches the detector. A threshold circuit will output a logic zero when the detector is obscured and a logic high when illuminated above the threshold setting. From the waveform shown in figure 8 an equal mark/space will result when the image is centrally located in the knife edge plane. Comparing (in an exclusive - OR digital gate) the detector output with a reference derived from the knife edge driving signal will result in no output thereby denoting a balanced (or null) condition. If the source is displaced to P1, its image will be located at a point beyond the knife-edge. As the blade is driven across the optic axis, the beam is interrupted for a much longer period than in the null case. The time during which the detector is illuminated is shorter. Comparison with the reference will result in an output related to the defocused condition. A similar argument holds when the source is displaced to P2 where in this case the detector is illuminated for a longer period than the null case. Hence, we have a means of locating the source at Po. A requirement which is evident in this experiment is the stability of the light source output. Assume that the image is centrally located and the threshold is set for the prevailing radiant power. A decrease in power below the threshold will cause a

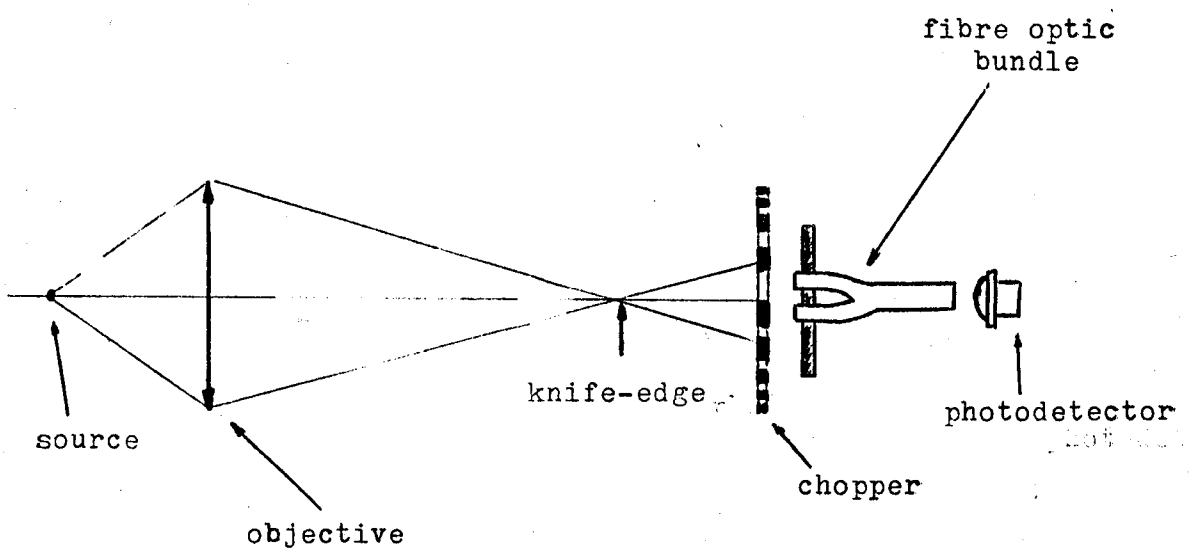
fibre optic
bundle
knife-edge
photodetector
source
chopper
objective

Figure. 10

complete loss of output. As a corollary to this discussion it can be seen that under defocused conditions, the irradiance is lower or higher than the set threshold thus resulting in one case to the situation stated above. It can be argued that the threshold can be set to a lower level to accommodate changes in intensity but various surface reflections will also need to be considered. Changes in source intensity can be compensated for if a ratiometric measurement is carried out. The threshold level will be continuously corrected and will depend on the average source intensity level. Another problem which needs to be kept in mind is the vibration generated by the knife edge driver. Since the motion is translational, a reaction will be transmitted to the supporting structure and may affect the absolute position of the lens. Although these problems are not unsurmountable, this system was shelved and another alternative proposed.

(b) Sequential sampling

This alternative; as the previous one; uses a single photodiode. Figure 10 is a simplified schematic similar to figure 7 except for the changes around the screen. The Foucault field falls on the screen as in the previous case except in this instance, two fibre optic bundles are equally spaced about the central axis of the system. The two bundles are subsequently "mixed" and located in front of the photodetector. The mixing is necessary to ensure that the bundle output is randomly distributed over the sensitive area of the photodiode. A rotating slotted disc chopper is located in front of the bundles. The position of the disc is such that the projection of the slot equals the spacing of the two bundles

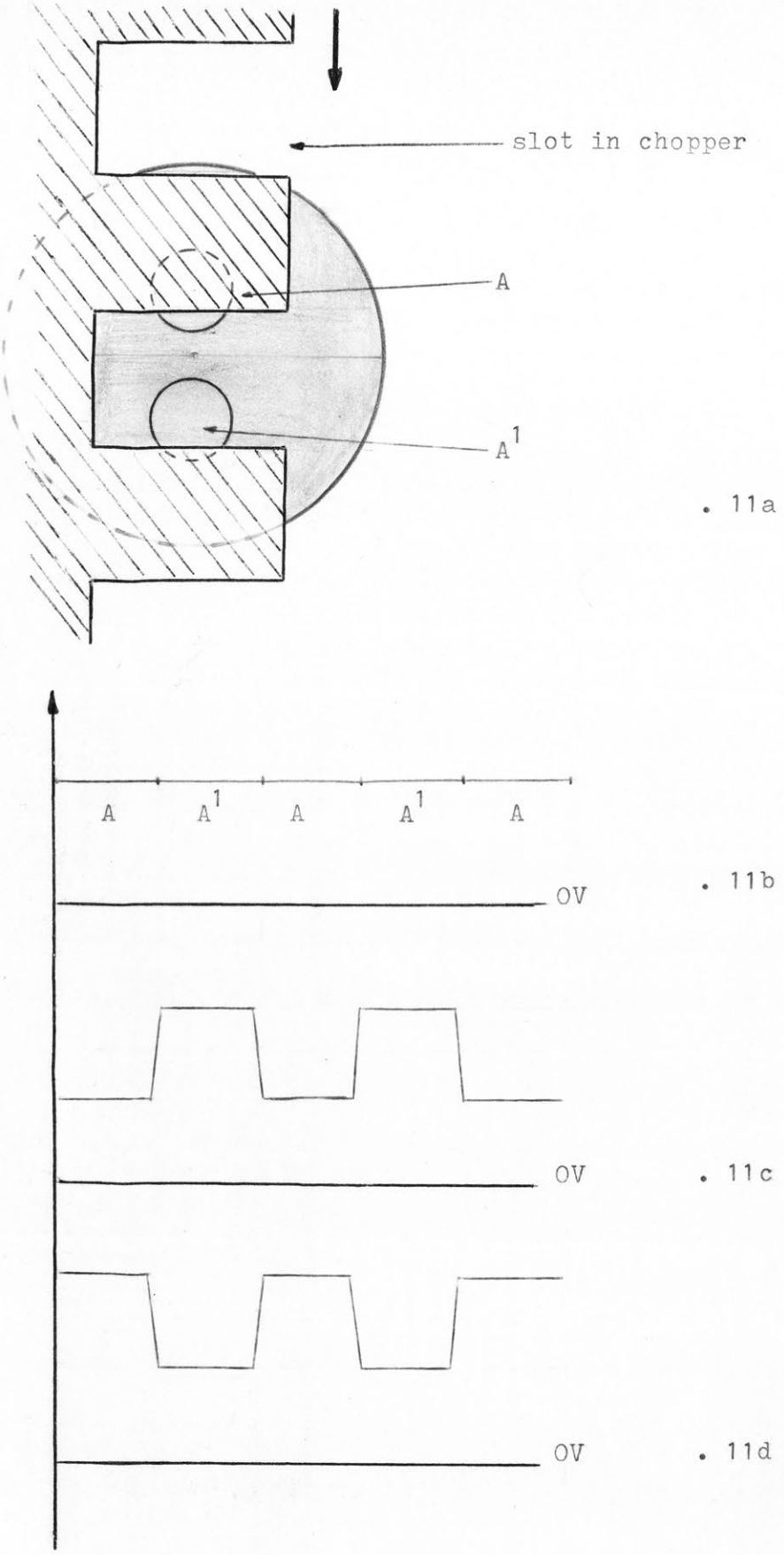

. 11a

. 11b

. 11c

. 11d

Figure. 11

With the help of figure 11 consider what happens when the disc rotates.

- The two bundles are equally illuminated (null condition).

As the chopper rotates in front of the two bundles, their end faces are alternatively obstructed and exposed. Assume bundle A is fully exposed and A^1 obscured. The photocurrent output will be a DC level as shown in figure 11b. When the roles are reversed, the DC output due to A^1 will be the same. When the shutters and slots on the dsic are in the position shown in figure 11a, sections of areas A and A^1 will be obstructed. The total area exposed will always be the same and equal to the end face area of either bundle. Since the irradiance on both areas is uniform, the output will be a steady level. Note that this property will later be used to position the chopper such that the photodiodes are spaced one slot width.

- The two bundles are unequally illuminated (defocused condition).

When the source is displaced, a defocused condition arises. For convenience assume A^1 is more strongly illuminated than A. When the shutter blocks A^1, the output due to A will be less than during the null condition. Conversely, when the shutter blocks A, the output due to A^1 will be more than the null condition as shown by figure 11c. When the source position is such that now A is more strongly illuminated than A^1, then figure 11d results.

The output from the fibre optic bundle under unbalanced conditions can be expressed as

$$(H - dH)\,a + (H + dH)\,(T - a)$$

where H = irradiance in mW/cm^2

dH = change in irradiance falling on A relative to the null condition

T = total receptive area of A in cm^2 = total receptive area of A^1

a = exposed area of A, hence exposed area of A^1 = (T - a)

Therefore, the generated photocurrent in mA is

$$I = S\,(H.T + dH\,(T - 2a))$$

where S is the diodes sensitivity in mA/mW

AC coupling the current will eliminate the H.T term hence

$$Iac = S\,dH\,(T - 2a)$$

For null conditions dH = O $\therefore$ Iac = o

For defocused conditions dH is positive or negative. Assuming dH positive gives

Iac = +STdH for a = o ie A obstructed

= O for a = T/2 ie shutter in central position

= -STdH for a = T ie A completely exposed.

for dH negative and the same sequence as above,

Iac = -STdH

= O

= +STdH.

This method therefore affords an improvement over the previous single photodiode since a change of dH results in an output of 2dH. From the previous statements, the following deductions become evident

- If the intensity falling on the end faces is uniform at null, any change in light source output should not affect the output.

- The output is directly proportional to the change in intensity under defocused conditions.

- The zero crossing always occurs for the same position of the shutter.

- The phase changes by 180° depending on which area is brighter.

- The fibre optic bundle and chopper automatically obtain the difference in intensity therefore eliminating the need for a differential amplifier.

- Since the output can be AC coupled, DC drifts due to temperature and leakage are avoided.

- Because the chopping frequency is fixed (within certain limits), a narrow band amplifier can be used to reduce wideband noise.

This simple and novel use of fibre optics produces a marked improvement in the detector performance and would in all likelihood be the system used in a prototype.

THE TRANSLATOR

Freedom from resonances in the bandwidth of interest and simplicity were the main factors which led to the selection of a piezoelectric element as the translator. Furthermore, the ability to obtain displacements in the nanometre region with an expected range of a few micrometres strengthened the decision that a ceramic element would be most suitable.

A Spectra-Physics piezoelectric translator model 560 was available for use but its full characteristics were not known. The manufacturer's specification was as follows:

Deflection		1.15 μm per 100V
Max sweep rate	ramp	2 k Hz
	sine	5 k Hz
Maximum voltage		2 k V
Angular variation		none.

Its electrical parameters were measured at a frequency of 10 000 radians and were found to be as follows: capacitance .0428 μF

parallelconductance .0007 m mho.

It was anticipated that the maximum displacement would occur near the maximum voltage thus giving a range of ±23 micrometres assuming the displacement direction is a function of polarity of the applied voltage. The identity of the ceramic material is not stated in the data brochure, but it is believed to be a stack of barium titanate ($Ba\ Ti\ O_3$) elements or probably a more advanced material such as lead zirconate-titanate (known as PZT). The unit was specifically made for continuous wave laser

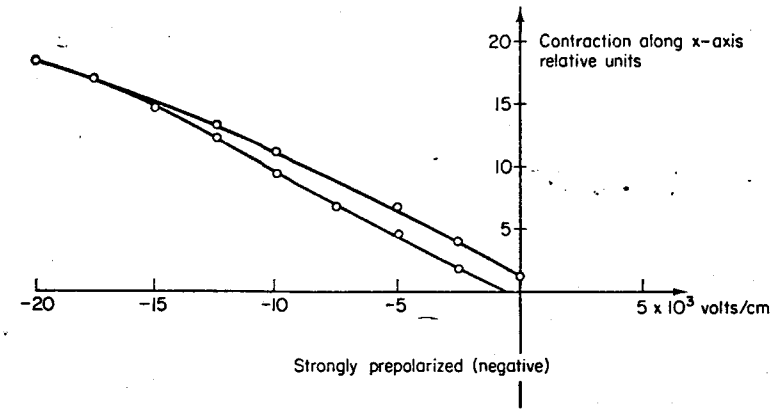

FIG. 5.17. Measured piezoelectric response of $BaTiO_3$ single-domain crystal.[81] Contraction along a axis is shown, rather than the accompanying expansion along the c axis. Note linear rather than quadratic nature.

Figure. 12 (after Jaffe(1971))

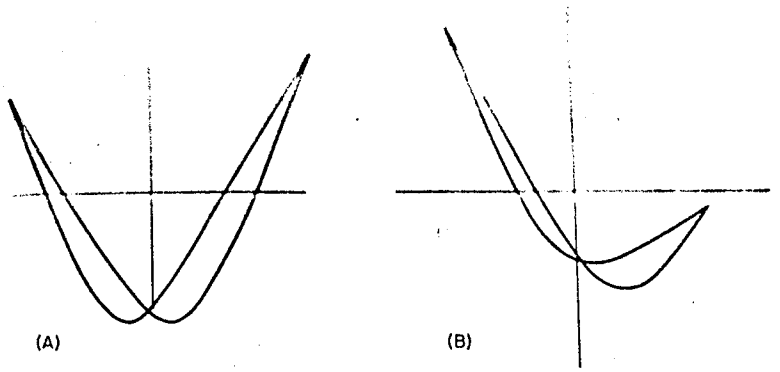

FIG. 5.15. Strain (ordinate) versus electric field (abscissa) loops for unpoled (A) and poled (B) barium titanate ceramic.[78] Peak field 10 kV/cm, total strain amplitude 4×10^{-5}.

Figure. 13 (after Jaffe(1971))

amplitude or frequency stabilization in interferometry.

Preliminary research was undertaken to discover the behaviour of piezoelectric ceramics. The general concept of piezoelectricity usually refers to a mechanical deformation when an appropriate crystal is subjected to an electric field. The displacement is proportional to the amplitude and sign of the applied field. Reading brought attention to two kinds of electromechanical effects

- (a) Piezoelectricity:- a phenomenon in which the displacement is a linear function of the applied electric field.
- (b) Electrorestriction:- in which the sign of deformation is independent of the polarity of the field and is proportional to even powers of the field.

Several other parameters and characteristics such as aging, creep, poling and hysteresis came to the author's attention as the ceramics properties were being investigated. Jaffe (1971) gives the following quantitative plots for barium titanate. A linear relation over a short range is shown but a hysteresis effect prevents the return trajectory following the forward path (see figures 12, 13).

Investigations by Ramsay (1962) in the use of barium titanate for fine movement control produced the following figures 14 and 15. The hysteresis, departure from non-linearity and quadratic behaviour upon field reversal are well demonstrated in these figures. Ramsay also points to a residual contraction which is gradually reducing with time.

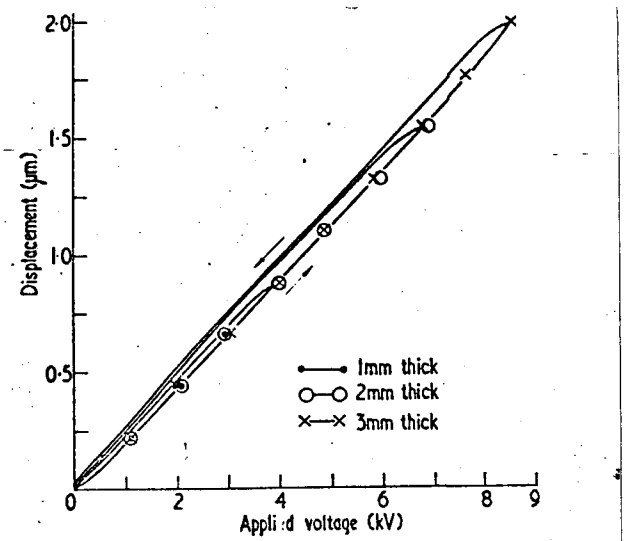

Figure 3. Movement as a function of applied voltage for ceramics 1, 2 and 3 mm thick, pre-polarized at 20 kv cm^{-1} for 1 hour at 140° c.

Figure. 14 (after Ramsay(1962))

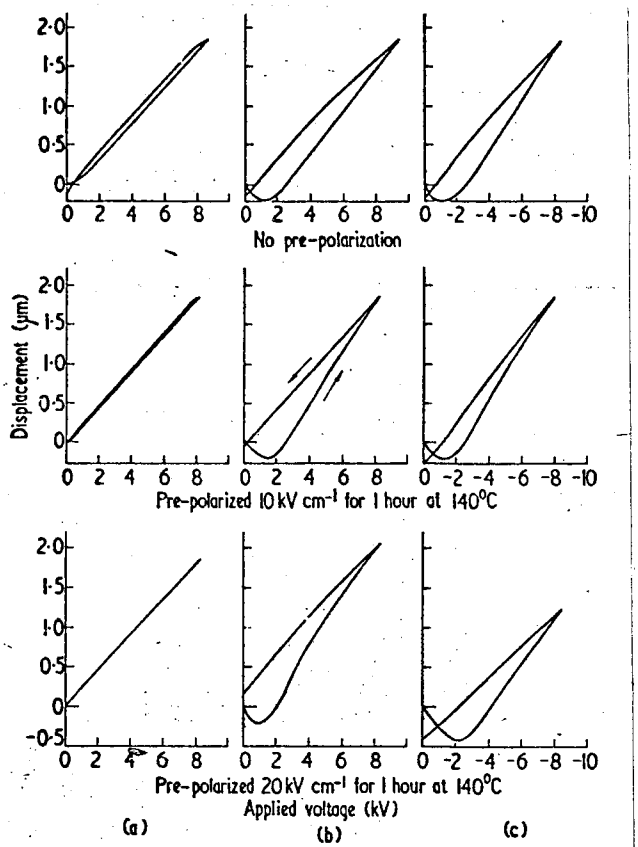

Figure 2. The effect of pre-polarization and the direction of the applied field on the movement of barium titanate transducers. (*a*) Movement as a function of applied voltage, the direction of the field (denoted by a positive sign) being the same as that of the pre-polarizing field. (*b*) Movement for the same field direction as (*a*) after prior application of a negative field. After cycling with a positive field, (*a*) is again obtained. (*c*) Movement as a function of applied voltage with a negative field.

Figure. 15 (after Ramsay(1962))

The time constant calculated from the capacitance and leakage resistance does not explain this slow creep. The notion that the element is supposed to behave similarly in either direction has, therefore, to be discarded. Unfortunately, this halves the displacement range to 23 micrometres only. Furthermore, non-linearities and hysteresis would play havoc with the original assumption that the ceramic displacement was linear. It becomes apparant that some means of linearizing the displacement with the input voltage must be sought.

Measurements

The following experiment was carried out to find the actual response of the "Spectra Physics" ceramic element. A variable DC supply was connected to a high voltage amplifier whose output was directly fed into the translator. A digital voltmeter was connected across the amplifier output to monitor and measure the voltage applied to the ceramic element. The translator itself was rigidly mounted on a granite surface plate which also supported a TESA electronic displacement indicator. The calibration, stability and linearity of the TESA were previously ascertained using a calibrated wedge. The wedge consists of two glass prisms whose hypotenuse surfaces were in contact with one another. Attached to the upper prism is a micrometer and vertical displacement of this prism is brought about when it is forced by the micrometer to move up the common contacting plane. The TESA displacement transducer was brought into contact with the top surface of the wedge and its linearity and accuracy determined. To verify that no errors arose due to the position of the pick-

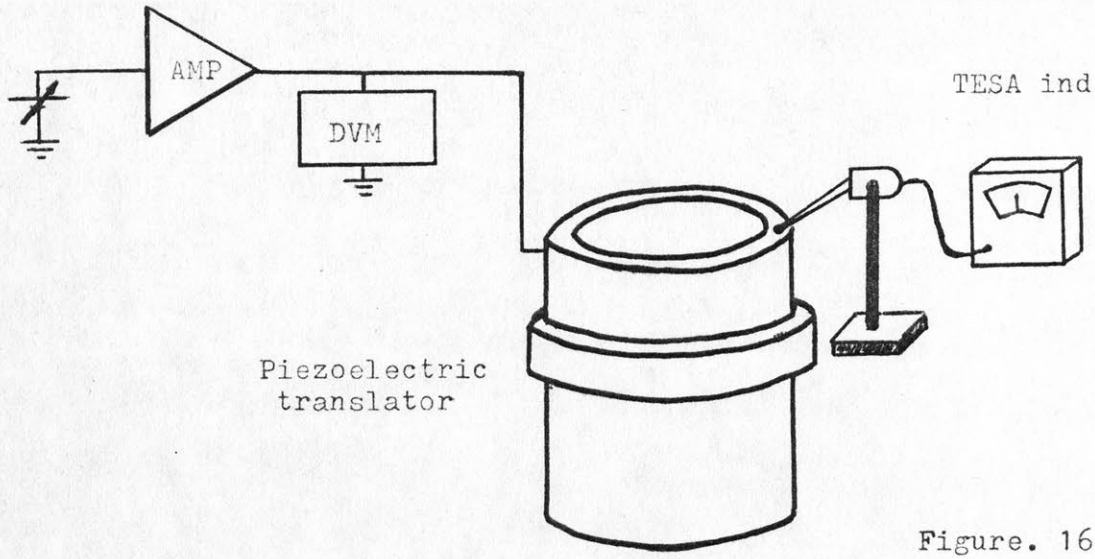

Figure. 16

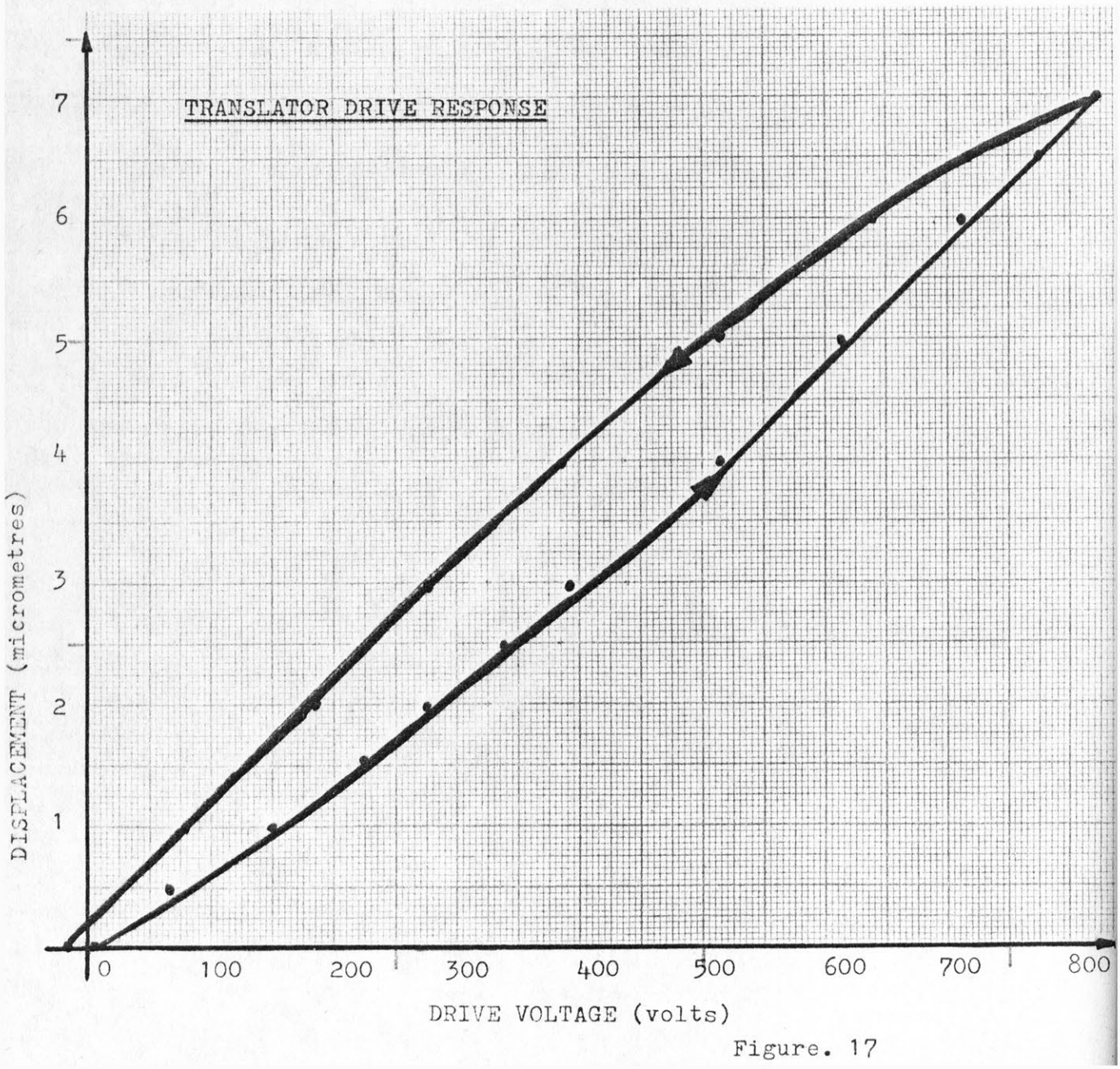

Figure. 17

up on the upper surface of the translator, the displacements were measured at various points along the rim. No deviations were detected between the readings taken at any of the selected points thus verifying within the accuracy of the transducer the specification of no angular deviation. The HT amplifier peak output was approximately +800 V and the full range of 2000 V of the ceramic element could not be examined. The measured displacement versus input voltage is shown in figure 18. Notice the different trajectory due to hysteresis. Also note the residual contraction of 0.25 μm when the drive voltage was returned to zero. From this graph, the displacement factor varies from 0.88 μm per 100 V to 1 μm/100 V depending on which trajectory line it is calculated. Figure 18 clearly depicts the hysteresis exhibited by the device. The hysteresis loop width depending on the peak amplitude from which the voltage is decreased. It is already apparent that it will be quite hard to linearize this kind of response. According to Ramsay (1962), the hysteresis loop width is reduced by prepolarization of the ceramic. Because of the wide loop obtained with our ceramic element, the author is led to believe that it may not have been prepolarized, or, if it was, aging may have affected the element and repolarization at the Curie point may become necessary. The latter was not carried out however. The data given for the ceramic properties does not give a true and complete picture of the product. The various instruments and publications reviewed revealed that most piezoelectric translators are normally used as nulling devices. In such cases, some other parameter such as light intensity or radiant power output is sensed and the piezoelectric element is driven to

Calibration of TESA electronic indicator model GN
Plant No S-59077

Range ± 3 μm

Method: Steps of 1 to 6 μm are introduced under the indicator sensor using a series of gauge blocks. The actual reading given by the index is then recorded and compared with the nominal displacement.

Gauge Block mm	Nominal Gauge Block difference μm	Scale marking μm	Reading μm	Error in reading μm
2.002	0	-3	-3.15	-0.15
2.003	1	-2	-2.05	-0.05
2.004	2	-1	-1.05	-0.05
2.005	3	0	0	0
2.006	4	+1	+1.05	+0.05
2.007	5	+2	+1.95	-0.05
2.008	6	+3	+2.90	-0.1

The uncertainty to be associated with each error is ± 0.1 μm.

14 July 1976

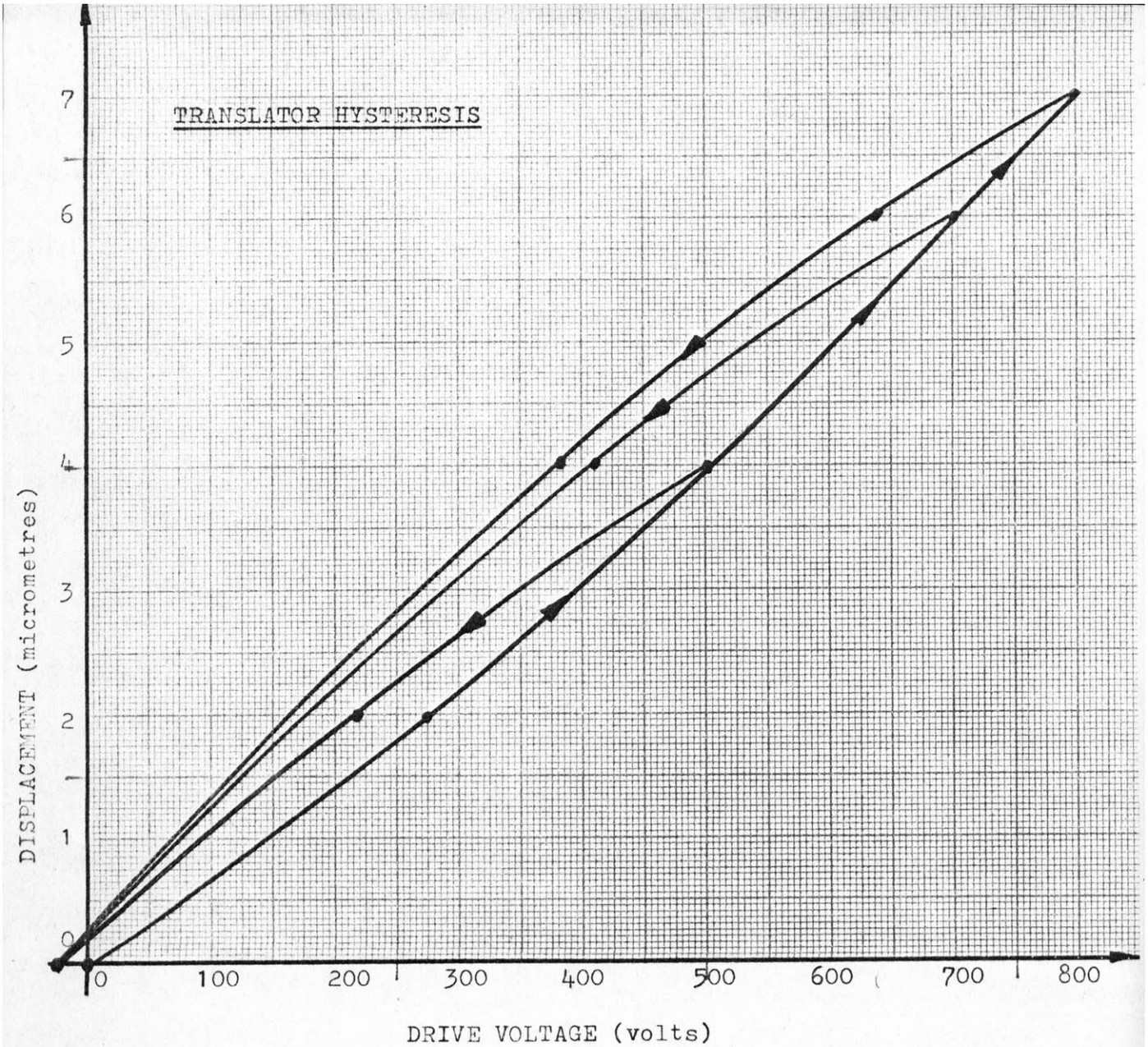

Figure. 18

Figure. 19
(after Jaffe(1971))

FIG. 5.18. Hysteresis loops for prepoled $BaTiO_3$ ceramic.[21] (AC fields of 1, 2, 5 and 7 kV/cm.)

null or maximize the sensed parameter. When used as a linear translator, capacitive sensing of displacement is almost invariably used. The displacement range usually encountered in interferometer systems using piezoelectric translators is 1.5 micrometres or less. This is much lower than the range expected to be achieved in this project. In these short ranges, the hysteresis is virtually non existent and the two curves collapse into a single line. Jaffe (1971) describes this behaviour on a graph which is duplicated here in figure 19. Jaffe also points out that owing to the maintenance of an applied alternating electric field, the ceramic tends to depole because of the combination of internal heating (due to hysteresis) and partial switching caused by the field. The conclusion which seems to stem from the study of the element's behaviour is that the element could be a $Ba\ Ti\ O_3$ rather than PZT as the latter has a superior overall performance. We are also led to conclude that the ceramic must be intended for very small excursions about a polarizing DC voltage. It is therefore doubtful if the maximum voltage and maximum drive specifications would apply for a 5 k Hz sine wave. That is, a 2 kV peak signal swing giving 23 μm displacements at the rate of 5 k Hz ! It also seems doubtful that this device can be used as intended as a linear displacement translator as a complex linearizing technique would be required.

Linearizing the translator

Since the translator exhibits a hysteresis and does not operate linearily, a linearization technique is necessary. This will entail a servo loop in which the position of the piezoelectric element is monitored and a correction applied to displace it to the required position. If the non-linear response

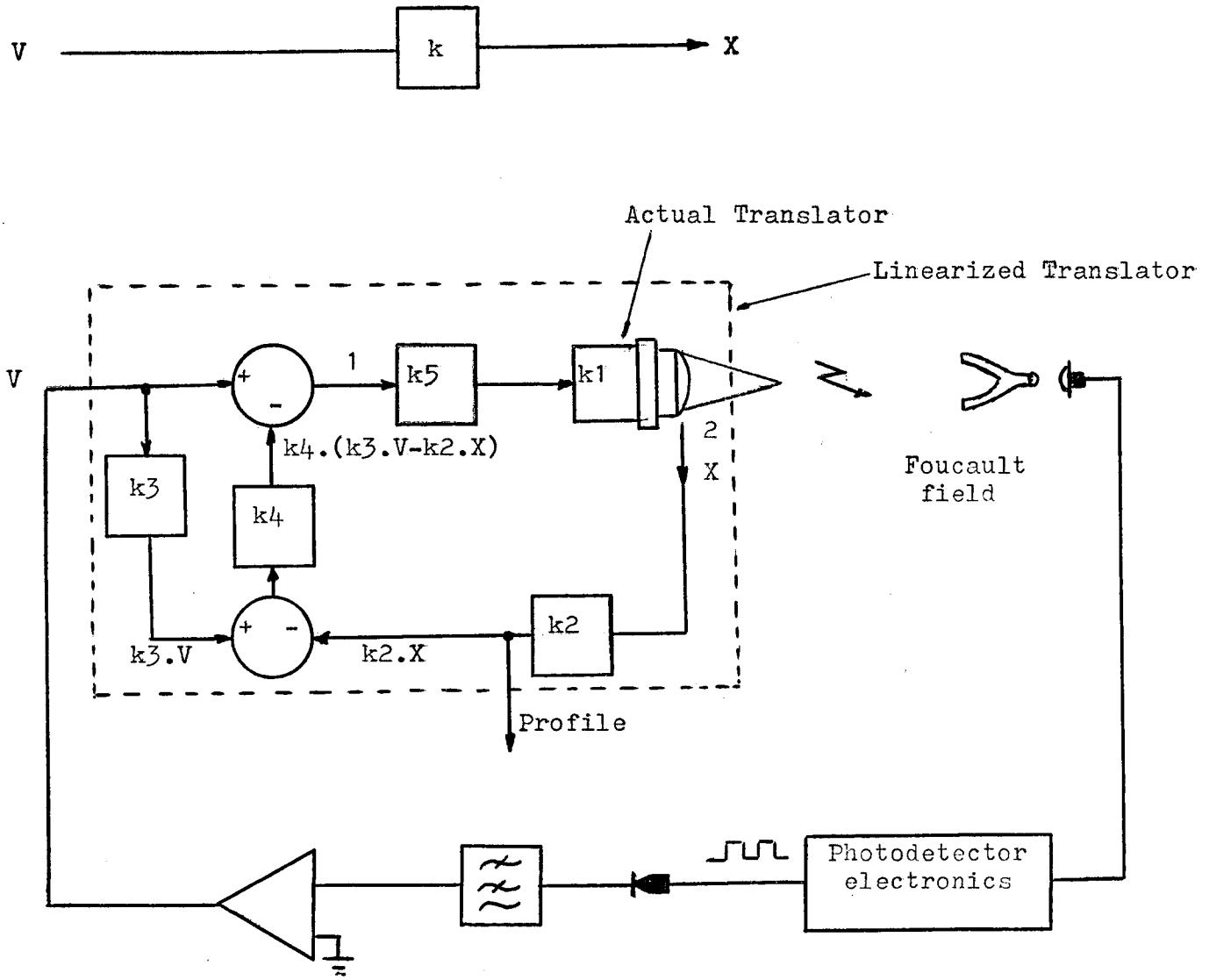
V
k
X
Actual Translator
Linearized Translator
V
+
-
1
k5
k1
2
X
k4.(k3.V-k2.X)
k3
k4
Foucault
field
+
-
k3.V
k2.X
k2
Profile
Photodetector
electronics

Figure. 20

was without hysteresis, a diode shaping network or some other non-linear gain technique could be employed to linearize the overall system. In the present case, hysteresis complicates the situation. The chief requirement from the translator is a linear displacement which is proportional to input voltage

ie $X = KV$ where X = micrometres (displacement)

V = voltage (drive)

K = constant ($\mu m/V$)

For this project, K is not a fixed value but depends on the amount of displacement experienced by the translator and the sign of the first time differential of the voltage. Therefore, the error which has to be fed back for correction has to differ depending which trajectory the voltage/displacement curve is traversing. A proposed technique for linearizing the box marked K but without providing for hysteresis is outlined in the following.

The elements shown in the dotted enclosure represent the linearized translator. The principle is as follows. A signal voltage V is amplified by k5 and drives the piezoelectric element with transfer function k1 producing a displacement X. The displacement is converted into a voltage by a linear transducer k2 which is then compared with the input voltage k3 V to produce an error. This error is added to the driving signal so that the desired position is achieved.

- Factor k1 is the transfer function of the piezoelectric element or any other electromechanical translator. Its dimensions are micrometres/volt.

- Factor k2 is the transfer function of the displacement transducer whose output is linear and proportional to the displacement generated by k1. Its dimensions are volts per micrometre.

- Factors k3, k4, k5 are dimensionless gain (or attenuation) constants. The signals at (1) and (2) are respectively

$$V - k4\ (k3\,V - k2\,X) \tag{4}$$

$$k5\ k1\ (V - k4\ (k3\ V - k2\,X)) \tag{5}$$

At (2), equation 5 must be equal to X, therefore

$$X = \frac{k1\ k5\ (1 - k3\ k4)}{(1 - k1\ k2\ k4\ k5)}\ V \tag{6}$$

The obvious case when the translator is linear, making k2, k4 and k3 zero gives $X = k1\ k5\,V$ - itself a linear expression.

Since k3, k4, k5 are fixed gain values, they are considered real with no phase shift (at least in the bandwidth of interest).

k2 is a real constant within a bandwidth which is expected to be wider than the piezoelectric element bandwidth.

No major resonances are expected from the piezoelectric element whose displacements are considered to be nil above 2 k Hz and no phase shifts are expected below this value. This point is open until the displacement transducer (k2) can give us a measure of the phase shift introduced by the piezoelectric element. If phase shifts are introduced, an appropriate lead, lag, or lead-lag network must be used for compensation. Hence apart from k1 continuously changing its real value, a stable system can be expected when the loop is closed.

If the open loop gain $k1\ k2\ k4\ k5 >> 1$ then $X \approx \frac{-V\ (1-k3\ k4)}{k2\ k4}$

we select $k3 = 1$, $k4 = 2$, then $X = \frac{V}{2\ k2}$ is independent of $k1$.

Using equation 6 and substituting typical values

$k1 = 0.8 - 1.6\ \mu m/100\,V$ as measured from hysteresis graph.

Assuming a mean value of $1.2\ \mu m/100\,V$, a deviation of up to 33% is expected because of the variation in $k1$

now, $k5 = 1000$, being a high voltage amplifier

$k2 = 1$ volt/μm.

Setting $k3 = 1$ and $k4 = 2$

then $X = \frac{-V\ k1\ k5}{1 - 2k1\ k2\ k5} = -\frac{1000\ V\ k1}{1 - 2000\ k1}$

for $k1 = 0.8 \times 10^{-2}$ $X = 0.533\,V$

1.2×10^{-2} $0.522\,V$

1.6×10^{-2} $0.516\,V$

Therefore an error of 33% due to the variation in $k1$ has been reduced to 2% which is a smaller deviation than that displayed by the original device. Referring back to figure 20, it is observed that the linearized piezoelectric element is only a component of the overall feedback scheme. Any residual displacement error due to hysteresis will be detected in the Foucault field and the amplified error fed to the translator for nulling. Because of hysteresis, the translator can assume two different positions for the same drive voltage, this is why the surface profile is directly obtained from the output of transducer $k2$ as indicated.

If the piezoelectric element were used as the translator, a linear displacement transducer would be required.

The development of this unit is a project in itself as obtaining the high sensitivity and linearity over a wide range would require considerable effort.

THE FEEDBACK TRANSDUCER

As discussed in the previous section, a transducer whose linear range and sensitivity exceeds the translator's performance is required. One other important parameter, the bandwidth, must also be considered at this stage. The speed of response must exceed the response of the piezoelectric translator. There are several transducers which were considered as possibilities for use in the system and some of the implementations in their use are described in the following:

(a) Lion's (1964) method; using a differential capacitor whose discharge rate is a measure of displacement versus capacitance. This method is presently used in a surface simulator (Bendeli &al 1974). It is capable of high resolution over a wide bandwidth extending to DC. The linearity however is limited to 0.2 of the gap spacing. A compromise must be reached between sensitivity and range as an increase in either parameter will decrease the other. Manufacturing this transducer requires a large degree of precision and skill in setting and maintaining the gap between the capacitor plates.

(b) Use of a capacitor to determine the oscillation frequency of an eg 10 M Hz crystal oscillator. Any slight variation in capacitance due to displacement will frequency modulate the crystal's fundamental frequency. After modulation, beating the output with a standard oscillator or using a discriminator can achieve an electrical output proportional to displacement. Such a system should be inherently linear as the frequency of oscillation is

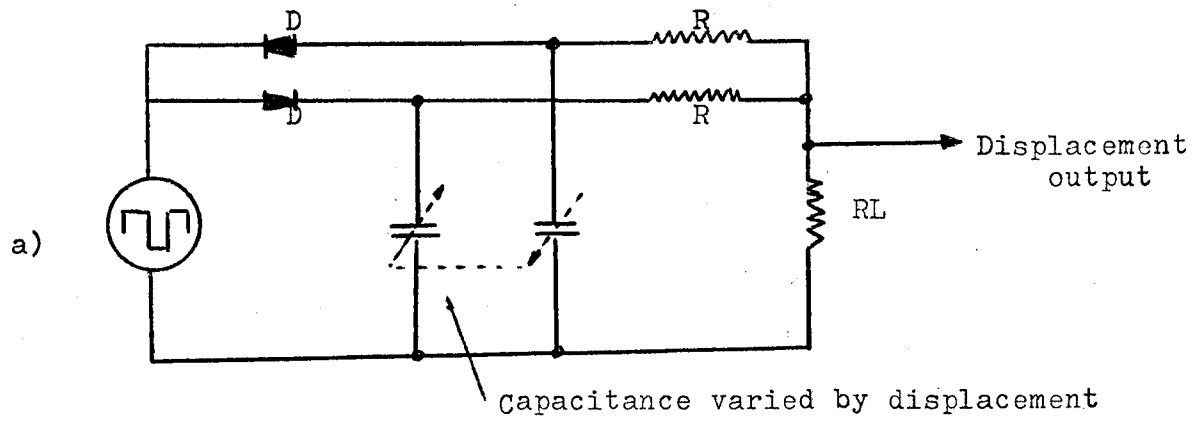

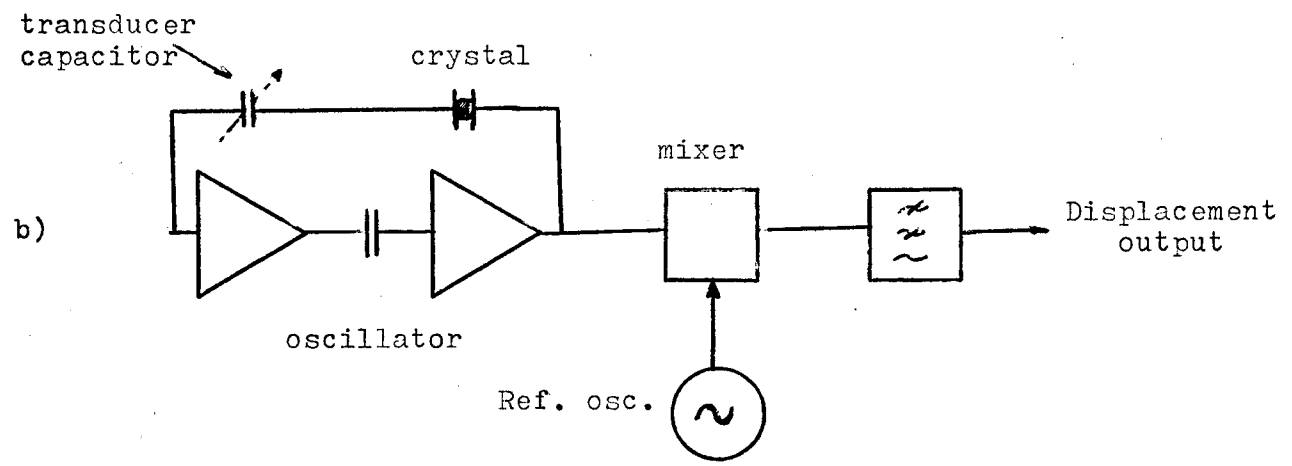

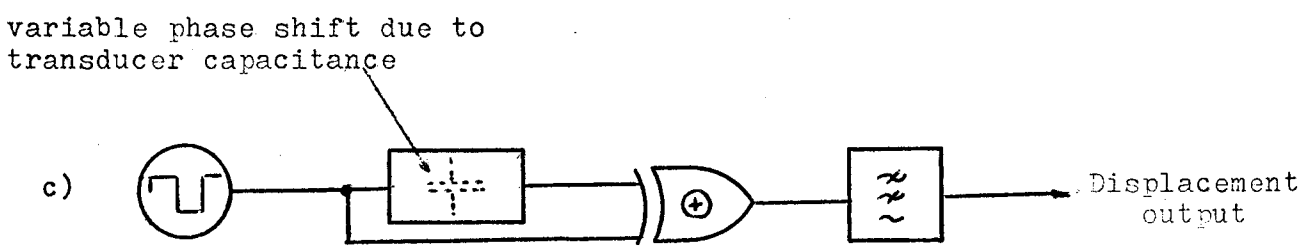

Figure. 21

Various capacitive transducer techniques

inversely proportional to the capacitance which in turn is inversely proportional to the gap spacing. However, any changes in pressure, humidity or temperature will affect the absolute value of the capacitor and therefore the output. A reference capacitor situated in the proximity of the sampling capacitor but not subjected to modulation can be used to compensate for environmental changes.

(c) Use of a capacitor in a phase shift network which is fed from a stable high frequency signal. Changes in capacitance due to linear displacement will produce a phase shift which can be detected by a phase comparator (eg a digital EX-OR gate). Sensitivities may be a problem as capacitance changes are usually small. Some sort of differential arrangement whose output is proportional to the difference between two capacitors rather than the absolute value of a single capacitor would be necessary to eliminate thermal transients.

In these methods, the capacitance is inversely proportional to displacement. It is conceivable that a different capacitor could be used where there is a change in area resulting in an inherently linear operation. Coaxial elements have been used but setting up and maintaining a precise and constant gap is a skilful and difficult assembly process. This displacement also has to be truly translational and not compounded with other wobbles and rotations.

(d) Since in the last few years the possibilities of interferometric measurement of length have been much advanced, it was felt that research in this direction might be more rewarding than redesign of standard equipment. Most interferometers basically operate with the detection of half wavelength displacements or separations (eg Michelson interferometer). Some methods have been described in the literature about the improvement of interferometric techniques by multiple reflections such that displacements much smaller than $\lambda/2$ can be detected (Saunders, 1957). Instruments have been produced where light beams are reflected several times between corner cubes or parallel mirrors to extend the resolution of a fringe count (Sakurai, 1974). Multiple reflections in an optical wedge have been used for examination of surfaces to provide a contour map of such but to the best of the author's knowledge no such technique has been used for fringe counting. Partly for this reason, partly because the resolution of the multiple reflections method over a given range is comparable with that achieved with a capacitor transducer it was decided to follow this line of development. Furthermore, this system's accuracy can also be directly traced to a wavelength standard. No other intermediary standards are necessary as would be required by methods a, b, c described previously.

The optical wedge displacement transducer

The "optical wedge" consists of two highly reflective surfaces whose planes form an angle denoted w "the wedge angle". A parallel beam of light enters the system and strikes the top surface at an incidence angle "I1". After reflection, the beam is directed to the bottom surface and the incidence angle in this case can be easily shown to be (I1-w). The beam travels between the two surfaces with a decreasing incidence angle after each reflection. Each decrement is equal to the wedge angle. Therefore, after the second reflection, the reflection angle is (I1-w), after the third, it is (I1-2w). By induction, it is clear that after N reflections, the reflected angle is I-(N-1) w. If the last incidence angle is zero, that is, the beam is normal to either of the surfaces, then

$$0 = I1 - (N-1)\,w$$

ie $I1 = (N-1)\,w$, and the ray will return by the original path

Once the beam is normal to a face, it takes another (N-1) reflections for the beam to have an incidence angle of I1. Total number of reflections is therefore

$$T = N + (N-1) = 2N-1$$

$$\text{ie } N = \frac{T+1}{2}$$

Hence $I1 = \left(\frac{T-1}{2}\right) w$ if the beam is to exit at the same angle at which it entered the system. Furthermore, the exit beam will retrace exactly the path of the original entry beam. Note that it is necessary that $I1 > w$ for the beam to correctly propagate along the wedge. The limiting condition of w = o (ie parallel surfaces) is of no practical consequence in this context as the beam never returns. The advantage of this system over a parallel plate system is the fact that the beam exits at the same spot

as it enters the wedge. The main property is therefore apparent; if I and w have the correct relationships, the input and output beam position will be independent of the separation between the surfaces. The wedge system behaves more like a corner cube. If the return beam is made to interfere with a reference beam, a set of fringes will result. It is not hard to visualize that if the number of reflections is large, a minute change in vertical position of the two reflections will generate much bigger changes in optical path. We therefore have a means of generating a sequence of fringes which can be totalized and used to give a direct reading of displacement to a high resolution without subdivision.

Wedge calculation

Given an initial separation of the two surfaces, the optical path between the two surfaces is dependent on the wedge angle and incidence angle. If the top (or bottom) surface is displaced from its initial position, what is the corresponding change in optical path length and fringe count knowing the wavelength of the incident beam? It is to be noticed that as the surfaces separate, the last reflection occurs further away along the wedge. Hence, it is important to determine the length of the surface required to allow a given number of reflections. Consider the wedge system described in figure 22

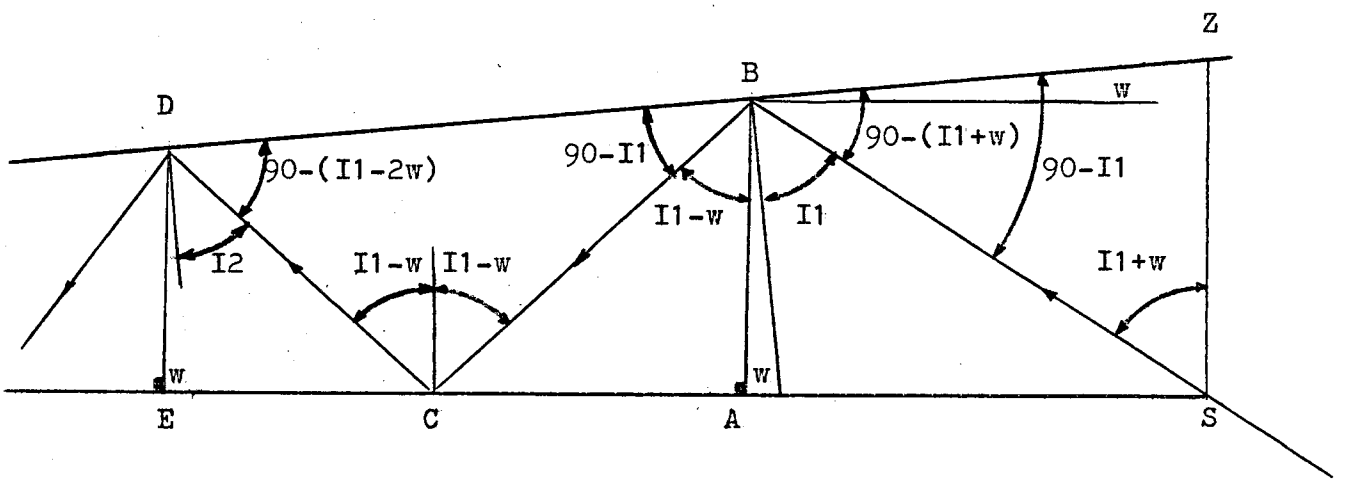

Figure. 22 The optical wedge

Initial separation at the mouth is SZ, wedge angle w, incidence angle I1

in triangle SAB, $AB = SB \cdot \cos(I1 + w)$

in triangle SBZ, $\frac{SB}{\sin(SZB)} = \frac{SZ}{\sin(SBZ)}$

$$SB = SZ \cdot \frac{\sin(SZB)}{\sin(SBZ)}$$

but angle $SZB = \frac{\pi}{2} - w$ and $SBZ = \frac{\pi}{2} - I1$

hence $$SB = SZ \frac{\cos(w)}{\cos(I1)}$$

Therefore $$AB = SZ \cdot \frac{\cos(w)\ \cos(I1 + w)}{\cos(I1)} \qquad (7)$$

Length $AS = AB \cdot \tan(I1 + w)$

Calling the new incidence angle $B = (I1 - w)$

then $AC = AB \cdot \tan(I1 - w)$

Therefore $CS = AS + AC = AB\ (\tan(I1 + w) + \tan(I1 - w))$ (8)

New height DE is calculated from the following:

in triangle DEC $DE = DC \cos(I2 + w) = DC \cos(I1 - w)$

in triangle DCB $DC = BC \cdot \frac{\cos(I1)}{\cos(I1 - 2w)}$

Therefore $$DE = BC \cdot \frac{\cos(I1)\ \cos(I1 - w)}{\cos(I1 - 2w)}$$

In ABC, $AB = BC \cdot \cos(I1 - w)$

hence $$DE = AB \frac{\cos(I1)}{\cos(I1 - 2w)}$$

An algorithm can be developed with the following steps:

$$DE = \text{old height} \times \frac{\cos(I1)}{\cos(I1 - 2w)} \qquad (9)$$

New incidence angle $= I2 = (I1 - 2w)$ (10)

and the series continues.

Total surface length is

$$AB\,(\tan(I1+w)+\tan(I1-w))+DE\,(\tan(I2+w)+\tan(I2-w))+\text{etc}\ldots$$

An attempt was made to find an analytical expression for the sum of this series but a computer iteration was much more straightforward and the numerical answer was rapidly calculated.

The consecutive heights are equal to

$$AB,\ \frac{AB\cos(I1)}{\cos(I1-2w)},\ \frac{AB\cos(I1)}{\cos(I2-2w)},\ \frac{AB\cos(I1)}{\cos(I3-2w)}\ \text{etc}.....$$

A computer program was developed to go through a looping procedure and determine all the following details given the initial parameters SZ, I, w.

The initial separation was set at 3 mm minus 4 micrometres and the separation was incremented in steps of 0.2 μm. The wedge angle was 12' and the calculated incidence angle is 9° 48' to sustain 99 reflections $I = \frac{(99-1)}{2} \times 12'$. These angles were chosen for convenience and relative ease of setting. It is angle w which is the limiting factor since its setting accuracy will determine the overall accuracy. An angle of 12' is not too small to be comparable with setting errors using precision angle measuring instruments. Furthermore, w is not required to be too large as I will be excessively large especially after 99 reflections. Since the reflectance of dielectric coatings drops off for beams which are off-normal, it is necessary that I does not depart appreciably from the normal direction since each reflection reduces the intensity of the reflected beam.

WEDGE DE.M.SE	INCIDENCE DE.M.SE	EXIT DE.M.SE	REFLEC-TIONS	SEPARATION MM.	SMALL HEIGHT MM.	SAMPLE MM.	DEVIATION MM.	PATH LENGTH MM.	FRINGE COUNT
.1200	9.4800	9.4760	99	2.996000	2.950484	13.039312	-.202860E-11	298.083793	0.
.1200	9.4800	9.4760	99	2.996200	2.950681	13.040183	-.229861E-11	298.103692	31.
.1200	9.4800	9.4760	99	2.996400	2.950878	13.041053	-.228439E-11	298.123591	63.
.1200	9.4800	9.4760	99	2.996600	2.951075	13.041924	-.210321E-11	298.143489	94.
.1200	9.4800	9.4760	99	2.996800	2.951272	13.042794	-.206768E-11	298.163388	126.
.1200	9.4800	9.4760	99	2.997000	2.951469	13.043665	-.205347E-11	298.183287	157.
.1200	9.4800	9.4760	99	2.997200	2.951666	13.044535	-.206057E-11	298.203186	189.
.1200	9.4800	9.4760	99	2.997400	2.951863	13.045406	-.199663E-11	298.223084	220.
.1200	9.4800	9.4760	99	2.997600	2.952060	13.046276	-.181899E-11	298.242983	252.
.1200	9.4800	9.4760	99	2.997800	2.952257	13.047147	-.229505E-11	298.262882	283.
.1200	9.4800	9.4760	99	2.998000	2.952454	13.048017	-.223110E-11	298.282781	314.
.1200	9.4800	9.4760	99	2.998200	2.952651	13.048887	-.214229E-11	298.302680	346.
.1200	9.4800	9.4760	99	2.998400	2.952848	13.049758	-.211386E-11	298.322578	377.
.1200	9.4800	9.4760	99	2.998600	2.953045	13.050628	-.206057E-11	298.342477	409.
.1200	9.4800	9.4760	99	2.998800	2.953241	13.051499	-.253308E-11	298.362376	440.
.1200	9.4800	9.4760	99	2.999000	2.953438	13.052369	-.244782E-11	298.382275	472.
.1200	9.4800	9.4760	99	2.999200	2.953635	13.053240	-.211742E-11	298.402174	503.
.1200	9.4800	9.4760	99	2.999400	2.953832	13.054110	-.190781E-11	298.422072	535.
.1200	9.4800	9.4760	99	2.999600	2.954029	13.054981	-.222045E-11	298.441971	566.
.1200	9.4800	9.4760	99	2.999800	2.954226	13.055851	-.220624E-11	298.461870	597.
.1200	9.4800	9.4760	99	3.000000	2.954423	13.056721	-.190781E-11	298.481769	629.
.1200	9.4800	9.4760	99	3.000200	2.954620	13.057592	-.214939E-11	298.501667	660.
.1200	9.4800	9.4760	99	3.000400	2.954817	13.058462	-.189004E-11	298.521566	692.
.1200	9.4800	9.4760	99	3.000600	2.955014	13.059333	-.211742E-11	298.541465	723.
.1200	9.4800	9.4760	99	3.000800	2.955211	13.060203	-.212808E-11	298.561364	755.
.1200	9.4800	9.4760	99	3.001000	2.955408	13.061074	-.230571E-11	298.581263	786.
.1200	9.4800	9.4760	99	3.001200	2.955605	13.061944	-.205702E-11	298.601161	818.
.1200	9.4800	9.4760	99	3.001400	2.955802	13.062815	-.208189E-11	298.621060	849.
.1200	9.4800	9.4760	99	3.001600	2.955999	13.063685	-.225242E-11	298.640959	880.
.1200	9.4800	9.4760	99	3.001800	2.956196	13.064555	-.206057E-11	298.660858	912.
.1200	9.4800	9.4760	99	3.002000	2.956393	13.065426	-.223821E-11	298.680757	943.
.1200	9.4800	9.4760	99	3.002200	2.956590	13.066296	-.235190E-11	298.700655	975.
.1200	9.4800	9.4760	99	3.002400	2.956787	13.067167	-.216360E-11	298.720554	1006.
.1200	9.4800	9.4760	99	3.002600	2.956984	13.068037	-.209965E-11	298.740453	1038.
.1200	9.4800	9.4760	99	3.002800	2.957181	13.068908	-.203215E-11	298.760352	1069.
.1200	9.4800	9.4760	99	3.003000	2.957378	13.069778	-.182609E-11	298.780250	1101.
.1200	9.4800	9.4760	99	3.003200	2.957575	13.070649	-.243361E-11	298.800149	1132.
.1200	9.4800	9.4760	99	3.003400	2.957772	13.071519	-.218847E-11	298.820048	1163.
.1200	9.4800	9.4760	99	3.003600	2.957969	13.072390	-.230216E-11	298.839947	1195.
.1200	9.4800	9.4760	99	3.003800	2.958166	13.073260	-.205347E-11	298.859846	1226.
.1200	9.4800	9.4760	99	3.004000	2.958362	13.074130	-.206057E-11	298.879744	1258.

TABLE. 1

Assuming a 95% reflection coefficient, after 100 reflections, the attenuation is $(0.95)^{100} = 5.92 \times 10^{-3}$.

Looking at the computer output in Table 1, the return beam exits the system at an angle labelled "EXIT". The return beam position relative to the position of the original incident beam is labelled "DEVIATION". The minimum length of the reflective surface required to sustain 99 reflections is termed "SAMPLE LENGTH". Total optical length is "PATH LENGTH". Incrementing the separation by 0.2 μm, a new path length is calculated and a fringe count is derived from the knowledge of the laser wavelength of 0.6328 μm. The expression (new path length - previous path length)/wavelength is used to derive the fringe count. Because of the attenuation after 99 reflections, it is necessary to use a laser rather than a high intensity mercury lamp. Furthermore, for a 3 mm separation, a coherence length of 290 mm is necessary and this is reaching the limit of the mercury lamp performance.

Examining the results when w is an exact submultiple of I, it is evident that the exit angle is exactly equal to the incident angle after 99 reflections and the deviation is 10^{-12} mm for a separation of 3 mm. The minimum length of reflective surface is 13.069 mm. The fringe count exhibits a linear relation with displacement.

Sensitivity to alignment errors

By varying the incidence and wedge angles, the sensitivity of the system to misalignment of the wedge components, and to the possibility of non-purely translational motion were investigated. With constant

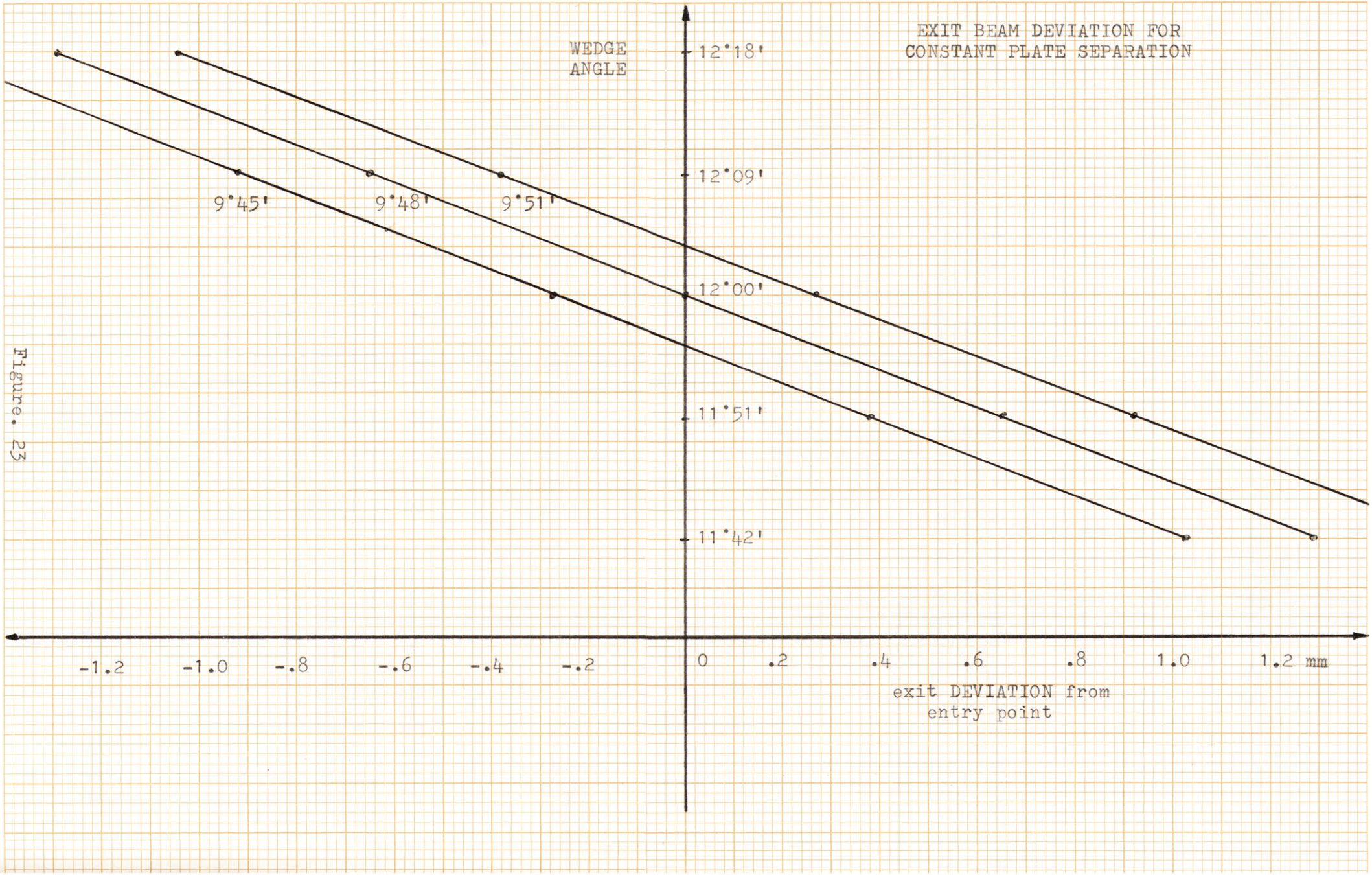
EXIT BEAM DEVIATION FOR
CONSTANT PLATE SEPARATION
WEDGE
ANGLE
12°18'
12°09'
12°00'
11°51'
11°42'
9°45'
9°48'
9°51'
-1.2
-1.0
-.8
-.6
-.4
-.2
0
.2
.4
.6
.8
1.0
1.2 mm
exit DEVIATION from
entry point

Figure. 23

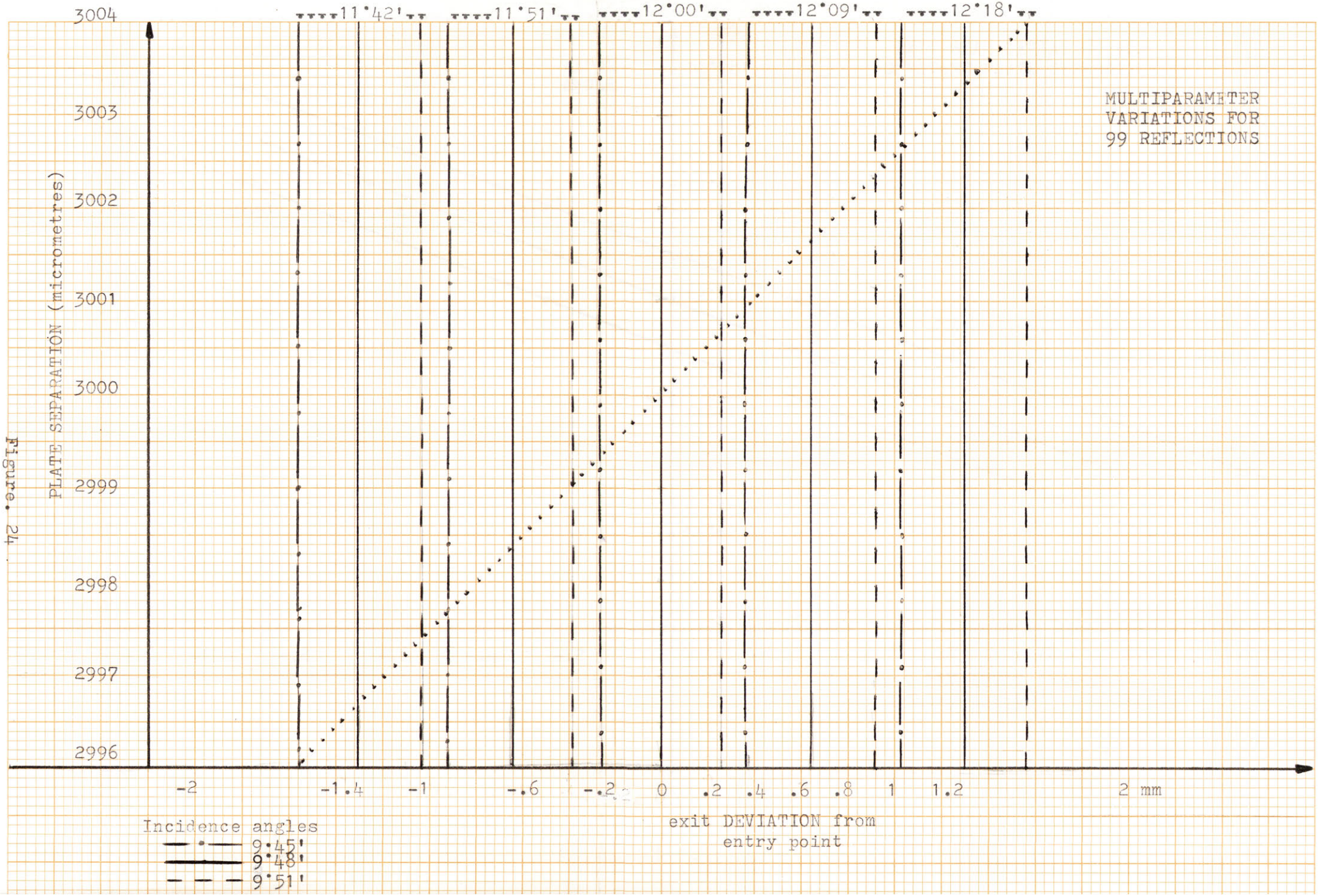
WEDGE ANGLE
11°42'
11°51'
12°00'
12°09'
12°18'
MULTIPARAMETER
VARIATIONS FOR
99 REFLECTIONS
PLATE SEPARATION (micrometres)
3004
3003
3002
3001
3000
2999
2998
2997
2996
-2
-1.4
-1
-.6
-.2
0
.2
.4
.6
.8
1
1.2
2 mm
exit DEVIATION from
entry point
Incidence angles
9°45'
9°48'
9°51'

Figure 24.

reflector separation, the incident beam varied from the nominal angle of 9° 48' by ± 3'. The deviation of the exit point from the entry point is shown in figure 23. For a constant wedge angle, as I varies by ± 3', the exit point deviates by ± 0.26 mm from the entry point. Varying the wedge angle also will give the family of lines shown in figure 23. If a photodetector has a sensitive area of less than 1 mm square, the exit beam would miss the detector if the angles are incorrectly set. As shown in figure 23, if the wedge and incidence angle are away from the nominal value, the exit point will be up to 1.5 mm from the entry point. However, looking at figure 24, if both wedge and incidence angles are away from the nominal value and although the exit beam can be up to 1.5 mm away from the entry point, its position remains fairly stable as shown by the family of vertical lines. Therefore, it is just a simple matter to move the photodetector initially by the appropriate amount so that the fringe field will always fall on the detector's sensitive area. Assume under worse case conditions that the entry beam position is fixed in space and the plate separation is compounded with a wedge angle shift from 11'42" to 12'18" as the reflector moves through a range of 8 micrometres. The incidence angle must necessarily change as w alters. The exit beam deviation will continuously increase by as much as 3 mm from its initial position as shown by the dotted line in figure 24. Since the specifications of the piezoelectric element gives a zero angular deviation, this problem will not occur. The transducer system appears to be quite tolerant on initial alignment errors as long as these errors remain fixed. The family of vertical lines in figure 24 have a very slight slope on them (slope shown

WEDGE DE.M.SE	INCIDENCE DE.M.SE	EXIT DE.M.SE	REFLEC- TIONS	SEPARATION MM.	SMALL HEIGHT MM.	SAMPLE MM.	DEVIATION MM.	PATH LENGTH MM.	FRINGE COUNT
.1142	9.4500	9.2136	99	2.996000	2.950965	13.232341	.102901E+01	297.982450	0.
.1142	9.4500	9.2136	99	2.996200	2.951162	13.233224	.102908E+01	298.002342	31.
.1142	9.4500	9.2136	99	2.996400	2.951359	13.234108	.102915E+01	298.022234	63.
.1142	9.4500	9.2136	99	2.996600	2.951556	13.234991	.102922E+01	298.042126	94.
.1142	9.4500	9.2136	99	2.996800	2.951753	13.235874	.102929E+01	298.062018	126.
.1142	9.4500	9.2136	99	2.997000	2.951950	13.236758	.102936E+01	298.081910	157.
.1142	9.4500	9.2136	99	2.997200	2.952147	13.237641	.102942E+01	298.101802	189.
.1142	9.4500	9.2136	99	2.997400	2.952344	13.238524	.102949E+01	298.121694	220.
.1142	9.4500	9.2136	99	2.997600	2.952541	13.239408	.102956E+01	298.141586	251.
.1142	9.4500	9.2136	99	2.997800	2.952738	13.240291	.102963E+01	298.161478	283.
.1142	9.4500	9.2136	99	2.998000	2.952935	13.241174	.102970E+01	298.181370	314.
.1142	9.4500	9.2136	99	2.998200	2.953132	13.242058	.102977E+01	298.201262	346.
.1142	9.4500	9.2136	99	2.998400	2.953329	13.242941	.102984E+01	298.221154	377.
.1142	9.4500	9.2136	99	2.998600	2.953526	13.243824	.102991E+01	298.241046	409.
.1142	9.4500	9.2136	99	2.998800	2.953723	13.244708	.102997E+01	298.260938	440.
.1142	9.4500	9.2136	99	2.999000	2.953920	13.245591	.103004E+01	298.280830	472.
.1142	9.4500	9.2136	99	2.999200	2.954117	13.246474	.103011E+01	298.300722	503.
.1142	9.4500	9.2136	99	2.999400	2.954314	13.247358	.103018E+01	298.320614	534.
.1142	9.4500	9.2136	99	2.999600	2.954511	13.248241	.103025E+01	298.340506	566.
.1142	9.4500	9.2136	99	2.999800	2.954708	13.249124	.103032E+01	298.360398	597.
.1142	9.4500	9.2136	99	3.000000	2.954905	13.250008	.103039E+01	298.380290	629.
.1142	9.4500	9.2136	99	3.000200	2.955102	13.250891	.103045E+01	298.400182	660.
.1142	9.4500	9.2136	99	3.000400	2.955299	13.251774	.103052E+01	298.420074	692.
.1142	9.4500	9.2136	99	3.000600	2.955496	13.252658	.103059E+01	298.439966	723.
.1142	9.4500	9.2136	99	3.000800	2.955693	13.253541	.103066E+01	298.459858	754.
.1142	9.4500	9.2136	99	3.001000	2.955890	13.254424	.103073E+01	298.479750	786.
.1142	9.4500	9.2136	99	3.001200	2.956087	13.255308	.103080E+01	298.499642	817.
.1142	9.4500	9.2136	99	3.001400	2.956284	13.256191	.103087E+01	298.519534	849.
.1142	9.4500	9.2136	99	3.001600	2.956481	13.257074	.103094E+01	298.539426	880.
.1142	9.4500	9.2136	99	3.001800	2.956678	13.257958	.103100E+01	298.559318	912.
.1142	9.4500	9.2136	99	3.002000	2.956875	13.258841	.103107E+01	298.579210	943.
.1142	9.4500	9.2136	99	3.002200	2.957072	13.259724	.103114E+01	298.599102	974.
.1142	9.4500	9.2136	99	3.002400	2.957269	13.260608	.103121E+01	298.618994	1006.
.1142	9.4500	9.2136	99	3.002600	2.957466	13.261491	.103128E+01	298.638887	1037.
.1142	9.4500	9.2136	99	3.002800	2.957663	13.262374	.103135E+01	298.658779	1069.
.1142	9.4500	9.2136	99	3.003000	2.957860	13.263258	.103142E+01	298.678671	1100.
.1142	9.4500	9.2136	99	3.003200	2.958057	13.264141	.103149E+01	298.698563	1132.
.1142	9.4500	9.2136	99	3.003400	2.958254	13.265024	.103155E+01	298.718455	1163.
.1142	9.4500	9.2136	99	3.003600	2.958451	13.265908	.103162E+01	298.738347	1195.
.1142	9.4500	9.2136	99	3.003800	2.958648	13.266791	.103169E+01	298.758239	1226.
.1142	9.4500	9.2136	99	3.004000	2.958845	13.267674	.103176E+01	298.778131	1257.

TABLE. 2

EDGE E.M.SE	INCIDENCE DE.M.SE	EXIT DE.M.SE	REFLEC-TIONS	SEPARATION MM.	SMALL HEIGHT MM.	SAMPLE MM.	DEVIATION MM.	PATH LENGTH MM.	FRINGE COUNT
.1218	9.5100	10.1424	99	2.996000	2.949964	12.866501	-.103131E+01	298.196158	0.
.1218	9.5100	10.1424	99	2.996200	2.950161	12.867360	-.103138E+01	298.216064	31.
.1218	9.5100	10.1424	99	2.996400	2.950358	12.868219	-.103145E+01	298.235970	63.
.1218	9.5100	10.1424	99	2.996600	2.950555	12.869078	-.103152E+01	298.255877	94.
.1218	9.5100	10.1424	99	2.996800	2.950752	12.869937	-.103158E+01	298.275783	126.
.1218	9.5100	10.1424	99	2.997000	2.950949	12.870796	-.103165E+01	298.295689	157.
.1218	9.5100	10.1424	99	2.997200	2.951146	12.871655	-.103172E+01	298.315596	189.
.1218	9.5100	10.1424	99	2.997400	2.951343	12.872514	-.103179E+01	298.335502	220.
.1218	9.5100	10.1424	99	2.997600	2.951540	12.873373	-.103186E+01	298.355408	252.
.1218	9.5100	10.1424	99	2.997800	2.951737	12.874231	-.103193E+01	298.375314	283.
.1218	9.5100	10.1424	99	2.998000	2.951934	12.875090	-.103200E+01	298.395221	315.
.1218	9.5100	10.1424	99	2.998200	2.952131	12.875949	-.103207E+01	298.415127	346.
.1218	9.5100	10.1424	99	2.998400	2.952328	12.876808	-.103214E+01	298.435033	377.
.1218	9.5100	10.1424	99	2.998600	2.952524	12.877667	-.103220E+01	298.454940	409.
.1218	9.5100	10.1424	99	2.998800	2.952721	12.878526	-.103227E+01	298.474846	440.
.1218	9.5100	10.1424	99	2.999000	2.952918	12.879385	-.103234E+01	298.494752	472.
.1218	9.5100	10.1424	99	2.999200	2.953115	12.880244	-.103241E+01	298.514658	503.
.1218	9.5100	10.1424	99	2.999400	2.953312	12.881103	-.103248E+01	298.534565	535.
.1218	9.5100	10.1424	99	2.999600	2.953509	12.881962	-.103255E+01	298.554471	566.
.1218	9.5100	10.1424	99	2.999800	2.953706	12.882821	-.103262E+01	298.574377	598.
.1218	9.5100	10.1424	99	3.000000	2.953903	12.883680	-.103269E+01	298.594284	629.
.1218	9.5100	10.1424	99	3.000200	2.954100	12.884538	-.103276E+01	298.614190	661.
.1218	9.5100	10.1424	99	3.000400	2.954297	12.885397	-.103282E+01	298.634096	692.
.1218	9.5100	10.1424	99	3.000600	2.954494	12.886256	-.103289E+01	298.654002	724.
.1218	9.5100	10.1424	99	3.000800	2.954691	12.887115	-.103296E+01	298.673909	755.
.1218	9.5100	10.1424	99	3.001000	2.954888	12.887974	-.103303E+01	298.693815	786.
.1218	9.5100	10.1424	99	3.001200	2.955085	12.888833	-.103310E+01	298.713721	818.
.1218	9.5100	10.1424	99	3.001400	2.955281	12.889692	-.103317E+01	298.733628	849.
.1218	9.5100	10.1424	99	3.001600	2.955478	12.890551	-.103324E+01	298.753534	881.
.1218	9.5100	10.1424	99	3.001800	2.955675	12.891410	-.103331E+01	298.773440	912.
.1218	9.5100	10.1424	99	3.002000	2.955872	12.892269	-.103337E+01	298.793346	944.
.1218	9.5100	10.1424	99	3.002200	2.956069	12.893128	-.103344E+01	298.813253	975.
.1218	9.5100	10.1424	99	3.002400	2.956266	12.893986	-.103351E+01	298.833159	1007.
.1218	9.5100	10.1424	99	3.002600	2.956463	12.894845	-.103358E+01	298.853065	1038.
.1218	9.5100	10.1424	99	3.002800	2.956660	12.895704	-.103365E+01	298.872972	1070.
.1218	9.5100	10.1424	99	3.003000	2.956857	12.896563	-.103372E+01	298.892878	1101.
.1218	9.5100	10.1424	99	3.003200	2.957054	12.897422	-.103379E+01	298.912784	1132.
.1218	9.5100	10.1424	99	3.003400	2.957251	12.898281	-.103386E+01	298.932690	1164.
.1218	9.5100	10.1424	99	3.003600	2.957448	12.899140	-.103393E+01	298.952597	1195.
.1218	9.5100	10.1424	99	3.003800	2.957645	12.899999	-.103399E+01	298.972503	1227.
.1218	9.5100	10.1424	99	3.004000	2.957842	12.900858	-.103406E+01	298.992409	1258.

TABLE. 3

in figure 23) except for the nominal I and w values.

For comparison with ideal conditions, the calculations for wedge and incidence angles which are non-ideal but whose setting can be accurately measured are shown in the following computer printout in Table 2, 3. For two extreme values of wedge and incidence angle, the behaviour is calculated as the plates are separated. As the two reflectors are separated over the range 3 mm $\pm$ 4 μm, the fringe count is within one count of the ideal situation (compare with Table 1).

The exit beam is shifted by $\pm$1.5 mm from the nominated entry path. Depending on the location and the sensitive area of the photodiode, the exit beam orientation may be such that it may still fall on the receptive area even though it suffers a deviation from its original path. From Table 2, 3 it is significant that the fringe count is constant for the non-ideal cases. This is not so surprising for when the top reflector tilts and changes the wedge angle (and consequently the incident angle) some optical paths are shortened while others are lengthened. On the average, the total path length does not alter much and fringe count is fairly consistent with the ideal case.

It is worth mentioning at this stage that an improved multiple path interferometer can be implemented using two corner cubes and a fixed mirror as described by Sakurai (1974). If one corner cube were attached to the piezoelectric element, it is evident that a large mass of optical glass will be permanently attached to the translator and may affect its characteristics. This is especially important if the translator is expected to be driven at

2k Hz. The wedge system previously described requires only one plane mirror which can in practice be very thin and light.

Light intensity consideration

After such a large number of reflections, the light intensity will drop since the reflection coefficient is not 100%. With modern zinc sulphide and thorium fluoride dielectric, coated mirrors with up to 21 layers can achieve a reflection coefficient as high as 99% and over for a particular wavelength. Assuming such a "tuned" mirror at 0.6328 μm with a reflection coefficient of 95%, the attenuation suffered by the beam after 100 reflections is 0.95^{100} or 5.92×10^{-3}. For an incident beam of radiant flux of 1 mW, the flux of the exit beam will be 5.92 μW. If the beam is condensed by a lens into an area of say 1 mm^2, the irradiance becomes 0.592 mW/cm^2. The radiant power response of a set of (5082 - 4205) Hewlett Packard PIN photodiodes available at NML is 1.5 $\mu A/(mW/cm^2)$. The generated photocurrent is equal to 0.62 μA (1.5 x 0.592 x 0.7; the 0.7 factor converts the sensitivity response to the wavelength of the He Ne laser). A voltage of 62 mV will be developed across a 100 K sensing resistor.

Electrical output considerations

The detection of a single fringe is not sufficient to provide information for the direction of travel of the bottom (or top) reflector plate. A second detector is necessary. Various techniques exist to extract phase information from such a system. Namely

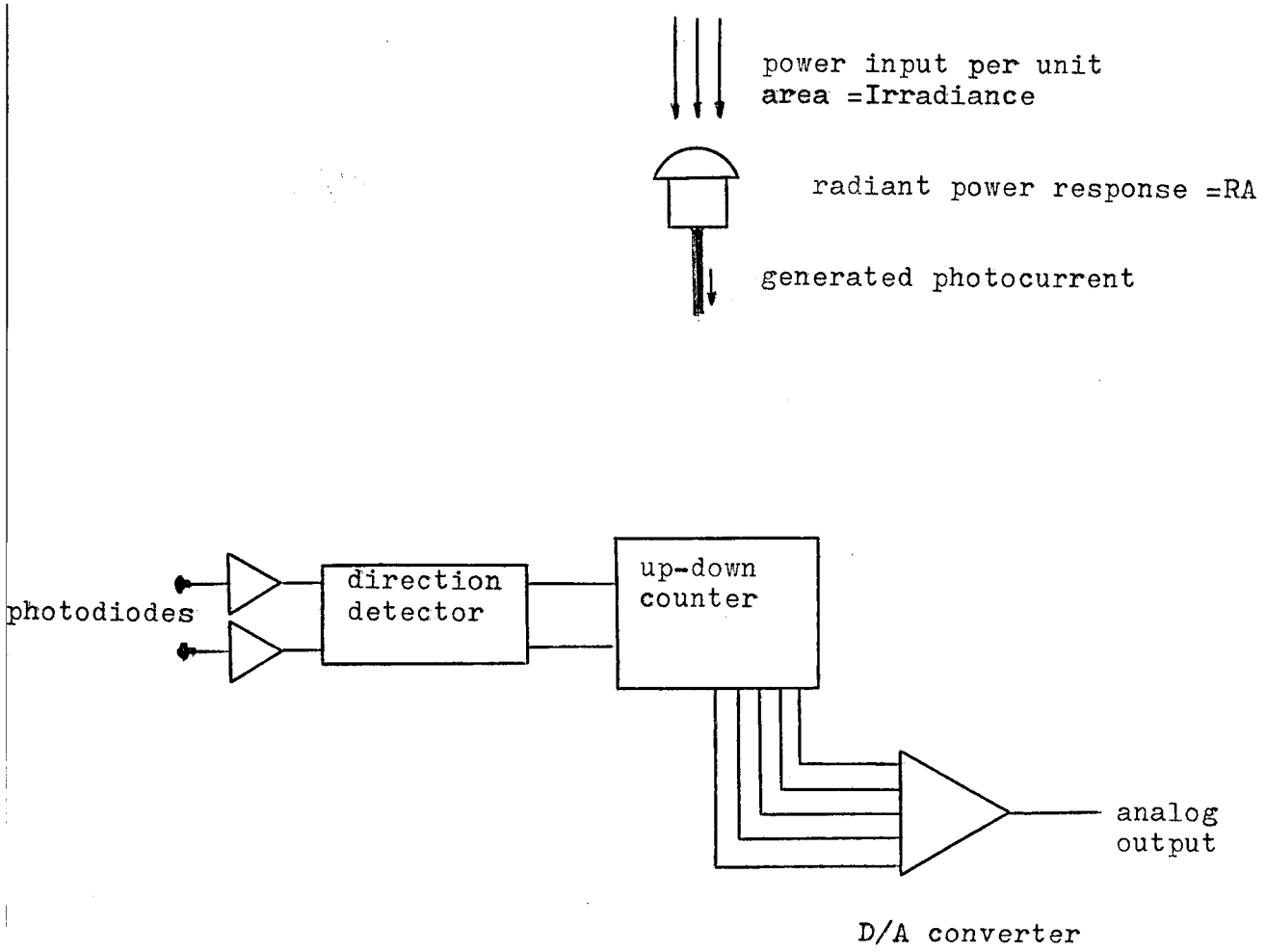
power input per unit
area =Irradiance
radiant power response =RA
generated photocurrent
photodiodes
direction
detector
up-down
counter
analog
output
D/A converter

Figure. 25

- split the entry beam into two beams with a $\lambda/4$ path difference between them and interfere the exit beams with a reference. This will produce two-fringe fields in quadrature. Detection can be sensed by determining the lead or lag of one field referenced to the other.
- Separation of the polarization components of the exit beam by using a beam splitter oriented at the polarizing angle to the beam.

Assuming that a scheme for obtaining two fringe fields at 90° and a fast photodetector mechanism has been implemented, the conversion from fringes to voltage can be achieved as shown in figure 25.

The signals received by the photodiodes are converted into pulses and a direction detector circuit determines whether an up or down count is to be registered. The binary count from the register is converted into an analog voltage by a D/A converter to drive a recorder and generate the necessary feedback signal for linearizing the piezoelectric element.

A count of 1260 is made for a range of 8 μm. For a range of 20 micrometres, a counter capability of 3150 would be necessary. A 12 bit D/A converter will permit a count of 4096 which is enough and will allow a range of 26 μm. Assume that a ramp of 2 k Hz is driving the translator through its total range of 20 μm, the translator is driven from 0 to 20 μm in 0.25 m sec and back to 0 in another 0.25 m sec. Number of counts per millisecond = 3150 x 4 = 12600 counts or 12.6×10^6 counts per second (12.6 M Hz !!). This result shows that a photodiode with a bandwidth of at least 12.6 M Hz

and a low noise amplifier to match it is necessary if the system has to keep up with all these counts for a 2 k Hz drive signal! This requirement is at present practically impossible as a great deal of noise will be present due to the wide bandwidth which necessarily must extend to DC. Furthermore, the D/A converter must settle in less than 40 nano seconds if it has to keep up with the least significant bits. A typical D/A converter classified as "fast" settles in 40 nanoseconds for 10 bits and 5 microseconds for 12 bits conversion.

Problems envisaged with this system

According to the calculations above, the bandwidth, sensitivities and capabilities required from the devices seem to exceed the present state of the art. Implementation may be difficult to achieve.

Due to the wide bandwidth of the photodiode and its amplifier, various thermal noise sources will be present. Because of the fast response required by the counter, it will be itself prone to spurious noise. Great care and precautions need to be taken to avoid noise pickup. The fringe counting technique leads itself to some troubles which can be overcome. Consider what happens if noise spikes suddenly hit the counter. The D/A converter will recognize the new count as a genuine change in the translator's position and will output a correcting voltage. The translator will therefore be shifted to a new erroneous position so that the error voltage is nulled.

Because of the settling time limitation of D/A converters, the maximum frequency driving the 12 bit converter previously noted is 200 k Hz. For the full range of 0 - 26 μm (4096 fringe count), the maximum frequency which drives the translator must not exceed $\left(\frac{4096}{2\times10^5}\right)^{-1}$ or 48 Hz. Alternatively, for a 2 k Hz driving signal, the maximum range is limited to $(2 \times 10^5 \times 0.5 \times 10^{-3})$ 100 counts or approximately 0.7 μm.

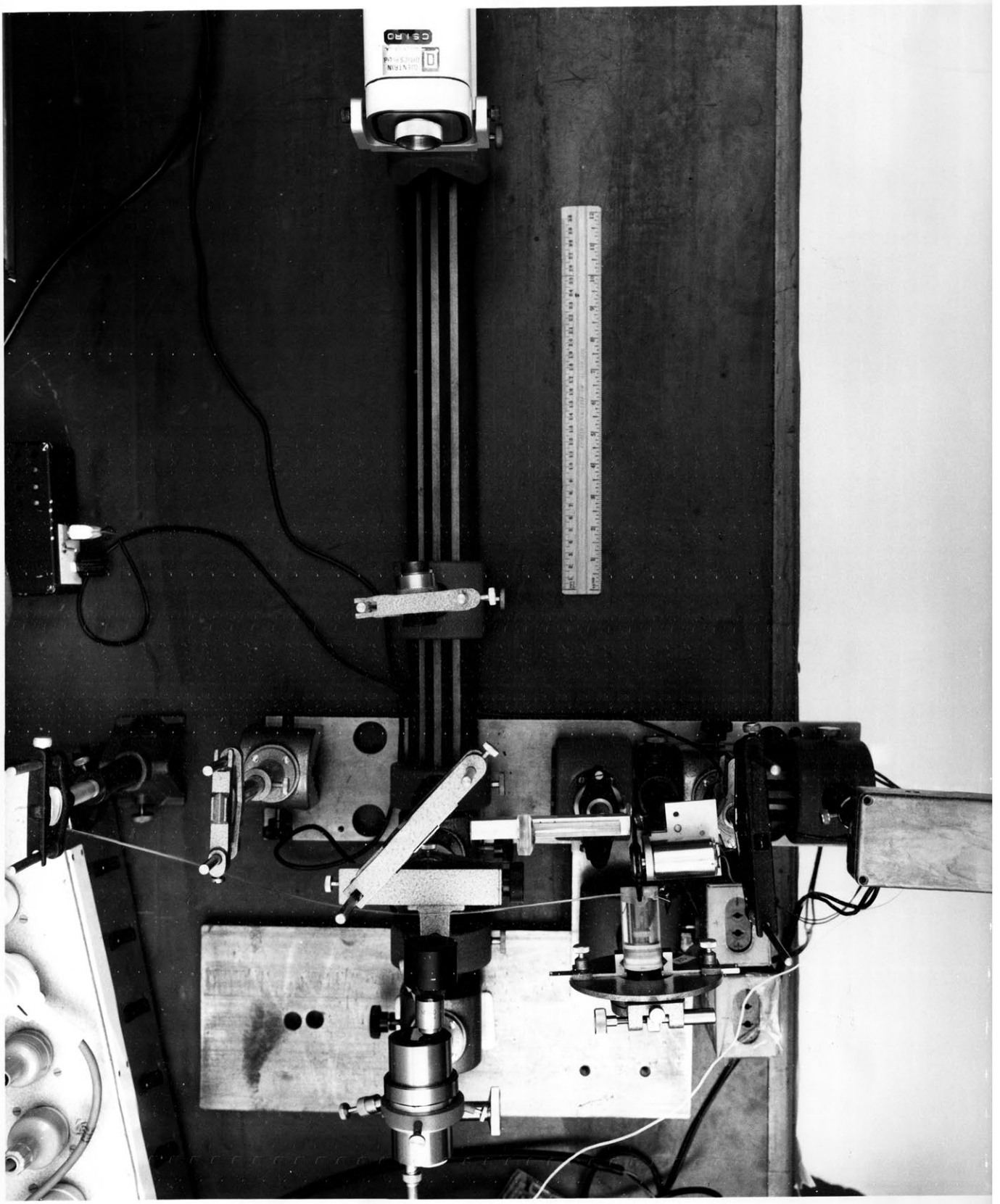

Figure. 26 Plan view of the apparatus

EXPERIMENTAL RESULTS AND APPARATUS

The best resolutions obtained during the preliminary investigation were around 1 μm whereas the theoretical figure is about 3 nm. The main limitation to reaching the required sensitivity was due to lack of an adequate detecting circuit, an inadequate fine control of the movement, mechanical vibrations, and optical misalignment. The next stage was to rebuild the apparatus on a single stable base.

Description of Apparatus

The photograph in figure 26, shows a plan view of the equipment and a diagram of the apparatus in figure 28. The main components are:

- A 0.5 mW HeNe laser which is used as the source of collimated intense light.
- Focusing lenses L1 and L3.
- A X40 Nikon objective lens L2 used to project the light spot on the surface to be measured.
- The piezoelectric element with a mirror attached to its driving member. The element is a means of achieving very small displacements. The hysteresis and non-linearities are unimportant as the mirror position is sensed by a Tesa electronic indicator.
- A beam splitter to deflect the spot image reflected from the surface.
- The knife edge.

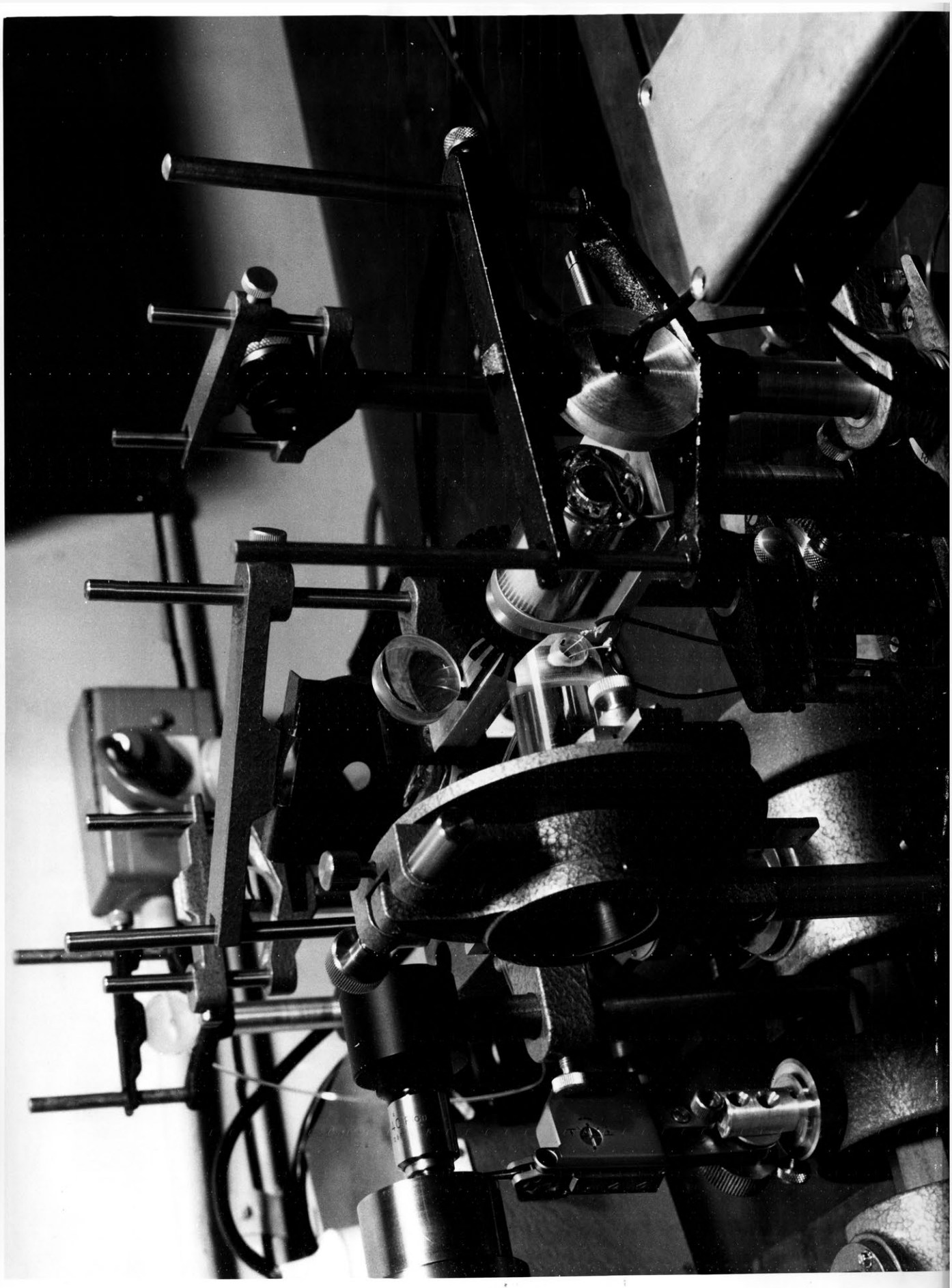

Figure. 27 Close-up of the optical set-up

- A chopper disc and fibre optic assembly whose function has been described earlier on pages 17 - 20.
- Sensing photodetector electronics.
- Reference photodetector. A long optical fibre illuminates the photodetector. The reference output is necessary to synchronize a lock in amplifier to the signal picked up by the sensing photodetector.

The operation of the apparatus is as follows:

Collimated light from the laser is focused by lens L1 into a diffraction limited image at the focal plane of L1. The light which falls onto and crosses the beam splitter illuminates the back surface of the objective lens L2. The Nikon objective L2 projects a spot with an approximate diameter of 1.5 μm onto the surface of the mirror held by the piezoelectric translator. The spot diameter is derived in Appendix I. The diffraction limited spot given by the objective required a minimum source diameter of 1.5 x 40 = 60 μm diameter. Since the diffraction limited image at the focal plane of L1 is 42 μm, there is no need of a circular aperture.

The light spot is reflected back through the objective and is deflected through 90° by the beam splitter. The image of the light spot falls in the plane of the knife edge. A mask with an aperture is placed in contact with the beam splitter to prevent any secondary images which are internally reflected by the beam splitter from reaching the knife edge. A close up of the knife edge, projection lens L4, chopper and fibre optic assembly is seen in figure 27.

The spot image is projected by L4 onto the two end faces of the fibre optic bundle. The chopper with forty slots cut along the circumference intercepts the image before it reaches the fibre optic end faces.

The light reflected by the back surface of the beam splitter is normally lost but it is made good use of in this apparatus. Focusing lens L3 collects this stray light and focuses it onto the end face of a 0.5 m long 1.5 mm diameter plastic monofibre. The fibre conducts the light to the reference phototransistor as indicated in figures 26, 27. The light fibre and phototransistor assembly is arranged such that the chopper intercepts the light path between the fibre end face and the phototransistor receptive area. As the chopper rotates, a reference signal is generated and simultaneously the sensing photodiode recieves alternate signals from the twin fibre optic bundle. The use of this collected laser light has another advantage compared to a separate light source and photodetector arrangement. Apart from providing the reference chopping frequency, the average light intensity of the laser can also be easily measured by this method. This can be simply achieved by measuring the peak output during the period when the phototransistor is illuminated. The intensity level as measured in this way can be used to make any gain or drift adjustment that is necessary if the laser output power varies.

- <u>The complete system</u>.

Apart from the basic hardware just described, there is a set of

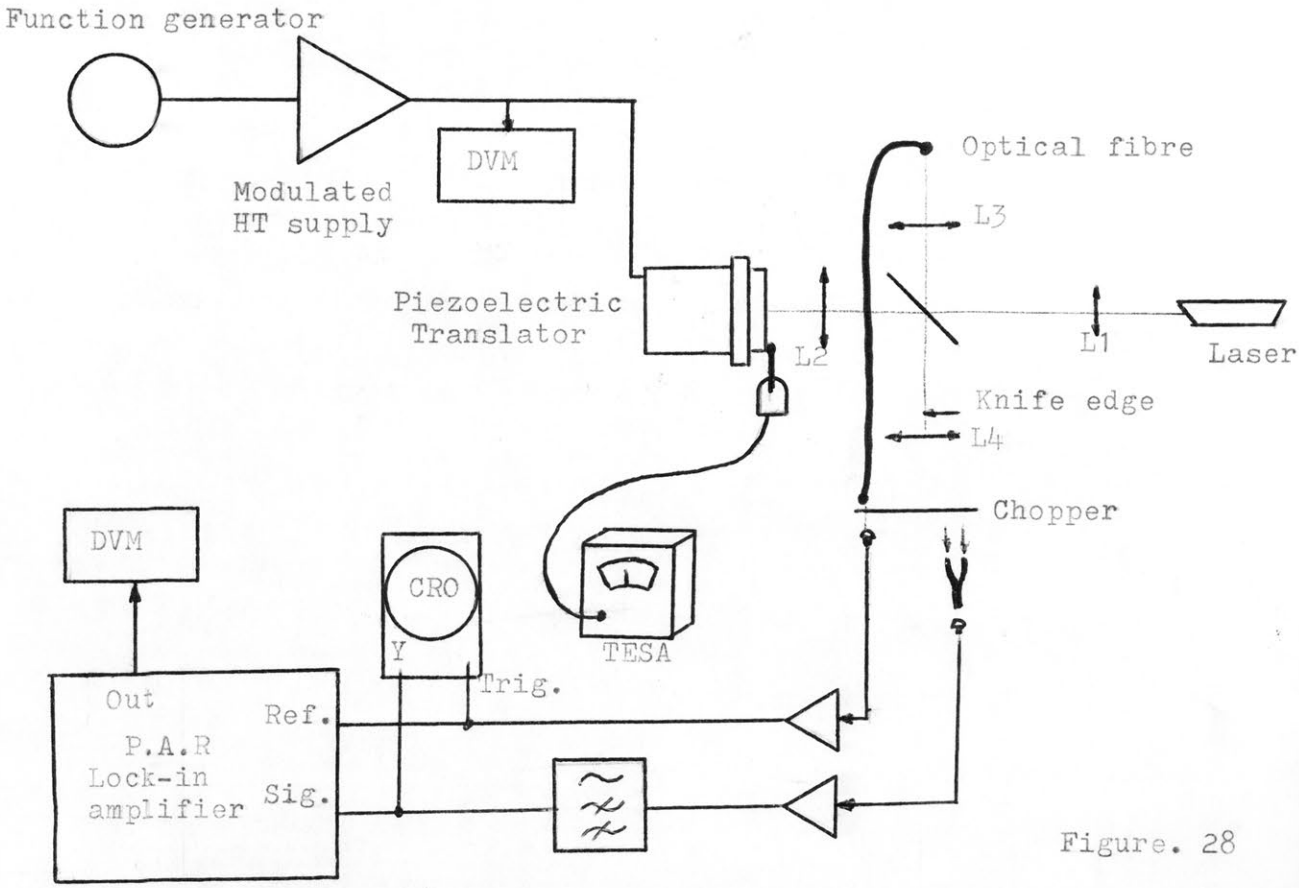

Figure. 28

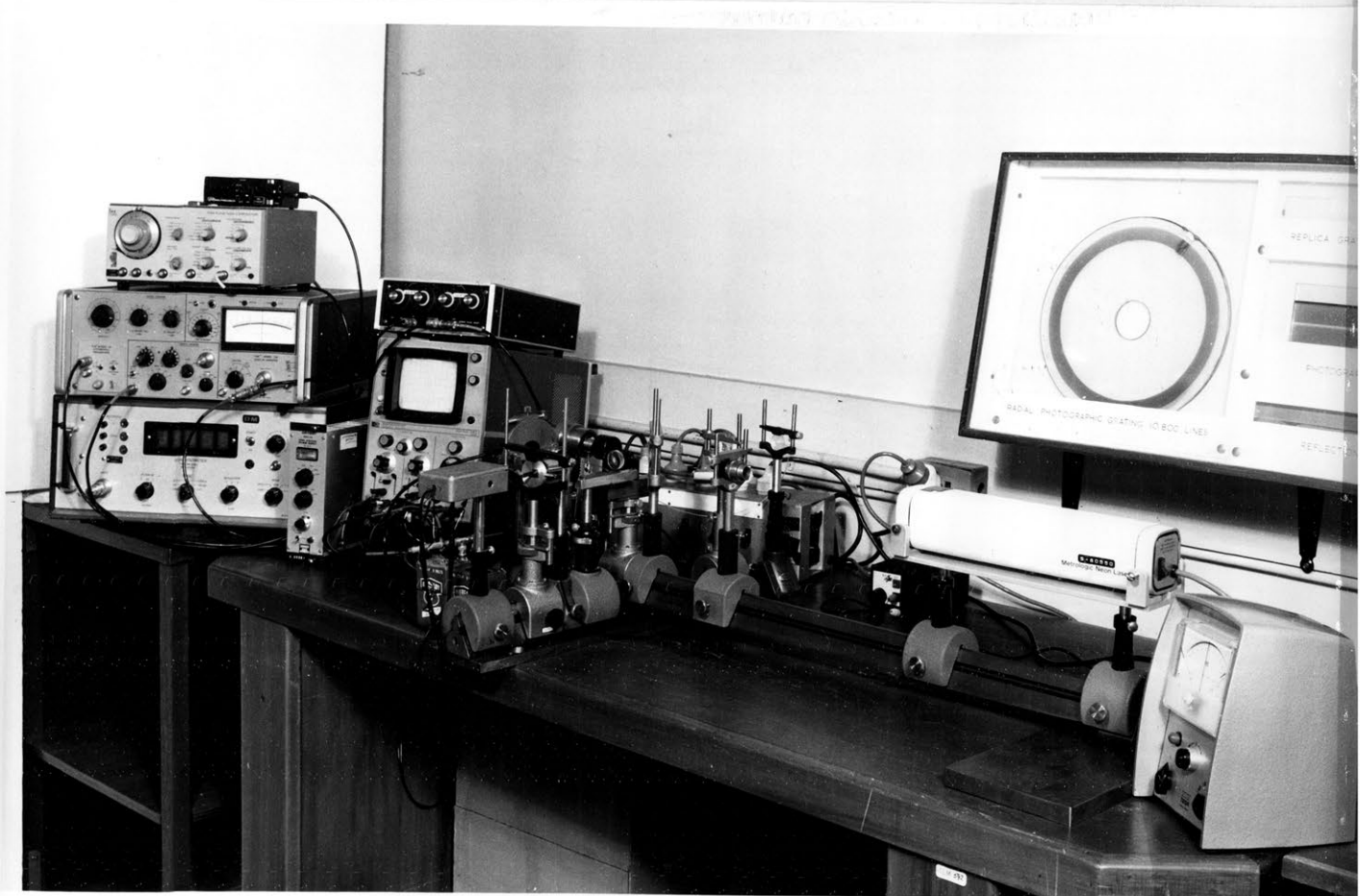

Figure. 29 Overall view of the whole apparatus

ancillary equipment which must be included to make up a complete measurement apparatus. Referring to figures 28 and 29 the role of each instrument is indicated in the following description. As previously mentioned, the position of the driving member of the piezoelectric translator is monitored so that a calibration of the apparatus can be performed. A commercial transducer ("TESA") using a LVDT (linearly variable differential transformer) rests against the driving end of the ceramic translator. Changes in mutual coupling in the transformer are sensed and amplified by the electronic indicator. On the highest sensitivity scale, a full scale deflection of 3 μm can be read. The scale is subdivided into 30 divisions and therefore a deflection of .05 μm can be reliably estimated.

The sensing photodiode output is fed to a high pass filter. The filter excludes any DC present in the signal. The DC arises from unbalance between the photodiode output and the DC offset control on the amplifier (see amplifier circuit figure 30). The filter output is then fed to an oscilloscope to observe and photograph the resulting waveforms. It is also fed to a Princeton Applied Research lock-in amplifier for synchronous detection and amplification. The PAR lock-in amplifier output is then measured with a digital multimeter. As previously mentioned, the reference phototransistor locks the lock-in amplifier and externally triggers the oscilloscope. A function generator is used to drive the high voltage power supply which can be modulated by either a varying DC level or a variety of waveforms. Unfortunately, the slow response of the supply

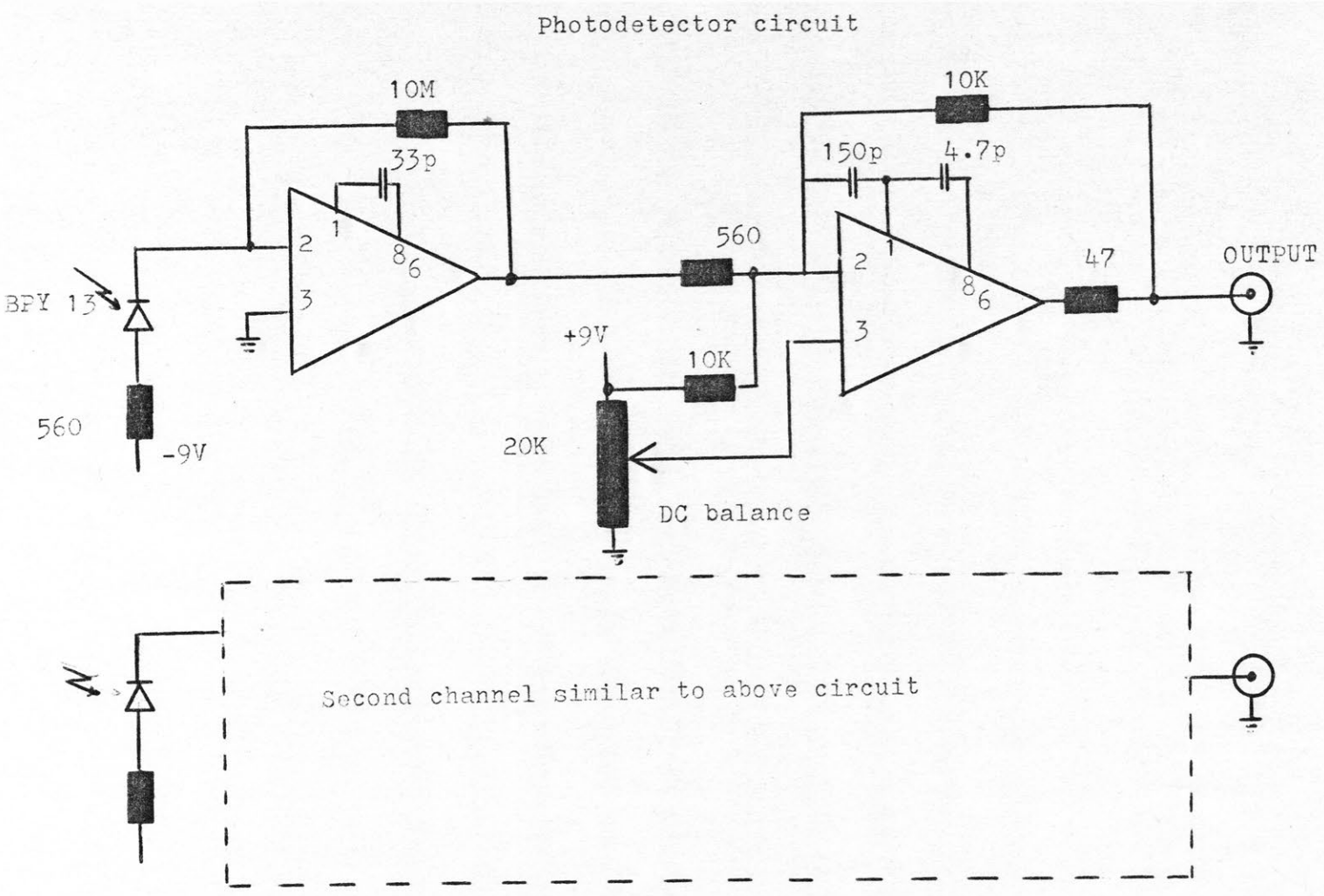
Photodetector circuit
10M
33p
10K
150p
4.7p
560
47
OUTPUT
BPY 13
560
-9V
+9V
10K
20K
DC balance
Second channel similar to above circuit
Operational amplifiers LM301A

Figure. 30

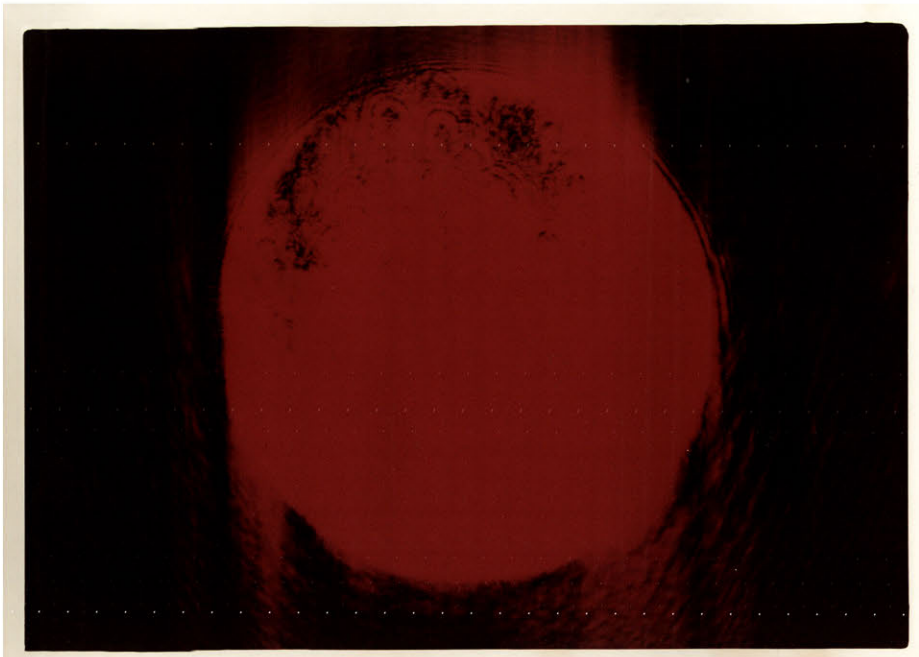

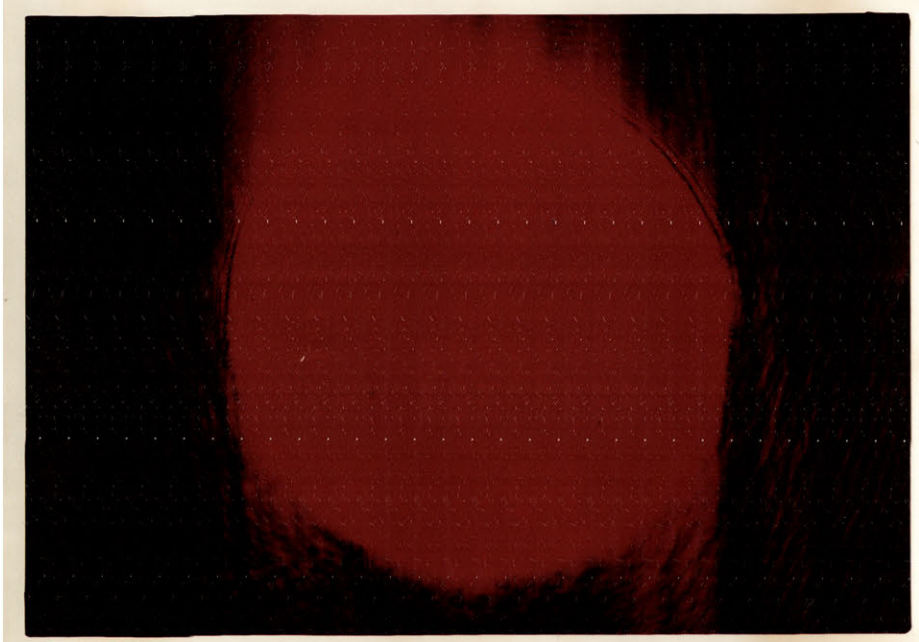

Null condition

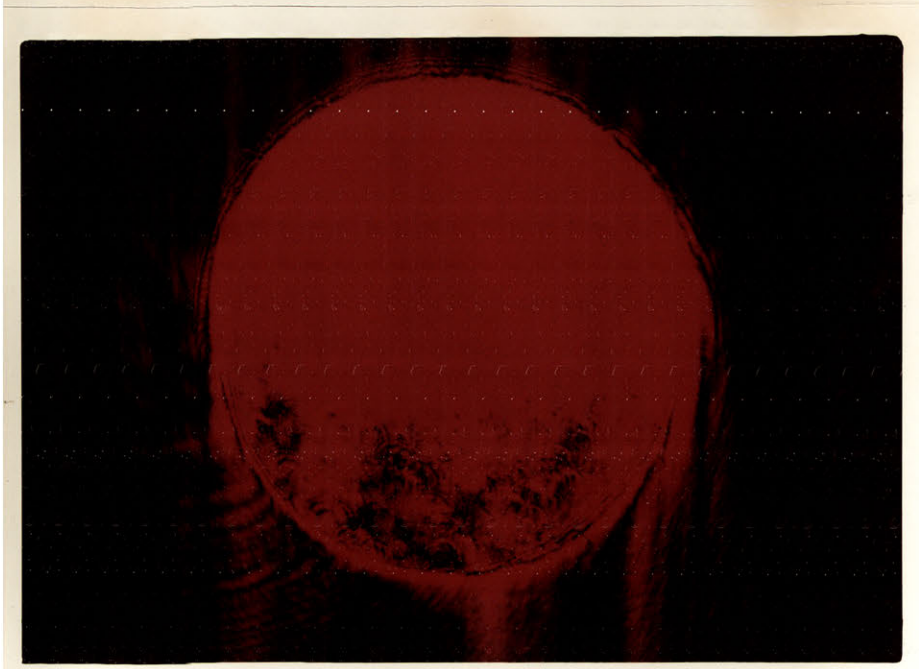

Figure. 31
The Foucault field

limits the modulation to a maximum of 5 Hz. A digital voltmeter records the DC voltage applied directly across the piezoelectric translator.

- Photodiode amplifier.

The circuit for the photodiode is shown in figure 30. This is a straightforward current to voltage converter. The IC amplifier is connected with a feedforward network to improve the slew rate and extend the bandwidth. The second amplifier is an inverting DC amplifier with a 47Ω at the output to decouple output cable and load capacitances and prevent output stage oscillation. An unconventional DC offsetting circuit is included to balance out the standing DC voltage generated by the alternating photodiode inputs (as described previously). The standard procedure is to string a potentiometer across the two supply rails and connect the wiper to one of the summing inputs via a resistor. Stability of both supplies is necessary to maintain a drift free offset. The balancing scheme designed by the author requires that only one supply be stable while still maintaining a full swing between the two supply rails.

- The Foucault image.

The area which the two fibre optic end faces sample is the Foucault field previously mentioned. These X10 photographs in figure 31 show the appearance of this field. The difference in intensity between the two half fields is more pronounced than appears in the photographs. To reveal the detail in the shaded half a long exposure was necessary and this has overexposed the brighter half of the film.

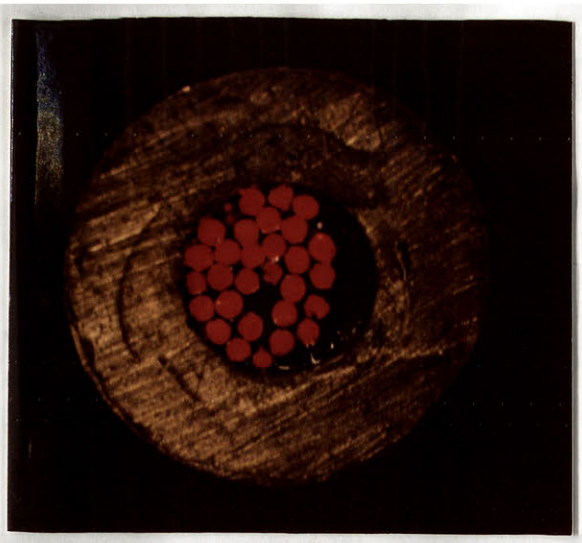

32.a

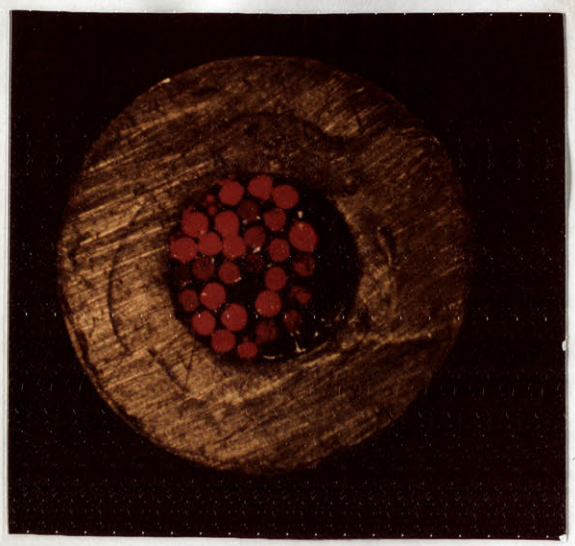

32.b

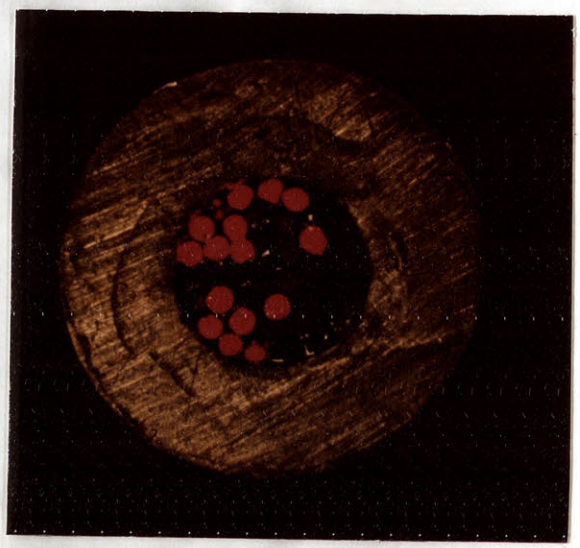

32.c

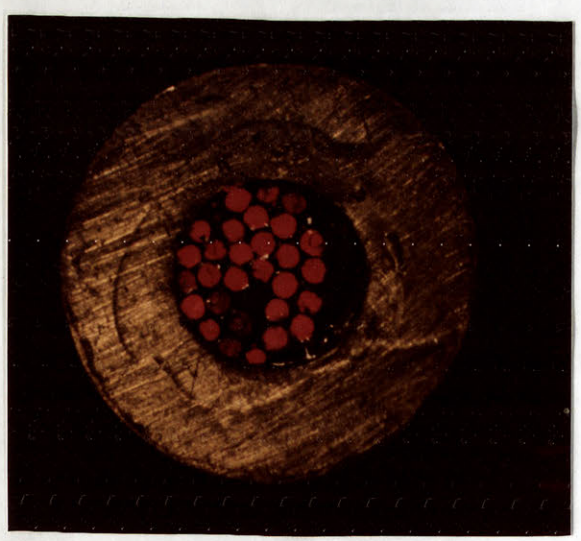

32.d

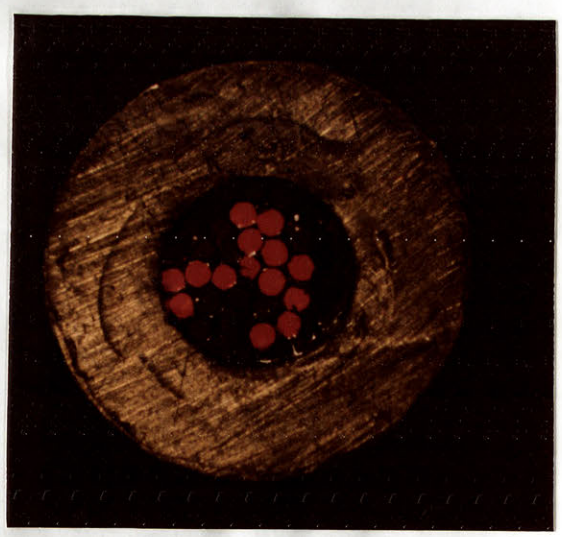

32.e

a-both end faces equally illuminated.

b-d-Foucault field randomized. Observe various intensities.

c-e-each end face alternately obscured and illuminated.

Figure. 32

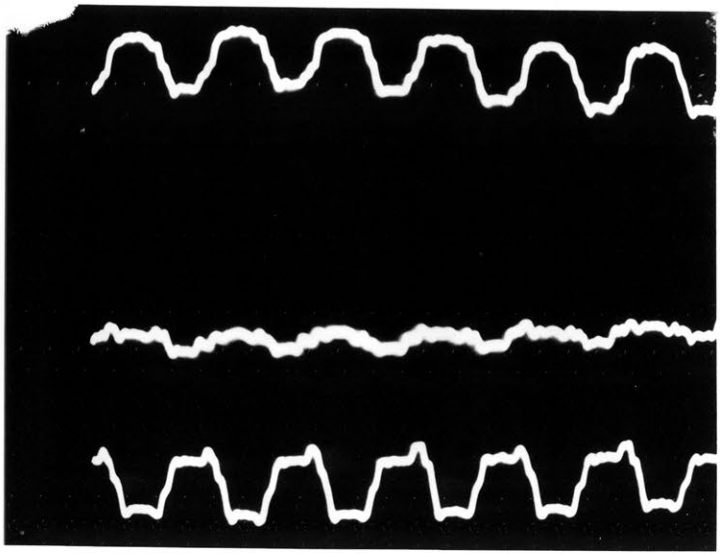

Null condition

Figure. 33 Photodiode output

- The fibre optic assembly

The assembly consists of two separate bundles, each containing 16 monofibres of 0.25 mm diameter each. The fibre bundle was prepared in the following way: firstly, the end faces are assembled and glued with an optical adhesive. Secondly, the loose ends of each end face are mixed in a common clamp and secured with optical adhesive. The ends are then polished. Photographs in figure 32 show the mixed distribution of the common end and the variation of light intensity when either or both halves of the Foucault field are illuminated. It will be noticed that the number of fibres in figure 32 c, e do not add up to 32 as expected. Two fibres from one end face must have cracked or bent at a sharp angle during assembly. This will result in an error during the null condition as different light intensities will be projected by each bundle on the photodiode.

Results.

- Nulling

The first result to be observed is the photodiode output under varying focusing conditions. The separation of the bundles was adjusted such that when each was illuminated by equal intensities, the resultant photodiode output is zero. The middle trace in figure 33 shows this output at null. The top trace indicates the output when the mirror is deflected back from its null position by 0.27 μm. The bottom trace is the output when the mirror is deflected ahead from its null position by 0.35 μm. The output when off-null is dependent on displacement and source intensity. The general purpose laser used in this experiment was

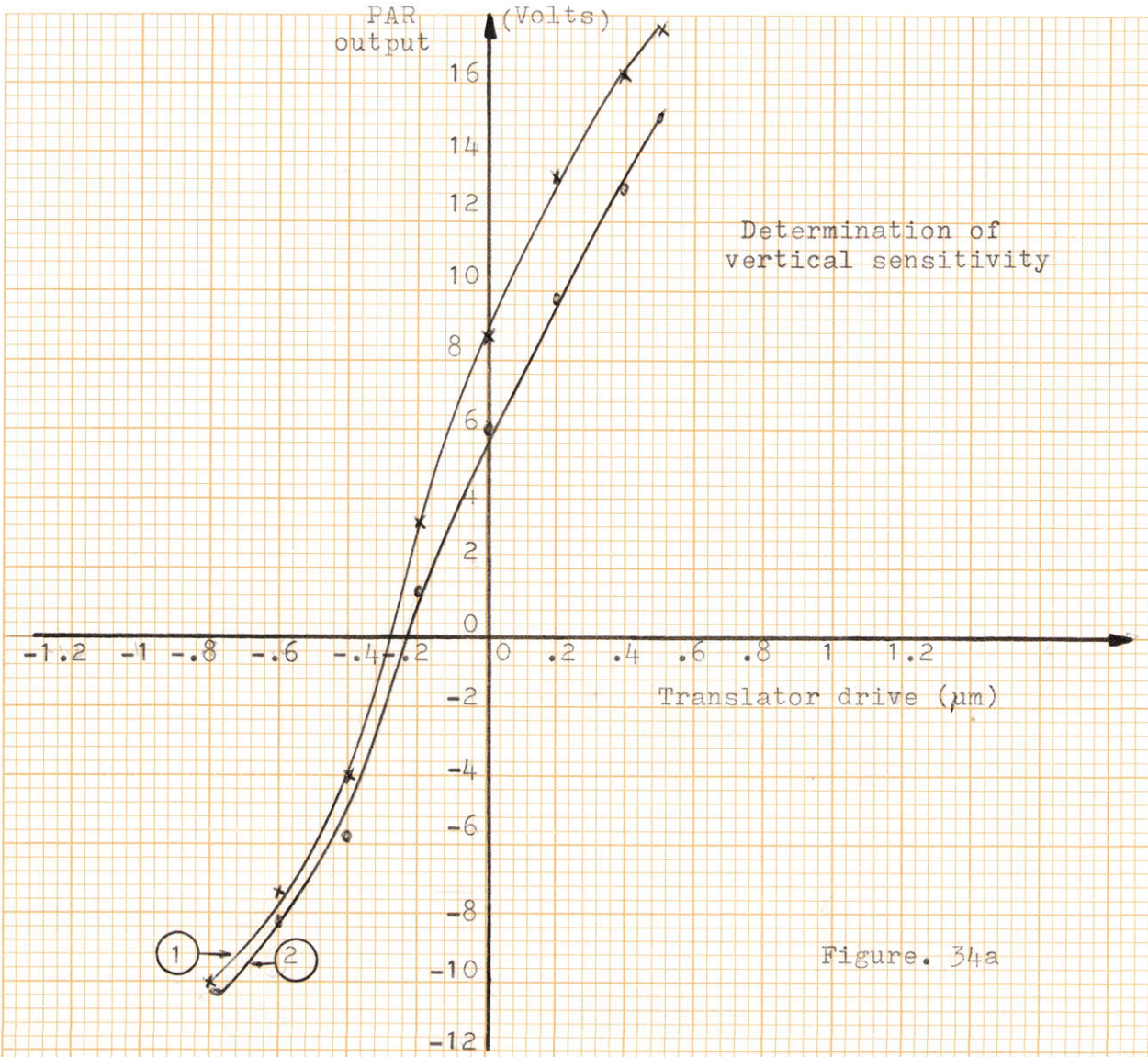

Determination of vertical sensitivity

Figure. 34a

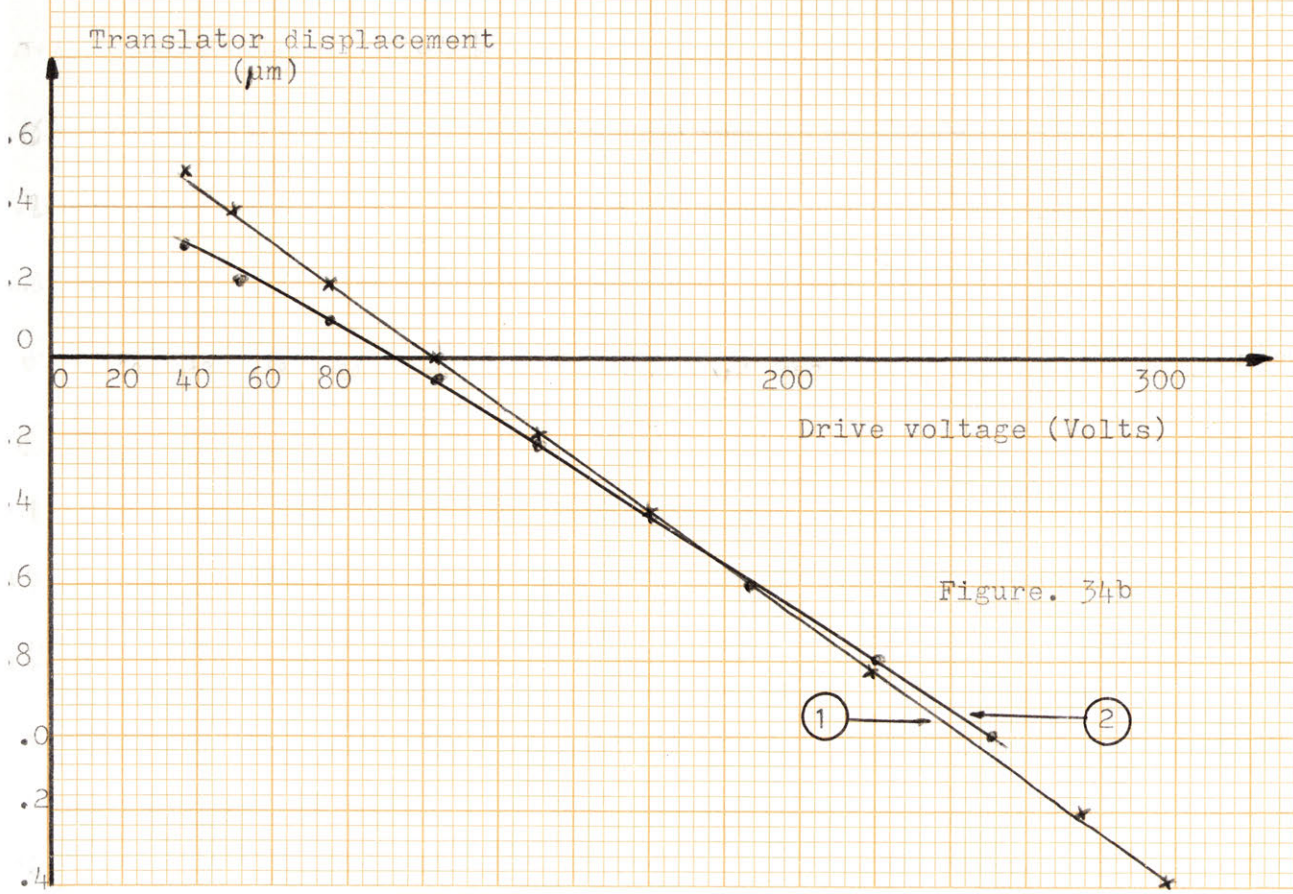

Figure. 34b

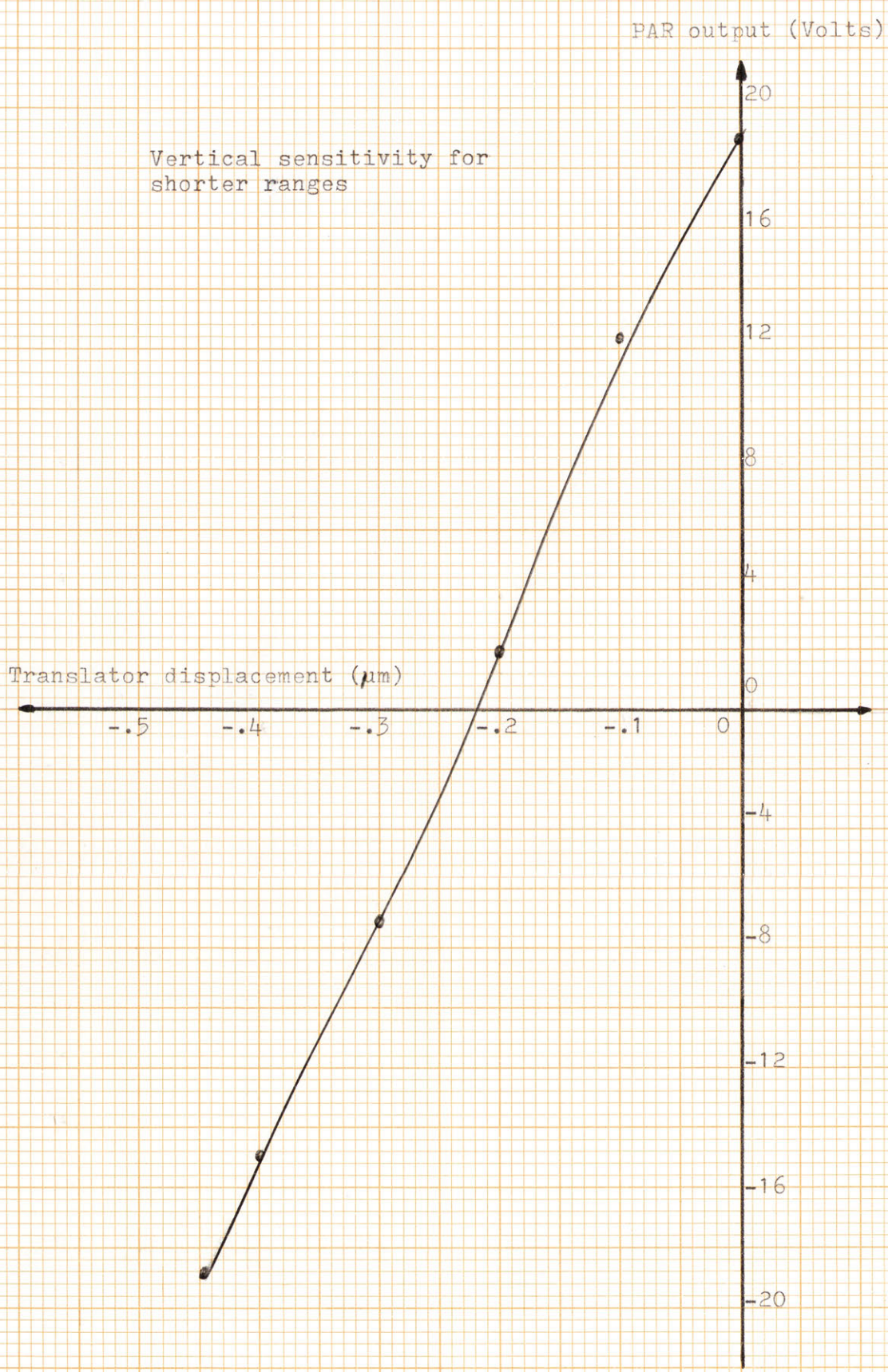
PAR output (Volts)
Vertical sensitivity for
shorter ranges
20
16
12
8
4
0
-4
-8
-12
-16
-20
Translator displacement (μm)
-.5
-.4
-.3
-.2
-.1
0

Figure. 35

not frequency or amplitude stabilized resulting in wide intensity changes during extended periods. Unfortunately, as the project was proceeding, the laser unit was failing more and more and it was later concluded that the laser was faulty. Measurement could only be performed for short periods. For the deflections just mentioned, the output voltage from the lock-in amplifier was 10V ± 0.5V therefore, the calculated sensitivity is 30 nm/V. Deflections smaller than the ones just mentioned can be observed as changes of 2V can be easily observed giving a resolution of better than 60 nm.

- Response linearity

The next set of results was obtained by driving the translator with various DC levels. The position of the mirror attached to the translator was measured by the TESA indicator to obtain accurate knowledge of the translator travel. The photodiode output was fed to the PAR lock-in amplifier whose input sensitivity was set at 100 mV and output gain was set at 1. Although an output gain of 10 and 100 can be selected, the readings under these conditions would be meaningless as the laser intensity drifts during the measurements resulting in an off scale value. The input parameter (drive voltage) is plotted versus mirror displacement and lock-in amplifier output. From runs 1 and 2 in figure 34a and b it will be noticed that the translator deflects linearly for short ranges but as mentioned earlier, hysteresis prevents the translator from following the same path for two similar runs. Over a short range of 0.4 μm, the photodiode output appears linear. The linearity worsens and the output levels off rapidly because the intensity on each half of the Foucault field reaches a

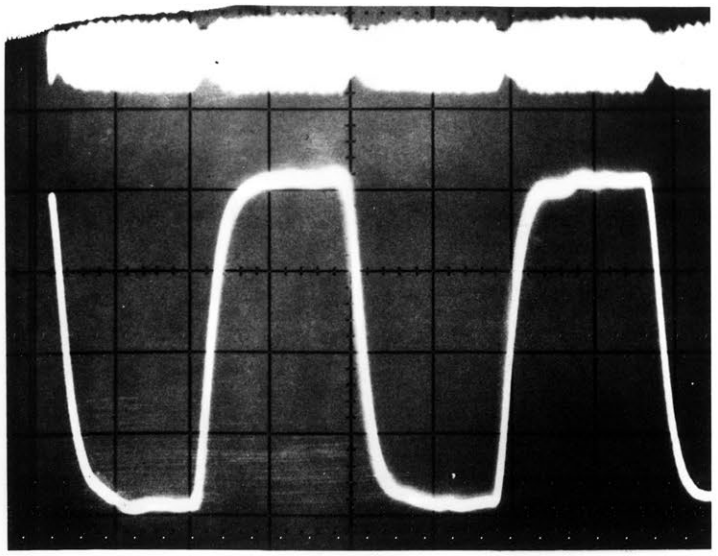

Figure. 36

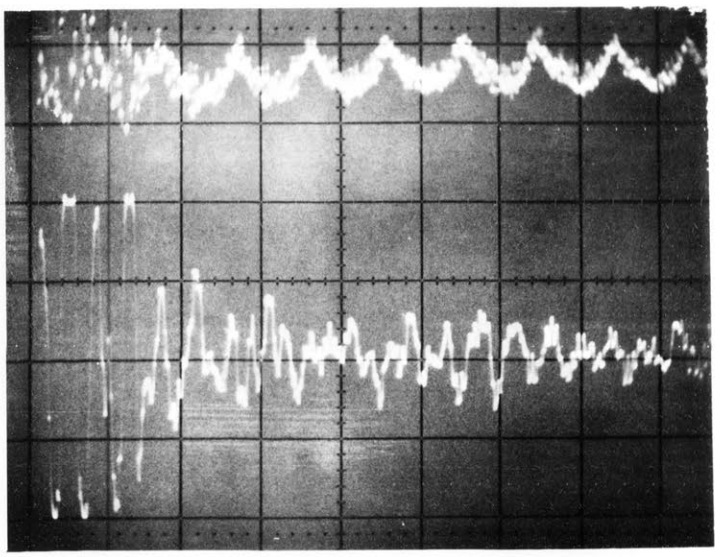

Figure. 37

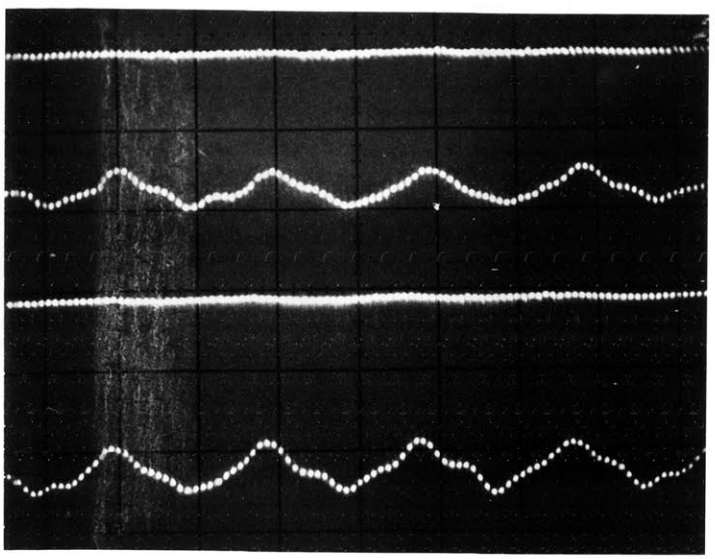

Figure. 38

maximum (or a minimum) from which it does not vary any more. Another set of readings was taken for a shorter range. The PAR input sensitivity was set at 50 mV and the output gain set at 1. The sensitivity as calculated from the graph in figure 35 is 0.45 μm/38V = 12 nm/V. The intensity variations limit the reading from the PAR output to within ± 2V. If the illumination source intensity is constant, a gain of 10 can be effected; resulting in a sensitivity of 1.2 nm/V.

- Dynamic response

Following the static measurements carried out on the system, simple dynamic measurements were made. As previously mentioned, the high voltage power supply can only be modulated by low frequency signals. A DC output of 128V was applied to the translator as this value corresponded to the position of the mirror when the light spot was focused on its surface. The photodiode output is adjusted for a null by carefully separating the fibre bundles. The power supply was then modulated by a ± 46V, 0.25 Hz square wave. The input sensitivity of the lock-in amplifier was set at 100 mV and the result appears in figure 36. The top trace shows the photodiode output and the bottom trace indicates the PAR output. Notice the dip in the top waveforms as the mirror position crosses the null condition during the rising and falling edges of the square wave drive. The TESA indicated an excursion of 0.55 μm. The CRO setting for the PAR output was 5V/division, hence the sensitivity was 27.5 nm/V - close to the sensitivity during static measurements. The photodiode amplifier bandwidth extends beyond 20k Hz and there is no reason why the system should not respond

faster. Because of the limitation of the power supply, another qualitative test was performed as follows. With the mirror in the null position, a small mass of 25 grams was dropped from a height of 5 cm on the edge of the laboratory bench. The impulse imparted to the bench deflected the optical equipment it supported. The impulse response as indicated by the PAR output is shown on the bottom trace of figure 37. Background structural vibrations and noise are displayed after the third division on the trace. There are two interesting features that can be seen in the top trace which represents the photodiode output. The signal appearing in the initial two divisions shows the impulse response which is contaminated with the 50 Hz modulation of the laser intensity. The 50 Hz modulation is due to ripple in the laser power supply. The first feature to be noted is the impulse response signal which has been extracted due to the use of a lock-in amplifier. The second feature is the complete rejection by the PAR of the intensity ripple during the null condition. It is worth mentioning that in the final prototype where the objective is servo controlled to maintain the null condition, intensity variations can be tolerated much more readily than at present and therefore an increase in sensitivity could be effected.

Further results.

As a matter of interest, the following simple variation was carried out. The dual fibre optic bundle was removed and a second photodiode was added to the existing photodiode amplifier. The chopper was shifted to be between lens L1 and the beam splitter. The reference signal was picked up directly at the focus of lens L3. With these changes, the two

photodetector version was quickly implemented and the photodiode outputs shown on the traces in figure 38. Each trace displays the switching between the cut off period of the beam and the period when the photodiodes are exposed to the Foucault field. It will be noticed that 50 Hz modulation ripple occupies approximately 25% of the output (CRO scale is 0.5V/division). For a displacement of 0.5 μm, the change in each output is only 0.1V. When the two signals were fed into the differential input of the lock-in amplifier only the least sensitive range of 500 mV could be used as overloading would occur in high ranges. Secondly, any slight unbalance in setting during nulling will worsen as the laser intensity drifts or fluctuates. Under similar conditions as the single photodiode set up, it was practically impossible to obtain a meaningful set of results because of intensity drifts. This further proves the efficacy of the single photodiode method.

CONCLUSION

This investigation revealed a few problem areas, some solutions and innovations which must be considered in the final design of the prototype. The first problem is the translator to be used in the servo network to drive the objective lens. According to the performance and high hysteresis exhibited by the piezoelectric element it seems obvious for extended ranges, this translator would be difficult to implement. An electromagnetic translator would be worth considering as an alternative. Secondly, the intensity of the light source needs to be reasonably constant as it will affect the sensitivity at null. This will demand an improved laser source - as an alternative it might be worth investigating the stability of semiconductor infra-red or junction laser sources. Thirdly, if the translator is non-linear or has resonances, a transducer will be required to correct for its errors. The transducer could well be capacitive because of the seemingly straightforward technique in achieving it. An optical wedge transducer (in the form of an interferometer) was derived and discussed but will command a separate project by itself. Several important factors about the wedge are worth repeating. It is a linear transducer with a resolution of 6.4 nm/fringe count and is only limited by the number of reflections between the two reflectors. The linearity is unaffected to some degree by setting or alignment errors and the accuracy is directly related to the laser wavelength.

One main innovation in this project is the use of optical fibres for sampling the signal from each half of the Foucault image. The vertical sensitivity ranged between 12 nm/V to 30 nm/V depending on the range

and the length of time during which the measurements were performed. A further improvement to 1.2 nm/V could be obtained if the illumination source intensity were constant. The horizontal resolution is limited by the spot size projected on the surface and is 1.5 μm. The completed prototype would incorporate a fixed optical probe assembly and the surface to be measured would be displaced under the probe. This will require that the surface to be measured is to be taken to the probe. The precise drive of the table supporting the work is another involved problem because of the large variety of objects to be accommodated and evaluated. If semiconductor infra red sources prove to be stable, then the whole optical assembly including the beam splitter, objective, translator, knife edge etc.... could conceivably be built in one "black box" which would be much simpler to drive across the surface than the other way round. If the latter can be implemented, then we have achieved an optical stylus which could be the direct replacement of a mechanical stylus profiling device.

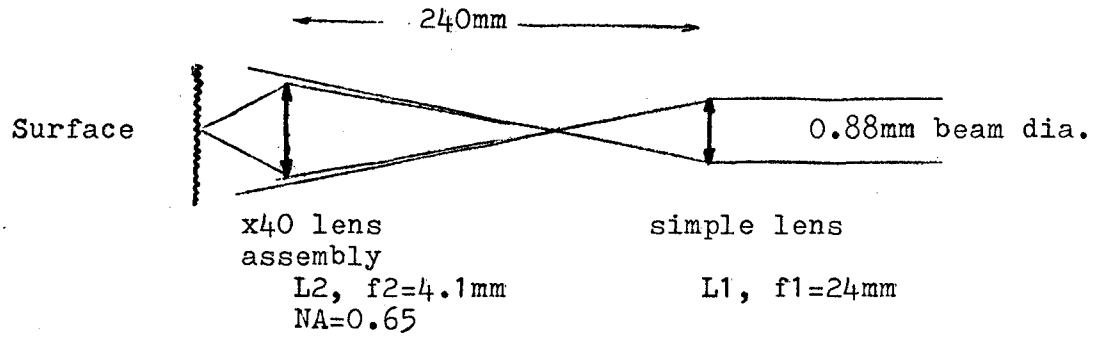
240mm
Surface
0.88mm beam dia.
x40 lens
assembly
L2, f2=4.1mm
NA=0.65
simple lens
L1, f1=24mm

Figure. 39

APPENDIX I

Estimation of the projected spot size

Since the size of the light spot projected onto the surface will limit the horizontal resolution of the apparatus, it is necessary to calculate the spot diameter. A simplified schematic is given on figure 39 and the spot size is calculated in the following:

(a) A parallel beam of light strikes the simple objective L1

The diffraction-limited spot size appearing at the focal plane of L1 is given by f1 x θ where θ = angular radius of Airy disc

$$\theta = \frac{1.22\,\lambda}{\text{aperture}} = \frac{1.22 \times 0.638 \times 10^{-6}}{0.88 \times 10^{-3}} = 8.845 \times 10^{-4} \text{ rad}$$

$\therefore$ Airy disc radius at f1 $= 24 \times 10^{-3} \times 8.845 \times 10^{-4} = 2.123 \times 10^{-5}$ m

$$= \underline{\underline{21.23\ \mu m.}}$$

(b) The diffraction-limited spot size at the focal plane of L2 is given by

$$\text{radius of spot} = \frac{1.22\,\lambda}{2\,n \sin(2\alpha)} = \frac{1.22\,\lambda}{2\,NA} = \frac{1.22 \times 0.638 \times 10^{-6}}{2 \times 0.65} = \underline{\underline{0.598\,\mu m}}$$

With a magnification of X40, the expected radius at f2 would be

$$\frac{21.23}{40} = 0.530\,\mu m$$

Since the diffraction-limited spot size is 0.598 µm, the expected radius at f2 cannot be smaller than 0.598 µm

$\therefore$ spot diameter at f2 $= 2 \times 0.598 = \underline{1.196\,\mu m}$

This estimation assumes perfect elements and an exact knowledge of the beam diameter. The true size would not be much larger than the minimum quoted diameter. A figure of 1.5 µm will therefore be used.

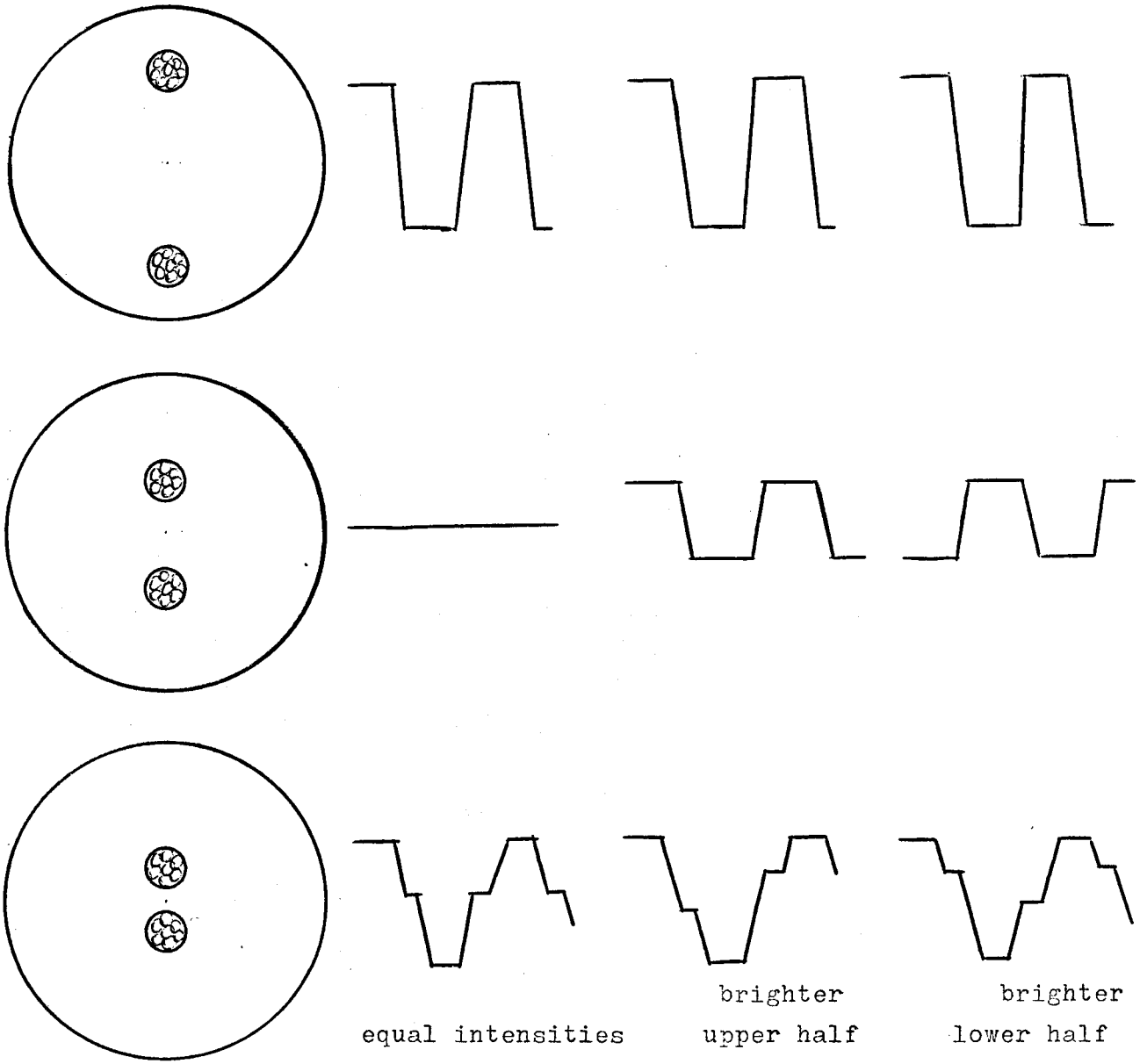

Fibre optic end faces separation
in the Foucault field.

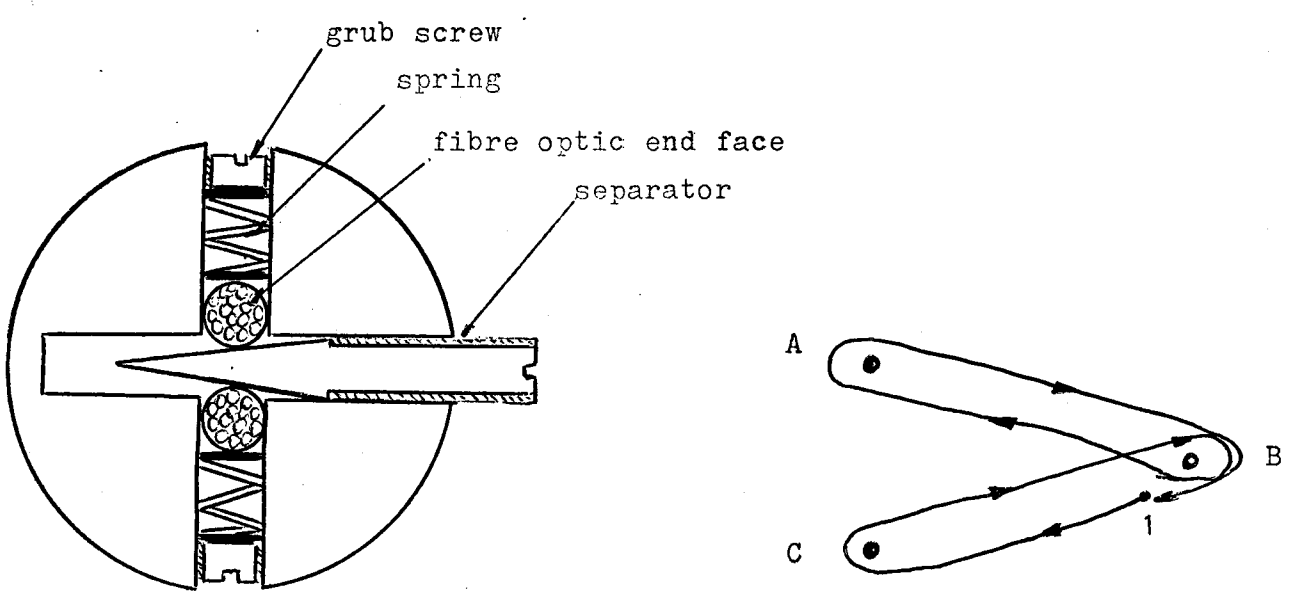

Figure. 40

APPENDIX II

Effect of wrong separation of the fibre optic end faces

- The figure shown opposite displays the various photodiode output waveforms that can be expected as the fibre optic bundle is adjusted in the Foucault field. Only when the bundles are correctly separated and centrally located will there be a definite relationship between focusing and defocusing conditions.

- The end faces of the fibre bundle were held in the adjustable separator shown opposite. Each end face is pressed by a spring onto the conical separator whose operation is self evident. As the separator is threaded in, the two bundles are precisely driven further apart until the required separation is attained.

- A better process to fabricate the fibre bundle is described in the following. Three pegs A, B, C are located on a base plate. Starting at a point 1, the continuous fibre is threaded around the pegs in the order shown. When the process is finished, each bundle is secured and a copper eyelet is fitted at each end A, B, C as the peg is withdrawn. The end faces are subsequently polished.

REFERENCES

ARNULF A. : Journal de Physique Vol 6 no 10 p 62 (1929)

BENDELI A, DURUZ J, THWAITE E. : Metrologia Vol 10 no 4 p 137 (1974)

DAVIES H. : Proc. Inst. Elec. Engineers Vol 101 p 209 (1954)

DEMMEL C. : Diss. TU. Braunschweig (1972)

DUPUY O. : Revue d'Optique Vol 43 p 217 (1964)

DUPUY O. : Proc. Inst. Mech. Engineers Vol 18 no 2 p 255 (1967)

EDWIN R.P. : Journal of Physics E. Sci. Inst. Vol 6 p 55 (1973)

JAFFE B. : Piezoelectric Ceramics. Academic Press London & NY (1971)

LION K.S. : Instrument & Control Systems Vol 37 no 77 (1964)

MOLLENHAUER C. : Intern. Conf. Surface Technology, SME, Pittsburgh IQ 73 - 613 (1973)

PHELAN R.J. : Applied Optics (USA) Vol 10 no 4 p 858 (April 1971)

PORTEUS J.O. : Journal of Optical Society of America Vol 51 p 123 (1961)

PORTEUS J.O. : Journal of Optical Society of America Vol 53 p 1394 (1963)

RAMSAY J.V., MUGRIDGE E.G.V. : Journal of Scientific Instruments Vol 39 p 636 (1962)

SAKURAI Y. : Bulletin of the Japan Society of precision Engineering Vol 8 no 2 (1974)

SAUNDERS J.B. : Metrology of gauge blocks NBS (1957)

SHARMAN H.B. : Proc. Inst. Mech. Engineers Vol 182 part 3K (1968)

TOLANSKY S. : Multiple beam interference microscope. Academic NY (1970)

WESTBERG J. : Intern. Conf. Surface Technology, SME, Pittsburgh IQ 73 - 613 (1973)

YOUNG R.D. : Review of Scientific Instruments Vol 37 p 275 (1966)

YOUNG R.D. : Physics Today Vol 24 no 11 p 42 (1971).

Metrologia 10, 137—143 (1974)

A Surface Simulator for the Precise Calibration of Surface Roughness Measuring Equipment

A. Bendeli*, J. Duruz** and E. G. Thwaite*

National Measurement Laboratory, CSIRO, Sydney, Australia (formerly National Standards Laboratory)

Received: May 8, 1974

Abstract

This paper describes apparatus which has been constructed for the calibration of stylus surface roughness measuring equipment by using a "simulated surface" generated by a vibration table. A differential capacitance position senser attached to the table is in a servo loop with the electromagnetic table drive. This arrangement allows the table to be driven to follow faithfully periodic and random signals over a wide range of amplitudes and frequencies and enables the static and dynamic calibration of surface roughness equipment. Accurately known displacements ranging from less than 10 nm to 4000 nm are obtainable and the frequency span is from dc to 800 Hz (3 dB). The calibration of the simulator remains stable within 0.5 % for periods of more than 6 months.

1. Introduction

Stylus profiling and averaging instruments are the most commonly used means for the precise numerical determination of surface roughness in both scientific and industrial applications. In these instruments a stylus attached to a transducer is drawn across the surface and produces an electrical analogue of the surface. The analogue signal may be treated in a number of ways — to give a profile of the surface at high magnification on a recorder, to give a direct readout of one of the many surface roughness parameters such as the "arithmetical mean roughness" (R_a), or processed by digital techniques.

The displacement of the stylus requires calibration statically or at very low frequencies to determine the scale and linearity of low frequency recording equipment. Dynamic calibration at frequencies of up to approximately 0.5 kHz is necessary to determine the transmission characteristics of averaging instruments with meter readouts.

Static calibrations have usually been made using steps of known height produced by wringing gauge blocks for relatively low magnifications, and lever arm devices or evaporated or etched grooves for high magnifications (see, for example, Reason [1] and Spragg [10]). Likewise, "roughness standards" have usually been used for calibrations in terms of R_a and other parameters. Aitchison [8] has described a plated chromium standard. These roughness standards are surfaces usually made by etching, evaporating, or machining processes and have a prescribed value of the roughness parameter; they are calibrated basically by computation from profiles recorded at known magnifications.

The methods of calibration just described have important limitations. For the static calibrations it is difficult to obtain satisfactory accuracies at the very high magnifications (50,000 and more) used in these instruments without having to rely on the trueness of the attenuators. There is also some difficulty in providing a sufficient number of calibration points throughout the ranges to determine linearity. Due to the restricted availability of "roughness standards" meter readings can only be calibrated at a few points. Obtaining sufficient homogeneity over the surface of the standard and the manufacture of standards at the extremities of the range (below 0.1 μm and above 1 μm R_a) are problems that have not been satisfactorily resolved. The stylii used in the instruments have finite radii (2 to 10 μm) and the inability of the stylus to reach to the bottom of structures is a limitation on the use of this type of standard in some circumstances. These problems of calibration are further discussed by Reason [3]. While the all-important frequency transmission characteristics for instruments have been determined using regularly spaced sinusoidal specimens which can be rotated to give a ratio of frequencies in excess of 10:1, and which were introduced by Sharman [2], a more direct and precise method is needed.

As an alternative to the methods of calibration mentioned above, this paper describes apparatus developed at the National Standards Laboratory that enables the calibrations to be made using a controlled vibration table — a "surface simulator".

Van Hasselt and De Bruin [4] have described a vibration system which they used to determine the transmission characteristics of roughness instruments and to provide a R_a calibration. The apparatus to be described differs from Van Hasselt and De Bruin's in that the table is included in a feedback system and this makes possible a flat response over a frequency range from dc to 800 Hz at the 3 dB point. The table will faithfully respond to a wide range of periodic and random signal waveforms and hold calibration for extended periods. The apparatus can be used to provide:

(a) the scale factor and linearity of low frequency profile recorders by applying a known dc or low frequency signal.

(b) The transmission characteristics in relation to the "Standard Instrument Transmission Characteristics", by applying a random signal to the table and measuring the corresponding output from the roughness equipment.

* National Measurement Laboratory, CSIRO, Chippendale, Sydney, Australia

** Present Address: Ballarat Institute of Advanced Education, Ballarat, Victoria, Australia.

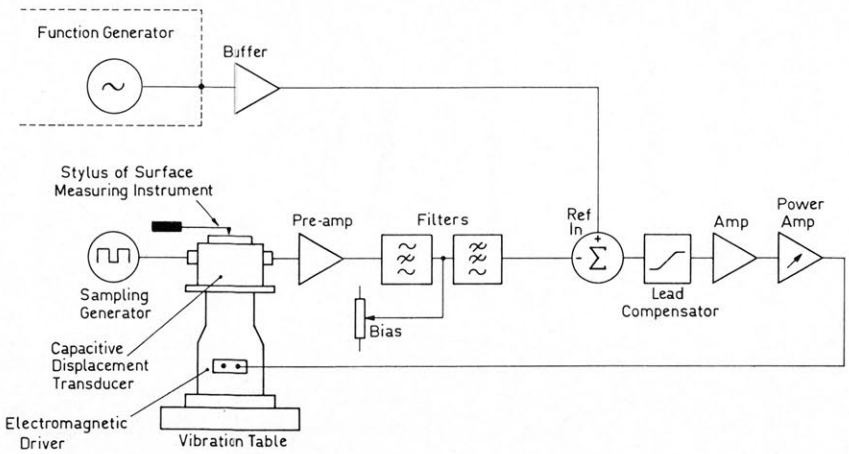

Fig. 1. Surface simulator block diagram

(c) Meter calibration in terms of a variety of parameters by applying signals which generate desired profile shapes and characteristics.

Because of the flat response, the table displacement can itself be determined accurately by static calibration and as the stylus does not traverse a rough surface its shape will not influence the result.

2. System Description

The arrangement of the servo system is conventional but the fact that highly stable and precise displacement characteristics are required for the table at very small displacements imposes a number of critical design problems. These problems relate particularly to the position sensing and the resonance characteristics of the table assembly.

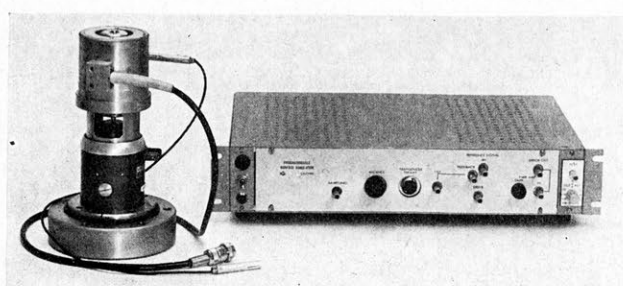

Fig. 2. Surface simulator system

A schematic diagram of the overall system is given in Fig. 1 and a photograph of the complete apparatus in Fig. 2. The major components of the system are the vibration table and the associated position sensor.

2.1 Operation

An electrical signal from a function generator or other source with a waveform analogous to the physical surface to be simulated is fed to the reference input where it is compared with a signal derived from the displacement transducer attached to the table. The difference signal is amplified and drives an electromagnetic transducer situated at the base of the vibration table. The top of the vibration table is consequently displaced synchronously with the waveform from the function generator. The pick-up stylus of the instrument to be calibrated rests on the vibrating member and follows the displacements.

2.2 The Vibration Table

The construction of the vibration table would ideally be such that its dynamic characteristics are free from any major resonances in the vertical direction, in

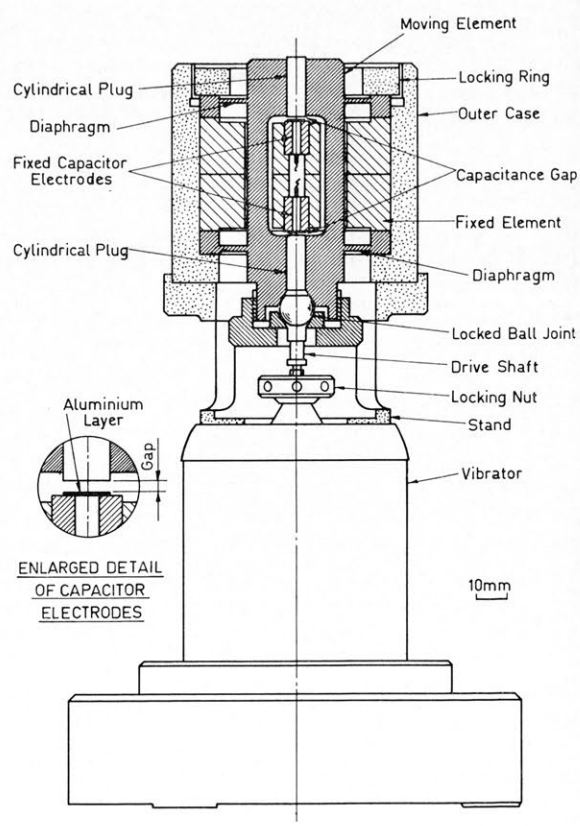

Fig. 3. Section of vibration table

the frequency range of interest, whilst being perfectly rigid in the horizontal plane. In order that the resonance frequency, which is proportional to $\frac{1}{2\pi}\sqrt{k/m}$ (where k is the spring constant of the suspension, and m the vibrating mass), be as high as possible it is necessary that k be large and m be small. A lower limit is placed on the mass reduction by the need for a rigid vibrating body. A heavy suspension, with large spring constant, if designed properly, will also help in the prevention of horizontal movement. However, the stiffer the suspension, the greater will be the force needed to drive the table and more heat will be dissipated in the structure because of the power required by the drive coil.

Various factors decided the shape that the table would take. To minimize the risk of vibrations in any directions other than that required, the moving element should be symmetrical about the central axis, along which the table is driven. A second requirement was that the differential capacitors used to monitor the position be situated with their plates centred on the central axis along which the motion takes place. This was to ensure that the motion being monitored was truly translatory motion along the central axis, and did not contain any effects due to rocking of the vibratory element. It was also decided to make the vibrating element from a single piece of material (i.e. to have no bolted or screwed joints in it) in order to reduce errors in the axial alignment of the capacitor plates, to reduce the risk of positional instability, spurious vibrations and stress concentrations all of which could affect the long term calibration and stability of the instrument.

(a) The Vibrating Element. Referring to Fig. 3, the vibrating element consists of a cylindrical member supported on a pair of diaphragms, the whole being machined from the solid. A large slot is cut from the centre of the cylinder to accomodate a fixed component and the two ends of the cylinder are bored to take a pair of accurately fitting steel plugs.

The diaphragms are rigidly supported at their edges. The design thickness was 0.25 mm which gives a design resonance of 500 Hz. The choice of thickness was a compromise between thick-walled diaphragms requiring a large driving force and having a high resonance frequency, and thin walls which would be difficult to manufacture, give lower resonances but require smaller driving force. The finished diaphragms were thinner than their design size and had a spring constant of 1.5×10^6 N/m. The total mass of the vibrating member (table and drive) is 0.6 kg which coupled to the spring constant has a resonance at approximately 250 Hz. Although the resonance peak is in the range of frequency of interest its effects, as will be seen later, are largely nullified by the servo-system.

The inner surfaces of the steel plugs fitted at both ends of the vibrating element form the moving conductors of a pair of differentially-connected capacitors — the earthed elements. These capacitors are used to monitor the position of the vibrating element relative to the housing. The positioning of the plugs is a critical adjustment in the assembly of the instrument as it determines the spacing of the capacitor plates. The stylus of the roughness instrument rests on the lapped top of the upper plug or on a small polished glass flat attached to it.

(b) The Fixed Element. The fixed element in its unassembled state is E shaped in plan, with the fixed electrodes for the differential capacitor being mounted on the central arm of the E (Fig. 3). The central arm of the E fits into the central slot of the vibrating element thus positioning the fixed conductors of the capacitors opposite their moving counterparts. The whole assembly is rigidly clamped in position as shown in the figure.

To minimize stray capacitance, a twin T network (Fig. 4) is mounted in the fixed element.

The capacitor electrodes are formed by evaporating aluminium layers on a pair of silver steel (high speed or tool steel) inserts fitted in ceramic plugs. This type of construction was adopted to minimize stray capacitance. The steel inserts and the ceramic plugs are cemented in position with an epoxy resin.

2.3 Monitoring Section

The displacement monitoring section of the surface simulator consists of the sampling generator, the capacitance transducer, and a filtering section. It is based on a capacitance displacement measuring technique due to Foldvari and Lion [5].

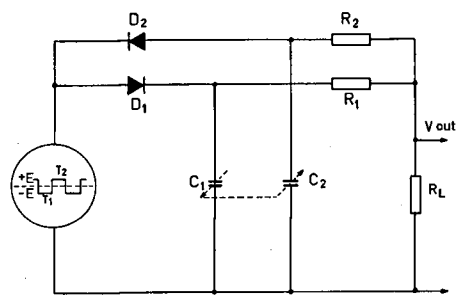

Fig. 4. Sensing circuit

A symmetrical high frequency waveform is applied to a circuit consisting of two switching diodes (D_1, D_2), two discharge resistors (R_1, R_2), a load resistor R_L, and the differential capacitor (C_1, C_2) as shown in Fig. 3 and 4. During the positive half cycle, C_1 is fully charged while C_2 discharges through R_1, R_2, R_L. Similarly during the negative half cycle, C_2 is charged to the supply's peak output and C_1 discharges through the resistors. The diodes switch in the appropriate capacitor during the corresponding half cycle. As the capacitor's plate position is altered, so is the discharge rate. A resultant dc component arising from unequal discharge rates will then relate displacement to capacitance.

Analyzing the circuit under ideal conditions with $R_1 = R_2 = R$, $T_1 = T_2 = T = 1/2\,f$, and with a symmetrical switching signal of amplitude E:

$$V_{OUT} = \frac{R\,(R+2\,R_L)\,V_A}{2\,T\,(R+R_L)}\left[(C_1-C_2)-\left(C_1 e^{-k_1 T}-C_2 e^{-k_2 T}\right)\right], \quad (1)$$

where $V_A = \frac{ER_L}{R+R_L}$, and $k_{1,2} = \frac{R+R_L}{R\,(R+2\,R_L)\,C_{1,2}}$.

For linearity of output with change in capacitance, the exponential terms have to be small. With $R_L \gg R$ and $k_{1,2}\ T \geqslant 5$ the error is $\leqslant 0.6\%$.

If then

$$\frac{1}{4\,RCf} \geqslant 5 \tag{2}$$

$$V_{OUT} = 2\,fRE\,(C_1 - C_2) = 2\,fRE\Delta C \tag{3}$$

where $C_1 - C_2 \propto 2\,ax/(d^2 - x^2)$.

However, for maximum sensitivity

$$\frac{1}{4\,RCf} = 1.75 \tag{4}$$

(see Lion [9]) which is incompatible with Eq. 2 and a compromise between sensitivity and linearity has to be made. Under non-ideal conditions where the switching signal is asymmetrical and $T_1 \neq T_2$, $R_1 \neq R_2$ then

$$V_{OUT} = 2fRE\Delta C + \frac{\Delta E}{2} + fR\Delta E \cdot \Delta C + fE\Delta T + 2fEC\Delta R$$

where ΔE, ΔT, ΔR are the differences between the voltage peaks, periods and discharge resistors respectively. It is therefore necessary that the magnitudes of these quantities are set equal and maintained at the absolute value within close tolerances if a linear response is to be obtained. Furthermore, stability of the discharge resistors and of frequency will determine the long term stability of calibration of the instrument.

The requirement of frequency stability was met by a crystal-controlled oscillator. The frequency was divided using a series of TTL JK flipflops to obtain a unity duty factor. The JK output is fed to a voltage translator switching between $\pm$ 28 V thus delivering a sampling waveform whose half-periods are equal and switching times identical. From the geometrical dimensions (area 27.5 mm^2, separation 7.5 μm) of the transducer capacitance, its value is calculated to be 32 pF. The frequency and discharge resistors are limited by two constraints. Firstly, their maximum value is determined by the linearity condition (Eq. 2) which, as we saw, is incompatible with the requirement for maximum sensitivity. Secondly, the sampling frequency must be higher than the expected bandwidth of the system and the values of the discharge resistors must be low to prevent hum pickup. A value of 56 kΩ and a frequency of 48 kHz was selected. An integrated circuit preamplifier was fitted as close as possible to the transducer element to present a low output impedance to the monitoring cable. The filter section consists of a series of band reject filters tuned at 48 kHz and 144 kHz to eliminate most of the sampling waveform components. A 16 kHz low pass filter provides further attenuation to the switching components. The output from the second filter represents the time variations of the surface simulator displacements. Although great care and precautions were taken in ensuring equal plate spacings of the transducer capacitors, matched discharge resistors, equality in mark-space ratio and switching voltages, an unavoidable residual dc component was present when the system was undriven. Cancellation of this term was carried out by adding a bias of equal but opposite polarity in the last filtering stage. For this adjustment a standard potentiometer was modified to operate using a viscous drive principle developed by King and Heeley [6].

2.4 Drive

This section describes the signal comparator and the drive which consists of the lead compensator, amplifiers, and an electromagnetic vibrator.

A high input impedance follower buffers the comparator from any loading caused by the type of signal generator. Associated with the buffer is a low pass filter with a corner point at 250 Hz which compensates for the peaking of the system's frequency response about this frequency. The buffered input is fed to the non-inverting terminal of a differential amplifier for comparison with the actual displacement as sensed by the capacitive transducer. The differential amplifier introduces a gain to compensate for the losses in the lead-compensator network. The measured open loop response of the system is given in Fig. 5.

Since a high open loop gain is necessary for an adequate speed of response, closing the loop with a

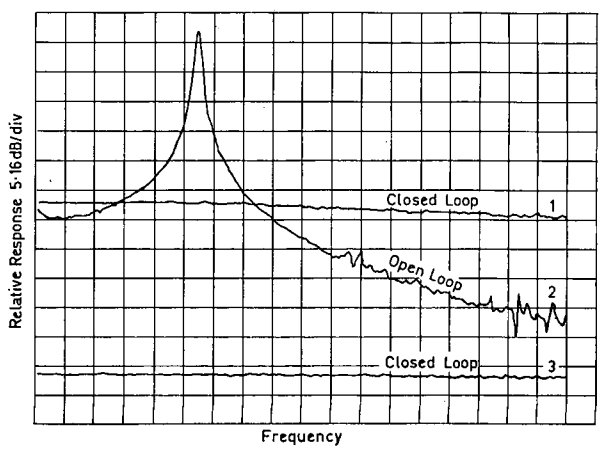

Fig. 5. System's transfer function. Graphs 1 & 2: max. frequency = 800 Hz, 44.76 Hz/div. Graph 3: max. frequency = 8 Hz, 0.44 Hz/div

resonance present in the bandwidth will only result in the production of a 250 Hz oscillator. It was thus necessary to incorporate a compensating network to introduce a phase shift at 250 Hz and make the system stable under closed loop conditions. Unfortunately, such a circuit, has a higher gain at higher frequencies than at dc. This characteristic creates a problem in the removal of noise and sampling frequency components. However, the driver's output at frequencies of 2 kHz and upwards is considerably reduced and the displacements produced by these components can be neglected as they are approximately 2.5 nm and less. An amplifier follows the compensator to provide further gain and to step up the error signal to the level required for driving the power amplifier to its full dynamic range. The power amplifier itself has a variable gain which is used in the final adjustments to optimise the system's step response. The transducer providing the actual mechanical drive is an electromagnetic vibrator (Ling-Altec, Model 201, a miniature unit used in small scale vibration testing). Overdriving the unit at low frequency is prevented by operating the vibrator from a current source consisting of a resistor in

series with the output of the power amplifier. This resistor limits the output current, increases the damping and reduces the resonance peak.

The vibrator is connected to the vibrating element via a drive shaft — Fig. 3. This shaft is coupled to the vibrating element by a locked ball joint, and to the vibrator by a locking nut. Adjustment during the assembly stage was achieved by screwing the shaft into the top of the vibrator armature until the two monitoring capacitances were equalized. This reduced any dc voltages resulting from inequality in the differential capacitor.

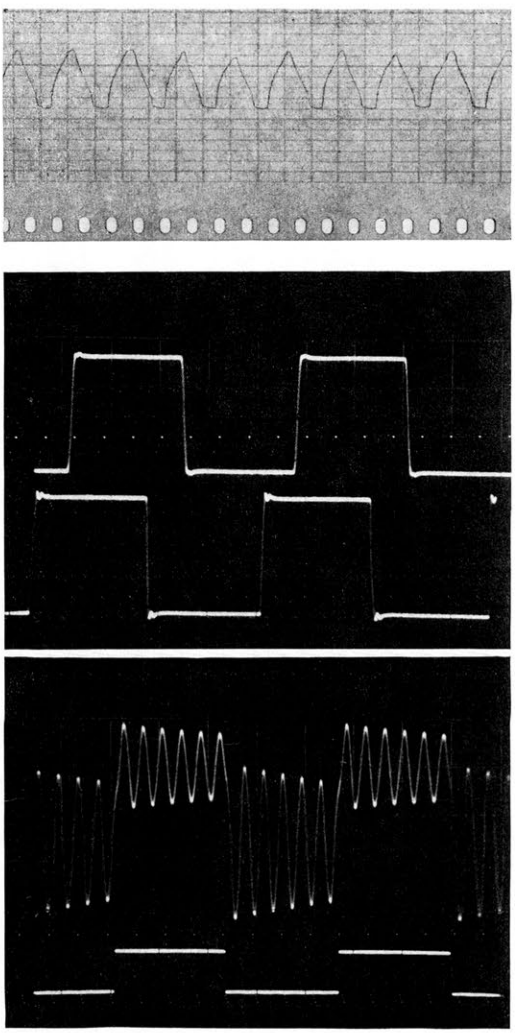

Fig. 6. Step response under various conditions. Scale: Vertical = 50 mV/div = 92 nm/div, Horizontal = 10 sec/div = 0.011 mm/div (b, c, d, e). (a) Roughness standard: R_a 0.077 μm, Peak to Valley Height: 0.266 μm, Horizontal Scale: 0.05 mm/div. (b) Closed loop response to a band limited driving signal. (c) Closed loop response. (d) Open loop response. (e) Driving signal

3. Performance Characteristics

3.1 Range

The spacing of each of the capacitor plates was set to 7.5 μm. The capacitance-displacement relation predicts a 1% deviation from linearity for a displacement of 1/3 of the gap and the displacement has been restricted to approximately this amount by limiting the current delivered to the drive. The resulting maximum range is ± 2 μm but could be increased if additional non-linearity can be tolerated.

3.2 Frequency Response

The measured open loop and closed loop responses of the table are given in Fig. 5. The responses were measured by driving the table from a pseudo-random noise source and using a digital spectrum analyser to determine the response at the various frequencies.

As mentioned earlier, the open loop response displays a resonance at 245—250 Hz while the closed loop response is substantially flat over the frequency range of interest — 3 dB down at 800 Hz.

The behaviour of the table is further illustrated by its response to a square-wave driving signal as shown in Fig. 6. The driving signal is shown at (e), the open loop response at (d), and with the feedback loop closed at (c). If the driving signal is band limited with a 1 kHz Bessel filter, the response (b) is obtained and the small amount of overshoot evident in (c) is further reduced. For comparison, the profile of a typical roughness standard is given in (a).

3.3 Table Calibration

To relate the driving signal to displacement the simulator requires calibration. Since the frequency response is essentially flat down to dc, this can be a static calibration. The calibration device needs a resolution in the nanometre region and a spherical-ended capacitance probe in conjunction with an ac inverse bridge of the type described by Clothier and Bairnsfather [7] has been used. The resolution obtainable with this apparatus is 2 nm.

The sensitivity of the simulator system measured at the transducer output is 0.543 V/μm. This value for sensitivity has remained stable to within ± 0.5% over a period of 6 months. If the instrument is calibrated before use the uncertainty is substantially reduced and the calibration factor can be relied upon to ± 0.1%.

The maximum departure from linearity for the displacement-voltage signal relationship does not exceed 25 nm at the extremities of the range and remains within 10 nm over a range of ± 1.5 μm.

4. Application

The following applications illustrate the variety of uses the surface simulator can be put to in the calibration of roughness measuring equipment.

4.1 Static Calibration of Profile Recorder

A series of levels from a low frequency staircase generator was applied to the reference input of the surface simulator which consequently displaced the stylus by known incremental steps. The record shown in Fig. 7 was made at a nominal magnification of 50000 times. The degree of non-linearity of the recording system is clearly indicated in the record.

4.2 Transmission Characteristics of Roughness Measuring Instrument

For the measurement of surface roughness parameters the wavelength content of the signal being

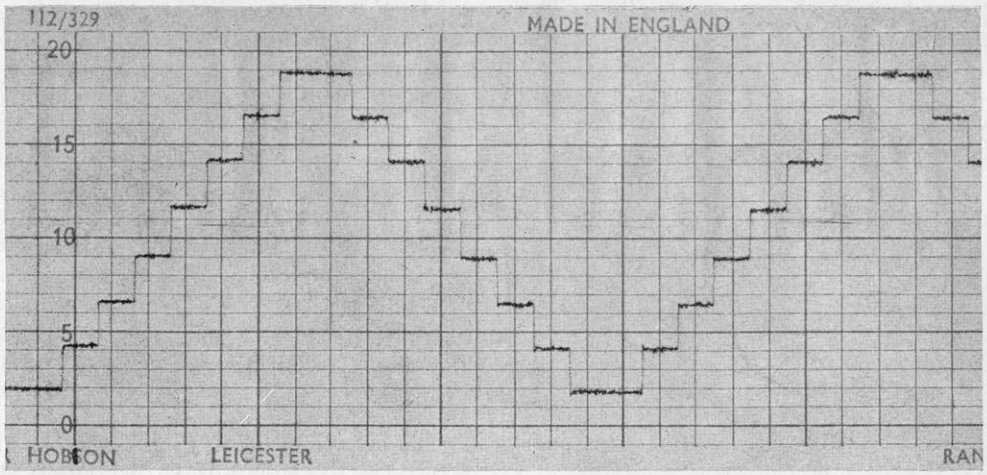

Fig. 7. Calibration of pen recorder. Talysurf: Model 3 on range 6. Scale: Vertical = 50 nm/div, Horizontal = 1 mm/div. Step displacement of the simulator 124 nm/step

processed is all important and the frequency characteristics of roughness measuring instruments are closely specified. These frequency characteristics can be measured with advantage using the surface simulator. A random signal containing all the frequencies in the range of interest is applied to the simulator which in turn stimulates the same frequencies in the roughness equipment. This signal can be recorded simultaneously before and after the filtering network and the ratio of the two records yields the transfer function for the network.

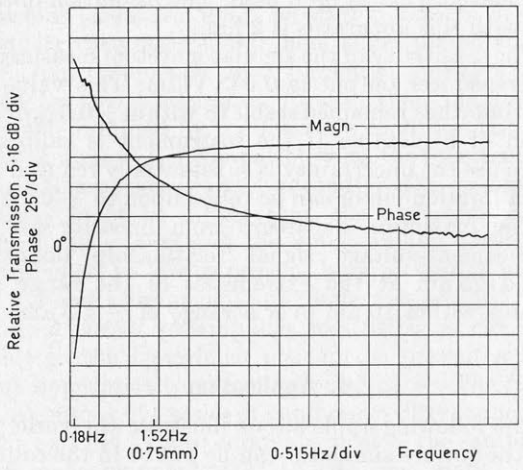

Fig. 8. Transfer function of Talysurf 0.75 mm Cut-off-Filter

Fig. 8 gives the measured frequency characteristics for the filtering network of a stylus roughness measuring instrument with a nominal cut-off setting of 0.75 mm. The curves were obtained using a Hewlett Packard Fourier Analyzer, Model 5451A.

4.3 Meter Calibration in Terms of Arithmetical Mean Roughness (R_a)

There are a number of alternative ways in which the simulator can be used to calibrate instruments fitted with R_a meters, or meters giving other parameters. The most straightforward is to apply a periodic signal of simple waveform (sine, triangular, etc.) and known amplitude to the simulator and to operate the roughness instrument normally. The stylus then moves across the surface of the simulator which generates a pseudo-surface having a known value of the parameter. An alternative which has been applied successfully is to modify the circuits controlling the integrating period in those instruments using relays, and to control the time of integration by an interval timer. When this modification can be made the traversing mechanism may remain stationary during the calibration and so eliminate any jitter which might be transmitted from the traversing mechanism to the stylus. The maximum value obtainable from the simulator of the mean arithmetic roughness (R_a) and the rms roughness (R_s) is approximately 2 μm.

A variety of waveforms have been used to calibrate the R_a meter of a Model 3 "Talysurf". The results for

Table 1. Calibration of R_a Meter — Model 3 "Talysurf" Units: μm

Full Scale Reading	Limit of Reading	Simulator Setting and Corresponding Meter Reading						
1		Simulator:	0.684	0.438	0.247	0.150	0.083	0.033
	± 0.01	Meter:	0.69	0.44	0.25	0.15	0.09	0.04
0.5		Simulator:	0.454	0.395	0.284	0.124	0.090	0.033
	± 0.005	Meter:	0.47	0.40	0.30	0.13	0.10	0.04
0.25		Simulator:	0.285	0.255	0.208	0.153	0.099	0.056
	± 0.003	Meter:	0.250	0.225	0.180	0.132	0.089	0.050
0.1		Simulator:	0.087	0.076	0.051	0.039	0.019	
	± 0.001	Meter:	0.087	0.077	0.052	0.040	0.021	

the calibration of the four most sensitive ranges are given in Table 1.

Acknowledgements. The detailed mechanical design of the vibration table was prepared by H. M. King and J. B. Weir of the Drawing Office of the CSIRO Division of Applied Physics. The apparatus was constructed by the Workshops of the Division.

References

1. Reason, R. E.: ASTME Intern. Conf. on Manufacturing Technology, Ann Arbor, Michigan, 1967
2. Sharman, H. B.: Proc. Inst. Mech. Engrs (London) **182**, Pt. 3K, 319 (1968)
3. Reason, R. E.: Intern. Conf. Surface Technol., SME, Pittsburgh, IQ73-613 (1973)
4. Van Hasselt, R., De Bruin, W.: CIRP Annalen **11**, 193 (1962/1963)
5. Foldvari, T. L., Lion, K. S.: Instr. Control Syst. **37**, 77 (1964)
6. King, H., Heeley, K.: J. Phys. E. **6**, 462 (1973)
7. Clothier, W. K., Bairnsfather, H.: J. Sci. Instr. **44**, 931 (1967)
8. Aitchison, P. M.: Australian J. Appl. Sci. **1**, 71 (1950)
9. Lion, K. S.: Instr. Control Syst. **39**, 157 (1966)
10. Spragg, R. C.: Proc. Inst. Mech. Engrs (London) **182**, Pt. 3K, 397 (1968)

Corrigendum Notice

Metrologia 10, 137-143 (1974). Bendeli, A., Duruz, J., Thwaite, E.G. : A Surface Simulator for the Precise Calibration of Surface Roughness Measuring Equipment

Page headings

... Simulator of ...

should read

... Simulator for ...

P.141 left column, caption of Figure 6

... Horizontal = 10sec/div = ...

should read

... Horizontal = 10ms/div = ...